Faculty of Science and Engineering

Department of Chemical Engineering

Breakup and interaction of immiscible liquid jets

Harisinh Parmar

This thesis is presented for the Degree of
Doctor of Philosophy
of
Curtin University

November 2014

Declaration

To the best of my knowledge and belief this thesis contains no material previously published by any other person except where due acknowledgment has been made.

This thesis contains no material which has been accepted for the award of any other degree or diploma in any university.

Signature: …….

Date: …….....

Abstract

Whilst emulsions have a wide applicability as explosives in mining industry, their precise and controlled use is highly important not only in minimising the resources, but also in reducing production of greenhouse gases. These emulsion explosives could be produced either on-site or elsewhere and transported to the mine-site. The onsite production of emulsion explosive is considerably safer in comparison with the offsite production which requires a relatively risky step of transportation. Offsite production of emulsion explosives involves various conventional methods; however, a micro reactor with multiple jets can be seen as target method for on-site production of micron sized and highly stable emulsion explosives. Consequently, emulsification process has been widely investigated in order to understand the effect of jet formation, jet breakup and droplet formation in micro reactors. However, there are a number of other important phenomena such as jet-jet interactions and jet instability that are not well understood. Hence, considerably more research is required to understand the effect of above mentioned factors on emulsification process.

The present work investigates the effects of multiple jet interactions and jet instability on droplet production and breakup using complementary stat-of-the-art experimental and computational techniques. Firstly, the dripping, jetting and jet breakup regimes of water in canola oil for single jet system have been studied in order to validate dripping, jetting and jet breakup mechanism. With this, the computational fluid dynamics (CFD) studies have been carried out for the single jet rectangular nozzle to analyse the effects of aspect ratio and volumetric flow rate on resultant droplet size. It was found that the modelling results were in good agreement with the experimental data, and for given nozzle dimensions, the equilibrium jet diameter increased with increasing volumetric flow rate. It was also examined that for a given liquid flow rate, the equilibrium jet diameter required for generating minimum sized droplets is a function of aspect ratio.

Furthermore, a CFD model was developed to identify the mechanism and dynamics of jet instability in single jet system. The simulation results were analysed to study the effect of instability on various parameters such as jet breakup, droplet formation and size of resultant emulsion droplets. It was found that at higher volumetric flow rates, the droplets size increased during jet breakup. In addition, both volumetric flow rate and continuous phase interfacial properties led to increase in instability with jet *swing* formation.

Finally, an extensive series of experiments of water in oil have been performed to understand mechanism and dynamics of jet-jet interaction and jet instability by varying dispersed phase flow rate, nozzle diameter and number of nozzles. In addition, computational fluid dynamics (CFD) simulations have been carried out to study interaction between two adjacent jets. It was found that the droplet diameters decreased with multiple jet interactions. Experimental and CFD analysis were in a good agreement for multiple jet system. It was found that the balanced induced pressure gradient between two jets resulted into regular jet breakup, droplet size reduction and shorter breakup length. It was also analysed that the critical distance between jets led to in-of and out-of phase phenomena with reduction in the size of droplets. The new insights provide an important basis to manipulate multiple jets, which produce better emulsion than single jet in micro reactors.

Acknowledgement

First and foremost, I would like to express my special appreciation and thanks to my supervisors Professor Vishnu Pareek and Dr. Chi Phan, you have been tremendous mentors for me. I would like to thank you both for encouraging my research. It would be an understatement to say that they have provided the whole-hearted support for this work both professionally and personally. Their in-depth advice, encouragement, easy accessibility and freedom for work helped me to explore new ideas and to complete the work in time.

Secondly, I would like to express my sincere gratitude to my external supervisor Prof. Geoffrey Evans for his valuable feedback and support during dissertation. I am thankful to my all supervisors for sharing ideas on many varied issues such as report writing, time management, presentation techniques, networking, exchange program encouragement etc. which helped me to develop my personal skills as well.

I would like to thank Dr. Yusuke Asakuma and Prof. Mikio Ouchi for his support during my exchange program in Himeji, Japan.

I would also like to thank my colleagues, Dr. Abhishek Sharma, Dr. Divyamaan Wadnerkar and Dr. Milin Shah, who ensured a pleasant working environment and helped in technical and non-technical matters. The support given by technical and IT staff, notably Ms. Karen Haynes, and Mr. Ross Hayes is worth mentioning. Timely help from the secretarial staff, namely Ms. Tammy Atkins is highly appreciated.

Finally, I am thankful to my parents and family for their support and patient during the tenure of my PhD. I would like to thanks my wife for her support before and during this dissertation. I also acknowledge everyone who has assisted me directly or indirectly in the completion of this work. Their assistance is invaluable and shall always be held in high regards.

Publications

Publications arising from PhD work at Curtin University are:

Peer reviewed journals

- Parmar, H., V. Pareek, C. M. Phan and G. M. Evans (2015). "Influence of jet–jet interaction on droplet size and jet instability in immiscible liquid–liquid system." Chemical Engineering Science 123(0): 247-254.
- Bhatelia, T. J., H. B. Parmar, C. Phan, V. K. Pareek, M. O. Tadé and G. M. Evans (2012). "Hydrodynamics of a rectangular liquid JET in an immiscible liquid–liquid system." The Canadian Journal of Chemical Engineering 9999: 1-5 http://onlinelibrary.wiley.com/doi/10.1002/cjce.20701/pdf.

International Conferences and proceeding

- Parmar, Harisinh; Pareek, Vishnu; Phan, Chi M and Evans, Geoffrey. Interaction between two moving jets in immiscible liquid-liquid systems: An experimental study [online]. In: Chemeca 2012: Quality of life through chemical engineering: 23-26 September 2012, Wellington, New Zealand. Barton, A.C.T.: Engineers Australia, 2012: [1]-[8].
- Pareek, V., H. Parmar, C. M. Phan and G. Evans (2011). "Breakup of multiple jets in immiscible liquid-liquid systems: A computational fluid dynamics study." CHEMECA 2011: Engineering a Better World: Sydney Hilton Hotel, NSW, Australia, 18-21 September 2011: 385.

- H. Parmar, Pareek, V., C. M. Phan and G. Evans (2013). “Influence of surfactant on liquid jet behaviour in another immiscible liquid." 9th World Congress of Chemical Engineering, Seoul, Korea.

In addition to the above publications, I have published on microwave studies, which was conducted in my exchange program at Hyogo University (Himeji, Japan) during the tenure of my PhD. Publications arising from this work are:

Peer reviewed journals

- Parmar, H.B., Asada M., Kanazawa Y., Asakuma Y., C. Phan, V. K. Pareek and G. M. Evans (2013).”Influence of microwave on water surface tension.” Langmuir (ACS Publications) (Accepted on 24 July 2014)

International Conferences and proceeding

- Kanazawa, Y., H. Parmar, Y. Asakuma, V. Pareek, C. M. Phan and G. Evans (2013). Surface tension of water with various kinds of salt under microwave radiation. Chemeca. Brisbane, Australia.
- Y. Asakuma , Kanazawa Y., H.Parmar, V.Pareek, C.M. Phan and G.Evans Surface tension profiles under various microwave radiation modes. In Society of Chemical Engineering Japan 2013 Sep 16, Okayama, Japan, No.K122
- Y. Asakuma , Kanazawa Y., H.Parmar, V.Pareek, C.M. Phan and G.Evans Influence of microwave radiation on water surface tension. In The Society of Separation Process Engineers, Japan 2013 May 24, Chiba, Japan, No.S1-9
- Y. Asakuma , Kanazawa Y., H.Parmar, V.Pareek, C.M. Phan and G.Evans Surface tension profiles under various microwave radiation modes. In ICCE 2013: International Conference & Exhibition on Clean Energy 2013 Sep 9 to 11, Ottawa, Canada, No.NDMRE-10

Table of Contents

List of Tables

List of Figures

Nomenclature

Alphabetical

$A_0 = Cross\text{-}sectional\ area\ of\ the\ nozzle\ (mm^2)$

$AR = Aspect\ ratio\ (X/Y)\ of\ the\ nozzle$

$a = Jet\ radious, mm$

$b = thread\ growth\ rate$

$$E_0(Eötvös\ number) = B_0(Bond\ number) = \frac{\Delta\rho\ g\ LL^2}{\sigma}$$

$C_2 = Constant$

$$C_a = Capillary\ number, C_a = \frac{\mu V}{\gamma} = \frac{Dynamic\ Viscosity * Characteristic\ Velocity}{Interfacial\ tension}$$

$$C_o = Courant\ number, \frac{\Delta t}{\Delta x_{cell}/v_{fluid}}$$

$d_e = equilibrium\ jet\ diameter\ for\ non\ circular\ nozzle, mm$

$d_0 = equilibrium\ jet\ diameter\ for\ \ circular\ nozzle, mm$

$d_d = dropelt\ diameter, mm$

$d_j = jet\ diameter, mm$

$F = force\ (g \cdot mm/s^2)$

$F_r = Froude\ number$

$g = Accelaration\ of\ gravity, 9800\ mm/s^2$

$I_n = modified\ Bassel\ function$

$k = Wave\ number$

$(ka)_{max} = Dimentionless\ wavenumber\ from\ instability for\ viscid\ liquid - liquid\ system$

$m = Mass\ flow\ rate\ (g/s)$

$n = periodicity\ of\ the\ motion\ around\ the\ jet's\ circumference$

$N = Factor\ which\ account\ for\ wave\ splitting$

$p = Pressure\ (g/mm \cdot s^2)$

$Q = volumetric\ flow\ rate\ of\ dispersed\ phase, mm/s$

$R_e = Reynold\ number$

$t = time\ (s)$

$U = Jet\ exit\ velocity, mm/s$

$U_A = Average\ jet\ velocity, mm/s$

$U_I = Interfacial\ velocity, mm/s$

$U_N = Dispersed\ phase\ average\ velocity\ through\ the\ nozzle, mm/s$

$U_t = Velocity\ of\ drop\ after\ detachment\ in\ mm/s$

u, v, w velocity components in x, y and z directions respectively (m/s)

$V = Volume\ of\ drop\ during\ and\ after\ formation, mm^3$

$V_d = Volume\ of\ dropelt\ in\ mm^3.$

$V_F = Volume\ of\ falling\ drop, mm^3$

VOF=Volume of Fluid

CSF= Continuum Surface Force

$\nu = Kinematic\ viscosity\ (mm^2/s)$

v_2=*jet superficial velocity (mm/s)*

$W_e = Weber\ number$

$x = dimensionless\ wave\ number$ * *refers to the disturbance which grows rapidly; (=ka)*

Greek symbols

$\alpha = Volume\ fraction$

$\beta = 0\ in\ the\ non\ jetting\ region$

$\beta = 0.286\sqrt{\Delta\rho g R_N^2/\sigma}\ in\ the\ jetting\ region$

$\Lambda = Actual\ wavelength\ of\ dominant\ wave, mm$

$\mu = Dynamic\ viscosity\ (g/mm \cdot s)$

$\mu_c = Viscosity\ of\ continuous\ phase\ , \frac{g}{mm \cdot s}$

$\sigma = Interfacial\ tension, N/m$

$\rho, \rho' = Desnities\ of\ continuous\ and\ dispersed\ phase\ respectively, g/mm^3$

$\psi = Harkins\ brown\ correctionfactor,$

$$V_D = \frac{2\pi R_N \sigma}{g\Delta\rho}\left[\psi + 1.648\frac{g\Delta\rho R_N U_N V_D^{1/3}}{\sigma U_t} - 0.875\frac{\rho_D R_N U_N^2}{\sigma}(1+\beta)\right]$$

$\Delta v_{2=S}$ *lip velocity (mm/s)*

$\Delta\rho = Difference\ in\ density\ between\ dispersed\ and\ continuous\ phase$

$\Delta\rho = Difference\ in\ density\ between\ dispersed\ and\ continuous\ phase, g/mm^3$

Chapter 1. Introduction

The interaction of two immiscible liquids in emulsification process has been of interest to the engineering community for more than a century. The problem has traditionally depends on different ways of liquid interactions and resultant emulsion quality. Most of the historical and recent literature focuses on the interaction between two liquids in the shear mixing process. However, the interaction of immiscible liquids, via injection of one liquid into the other, is gaining more interest as improved processes are sought.

1.1 Background

Many industrial processes rely on immiscible liquids interactions and hence the production of micro emulsion is an area of great current interest, particularly in the mining emulsion explosive arena. Interestingly, one of the most common emulsions in day to day life is milk which is a biological process of lactation of fat globules. In addition, asphalt, used for building roads, is also an emulsion formed from enormous mixing of different materials. Recently, water in diesel micro emulsion has been used in diesel engines not only to reduce both No_x and particulate matters but also improves combustion efficiency (Yahaya Khan, Abdul Karim et al. 2014). It is also very promising to use this technique to enhance oil recovery (Thomas 2008) or even to help with drug delivery system in pharmaceuticals (Buszello and Muller 2000). Furthermore, ink-jet printing technology is widespread as manufactures try to improve printing resolution as well as advancement in three dimensional printing.

Various techniques have been utilised for forming emulsion in the engineering industries for many years. Industrial emulsification processes can be mainly classified into shear mixing and injection of one liquid into the other as shown in Figure 1-1. In the shear mixing process, one liquid is mixed with the other immiscible liquid and have been stirred until desired emulsification achieved, however; high energy consumption and little control on droplet size distribution has been prominent.

Membrane emulsification involves injection of one liquid into the other through porous media (Okochi and Nakano 2000) for the micron size emulsion production, however; high pressure drop and lower rate of emulsion production is making this method commercially undesirable. Furthermore, flow focusing (Anna, Bontoux et al. 2003, Martín-Banderas, Flores-Mosquera et al. 2005, Xu, Hashimoto et al. 2009) and T-junctions(Nisisako, Torii et al. 2002, Garstecki, Fuerstman et al. 2006) are also used for the controlled emulsification processes. However, higher production rate remains a challenge due to higher pressure drop. The injection of liquid via various size of orifice (s) is one of the technique in which controlled emulsion size can be achieved with the higher rate of production.

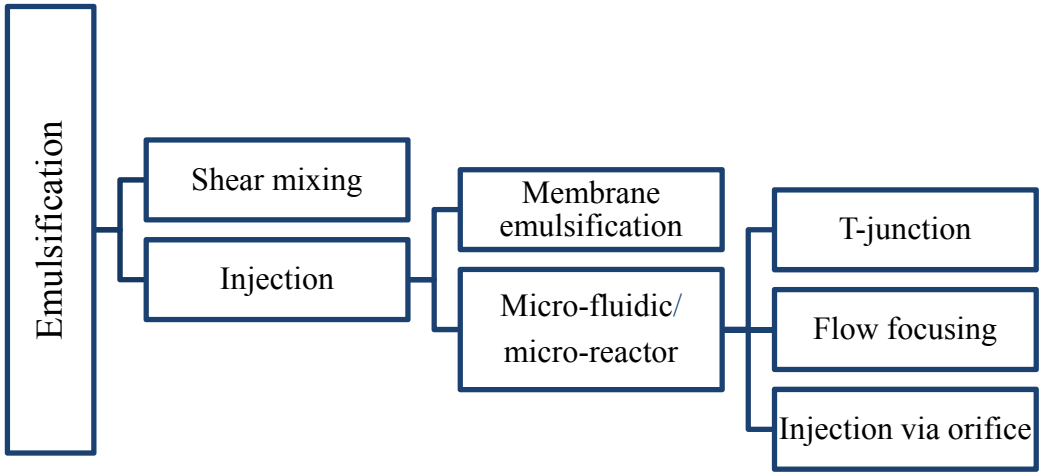

Figure 1-1: Classification of the emulsification processes.

Although multiple jet/orifice system can be used for the higher production rate; emulsion production with multiple jet system is complex mixing process with several physical and operational challenges. Knops, Slot et al. (2001) and Gunawan, Molenaar et al. (2002) studied implications of expending multiple jet system experimentally and numerically. They studied on the effect of the jet flow rate, viscosity and density of dispersed and continuous liquid and distance between jets in case of multiple jet system. The authors have shown that promising research can be carried out to study these implications as they adversely affect the emulsion quality.

In this work, these implications have been studied to understand their effects on the size of emulsion droplets and jet instability.

1.2 Approach

In this study, the jet breakup for single and multiple laminar axisymmetric water jets into canola oil have been studied using experimental and computational technique. In this system, dispersed phase was pushed into continuous phase from the top of the column and drop formed on the nozzle tip at low flow rate. Further, continuous jet has been formed at higher flow rates and jet(s) has been breakup into droplets. In this research project, CFD simulations have been used to study the liquid jet formation and subsequent detachment into droplets. The ANSYS Fluent v14 was used which is a control-volume-based technique to convert the governing equations into algebraic equations that can then be solved numerically. The governing equations used were the mass conservation equation for each phase and the momentum equation. Volume of fluid method (VOF) applied to capture the liquid–liquid interface during jetting and droplet formation. The interfacial tension between the two phases was implemented using the continuum surface force (CSF) model proposed by Brackbill, Kothe et al. (1992).

This study has been split into three main parts. Firstly, dripping, jetting and jet breakup phenomena of water jet in canola oil for single jet system have been captured using high speed camera (at 125 frames per second). Moreover, CFD simulations have been use to validate the phenomenon. With this, dripping, jetting and jet breakup analysis has been carried out for single jet system. CFD simulations have been further used to analyse the effects of aspect ratio and volumetric flow rate on resultant droplet size for rectangular nozzle. In the second part of this study , this immiscible liquid system has been examined for instability during emulsification and hence the effect of instability on emulsion quality. The CFD simulation results were analysed to study the effects of instability on jet breakup, droplet formation and size of resultant droplets. An extensive series of experiments of water in canola oil have been performed to understand mechanism and dynamics of jet interactions and

instability by varying dispersed phase flow rate, nozzle diameter and number of nozzles in the final part of this study. In addition, computational fluid dynamics (CFD) simulations have been carried out to study interactions between two adjacent jets. The effects of critical distance between multiple jets on jet formation, jet breakup length and droplet size were also studied.

1.3 Scope and objectives

This thesis focused on the hydrodynamics of emulsification process. The main aims of this research are to study the fundamental of jetting behaviour, drop formation and instability during emulsification. Furthermore, the influence of various parameters such as volumetric flow rate, nozzle size, space between adjacent nozzles and viscosity of dispersed and continuous phases, are investigated. The specific objectives are as follows:

1. To study dripping, jetting and jet breakup phenomena in single jet emulsification.
2. To investigate the effects of instability phenomenon on the emulsification process and droplet size.
3. To examine the interaction between adjacent jets, in combination with the aforementioned effects, on the emulsification process and droplet size.
4. To quantify the relationship between jet distance and the resulting droplet size.
5. To elucidate the underpinning mechanisms of the experimental results by the simulations.

1.4 Organisation of the thesis

This thesis is organized into six chapters and an appendix. An introduction to the emulsification process and current challenges has been given in the first chapter with focus on the research objectives of this study. The second chapter describes previous work in the area of emulsification more specifically jet formation, jet breakup,

volume of droplets and sets the groundwork and objectives for the rest of this work. The third chapter describes detailed experimental setup and procedures. Simulation methodologies were also described in this chapter. Single jet experimental and simulation results follow in the fourth chapter with single jet instability modelling. Multiple jet experimental and CFD analysis were discussed in fifth chapter with concluding remarks and recommendations for future work following in the sixths. The appendix presents the data used to develop all graphs and tables. The structure followed for completion of this thesis is given in Figure 1-2.

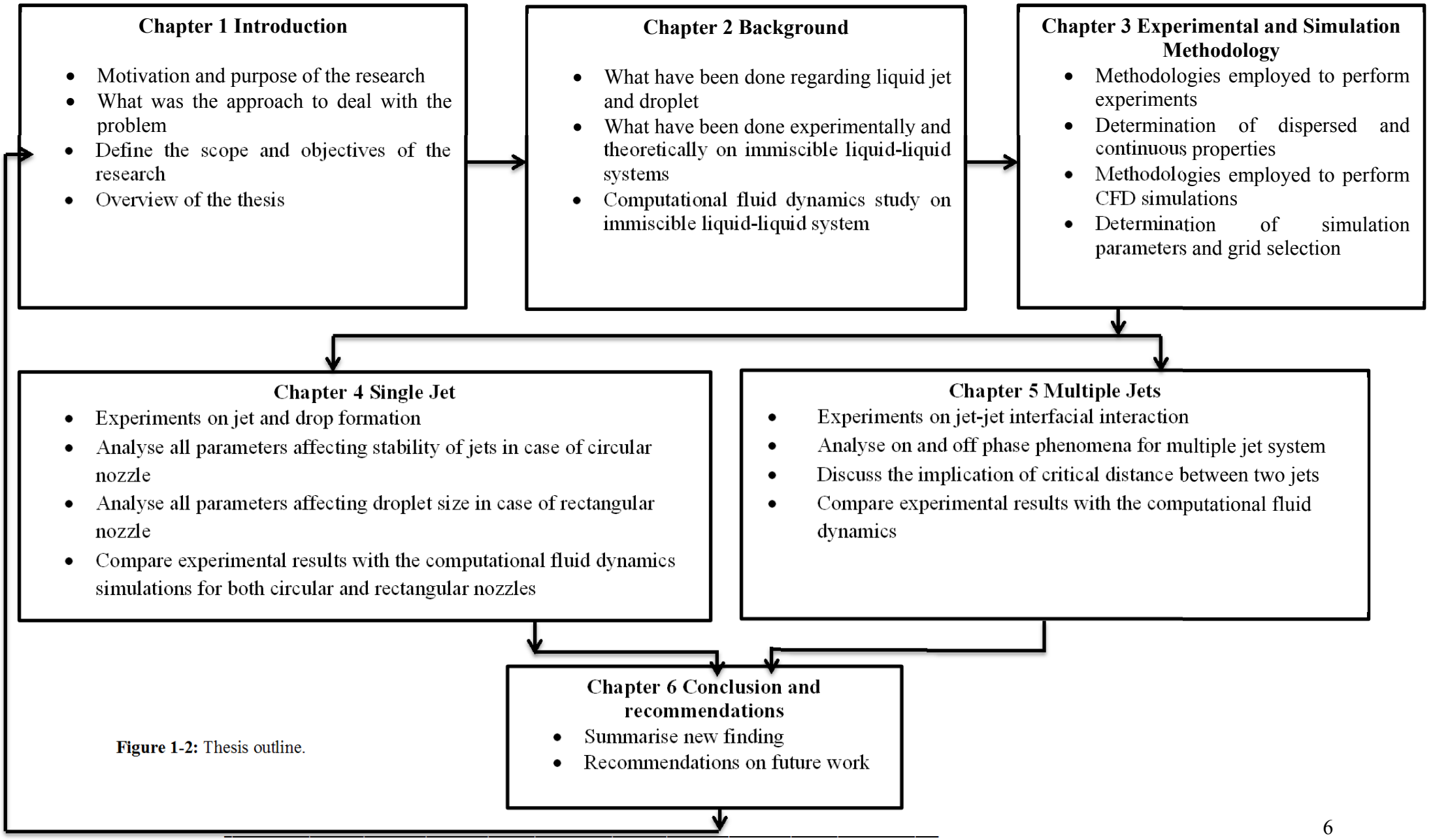

Figure 1-2: Thesis outline.

Chapter 2 Literature Review

The miniaturisation of chemical reactors offers many fundamental and practical advantages for all chemical industry, which is constantly searching for solutions to achieve control over product quality, throughput, and environmentally friendly methods with a high degree of chemical selectivity and low carbon footprints (Ehrfeld, Hessel et al. 2000, Fletcher, Haswell et al. 2002). Miniaturization allows measurements to be performed with a device that consume less space, materials, and energy and often has higher reaction rate. These devices can be fabricated in parallel by batch processing at low cost and, in particular, a dramatic improvement of performance is achievable by integration of a multitude of miniaturized functional elements. Micro reactors are widely used in chemical industry for the production of water-in-oil (W/O) and oil-in-water (O/W) emulsions and drug delivery system in pharmaceuticals.

With this improved performance of these reactor, emulsion production via micro channels has been of interest for many chemical industries. However, detailed study of complexities involved with the jet and droplet formation for the multiple jet system required to produce quality emulsion droplets. Numerous research, most notably Tomotika (1935) and Chandrasekhar (1961), have been published over the years describing the theory of jet breakup. Recently, many studies, Homma, Koga et al. (2006) and Garcia and Gonzalez (2008), on jet breakup and droplet formation were carried out using computational fluid dynamics to capture the jet breakup phenomena.

2.1 History of liquid jets research

The original work on liquid jet and instability was carried out by Savart (1833), who investigated falling-off phenomena of liquid jet at the bottom of the reservoir. Figure 2-1 shows drop breakup dynamics observed by Savart (1833); in which, Perturbations grow on the jet, until it breaks up into drops, at a point labelled "*a*" and an elongated neck was observed near "*a*". Moreover, "satellite" drop is also visible

between two drops. Drop break up resulted from growing perturbations therefore drop continue to oscillate around the spherical shape even after the breakup. The author was managed to produce the complete picture of the actual process which was taking place in very short time scale. Despite the fundamental insight, the author could not be able to recognise the source of instability which led to the eventual break up of this liquid jet. Savart (1833) however mentioned that the mutual attraction between molecules leads to a sphere shape, around which oscillations take place. Moreover, the groundwork for the surface tension which is the driving force behind drop breakup, was carried out by Young (1804) and Laplace (1805). It is also noted that the mutual attraction of molecule also occurs inside the drop not only on the surface.

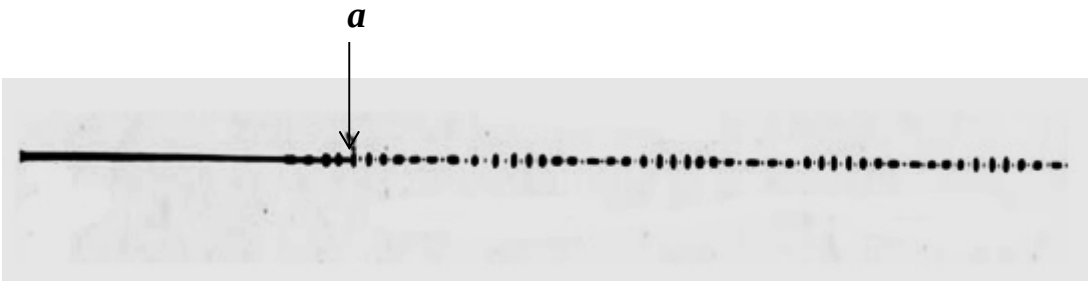

Figure 2-1: Breakup of liquid jet diameter of jet was 6 mm (A figure taken from Savart's original paper (Savart, 1833)).

Subsequently, Plateau (1843) studied drop breakup by developing his own "Plateau tank". He eliminated gravity effects by suspending a liquid bridge in another liquid of the same density inside the tank. From these studies, Plateau (1849) confirmed the crucial role of surface tension in jet breakup. Any perturbation which leads to a reduction of surface area is favoured by surface tension. This makes all sinusoidal perturbations unstable when its wavelength longer than 2π (Eggers 2006). Figure 2-2 offers some interesting insight into the nonlinear dynamics of jet breakup. Initially, thin elongated thread forms, which has its minimum in the middle. Finally, three satellite drops forms in which satellite drops on left and right hand side are even smaller indicates that the final stage of breakup are more complicated. The thread breakup occurred at four places instead of the middle.

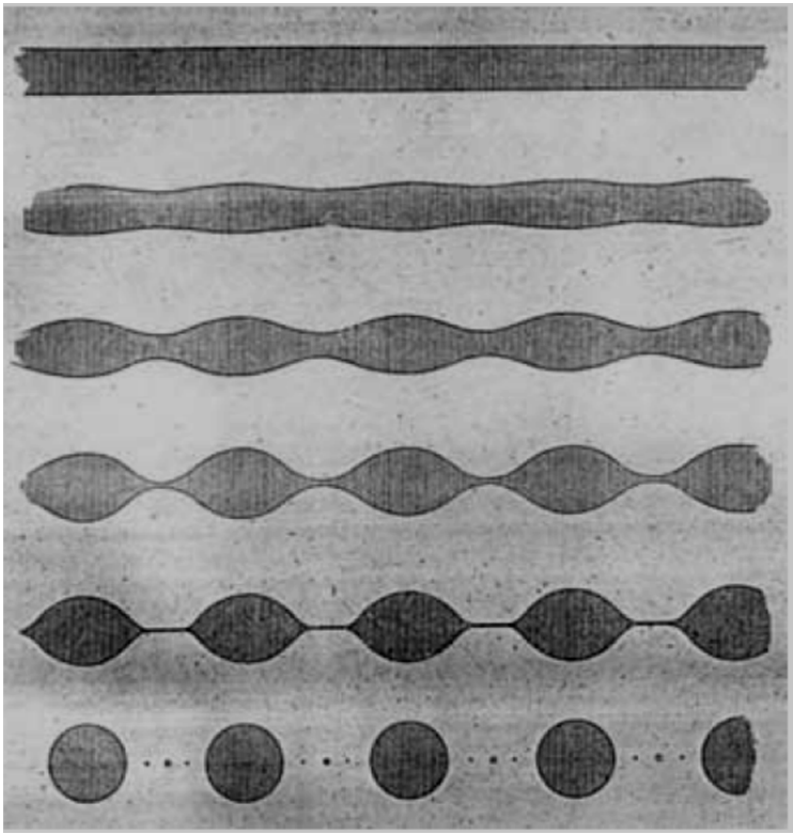

Figure 2-2: Breakup of liquid column of oil in a mixture of alcohol and water (Plateau 1849).

Rayleigh (1878) proposed a model describing jet break up mechanism and argued that the jet instability was the result of one of two causes: dynamic breakup or capillary forces. In addition to reviewing previous studies of Plateau (1873) and Helmholtz (1869), Rayleigh developed equations to predict the dynamic and capillary breakup of these liquid jets. Later on, Rayleigh (1891) published experimental pictures which is shown in Figure 2-3. However, these pictures were produced by a single short spark, so they only transmit a rough idea of dynamics of the process but satellite droplets are clearly visible. These droplets were produced between elongated necks between two main drops. The important point to note how these sequential photographs showed the formation of satellite droplets.

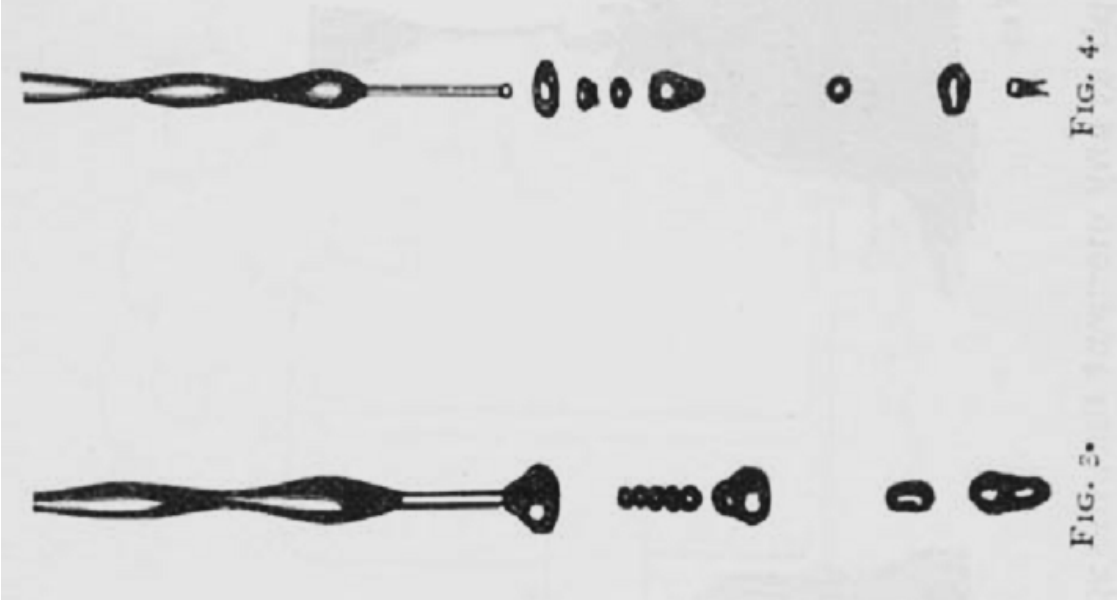

Figure 2-3: Photographs were taken by Rayleigh (1891) with the help of short electric spark.

In the jet breakup mechanism proposed by Rayleigh (1878), the most amplified wave length ($\Lambda \approx 4.5$ jet diameters) was one of the critical components of his linear breakup analysis. He analysed the linear stability of an infinitely long axisymmetric cylinder of an inviscid incompressible fluid, with initial radius $r = R$, which is subjected to small sinusoidal disturbances of wavelength Λ_ω from this equilibrium This leads to the radius having the form $r = R + \delta\, cos(kz)\, cos(n\emptyset)$, where δ is a small initial disturbance, *k* is the wavenumber ($k = \frac{2\pi}{\Lambda_\omega}$), *n* is an integer, *z* represents the distance along the central axis of the cylinder and ϕ is the azimuthal co-ordinate. Using the standard equations of motion and assuming that disturbances in the form $exp\,(i(kz - n\emptyset) + \Lambda t)$, where *t* is time, Rayleigh was able to derive a dispersion relation as per Equation 2.1.

$$\Lambda^2 = \frac{\sigma(kR)}{\rho R^3}\,(1 - n^2 - k^2R^2)\,\frac{I'_n\,(kR)}{I_n(kR)'} \tag{2.1}$$

Where σ is the surface tension, ρ is the density of the liquid, I_n is the modified Bessel function of the n[th] order and I'_n is the derivative, defined by $I'_n = (\frac{d}{dr}\, I_n\,(kr))|r = R$.

Values of $R_e(\lambda) > 0$ cause the amplitude of the disturbance to grow with time, and so $R_e(\lambda)$ is defined as the growth rate of the disturbance. $I_n(\lambda)$ is the wave frequency. The integer n is the periodicity of the motion around the jet's circumference. For values of $n \neq 0$, $\Lambda^2 < 0$; this corresponds to neutrally stable waves, where λ is purely imaginary and $R_e(\Lambda) = 0$. Waves for which $R_e(\Lambda) < 0$ are stable. However, for $n = 0$, $R_e(\Lambda) > 0$, corresponding to a growing amplitude for $0 < kR < 1$. This mode is axisymmetric and it is possible to use the recurrence formulae for Bessel functions (Equation 2.2)

$$I_{n-1}(x) + I_{n+1}(x) = \frac{2n}{x} I_n(x),\ I'_n(x) = \frac{1}{2}(I_{n-1}(x) + I_{n+1} \tag{2.2}$$

to arrive at the dispersion relation for the unstable axisymmetric disturbances (Equation 2.3)

$$\Lambda^2 = \frac{\sigma(kR)}{\rho R^3}(1 - k^2R^2)\frac{I_1(kR)}{I_0(kR)} \tag{2.3}$$

The most unstable mode is the value of k corresponding to the maximum of $R_e(\lambda)$. The disturbance which grows most rapidly occurs for $kR \approx 0.697$, which has a wavelength $\lambda_\omega \approx 2\pi R/0.697 \approx 9R$, the so-called famous Rayleigh mode. At this wavenumber the perturbation grows fastest and kR governs the size of the droplets produced. The corresponding growth rate is $R_e(\Lambda) \approx 0.34\,(\sigma/\rho R^3)^{1/2}$, which yields a characteristic break-up time, $t_b \approx 1/R_e(\Lambda) \approx 2.94(\rho R^3/\sigma)^{\frac{1}{2}}$. For $kR > 1$, λ is imaginary and the disturbances do not grow with time. Validation of the results were done against the well-known experiments of Savart (1833) , and was found to be in good agreement.

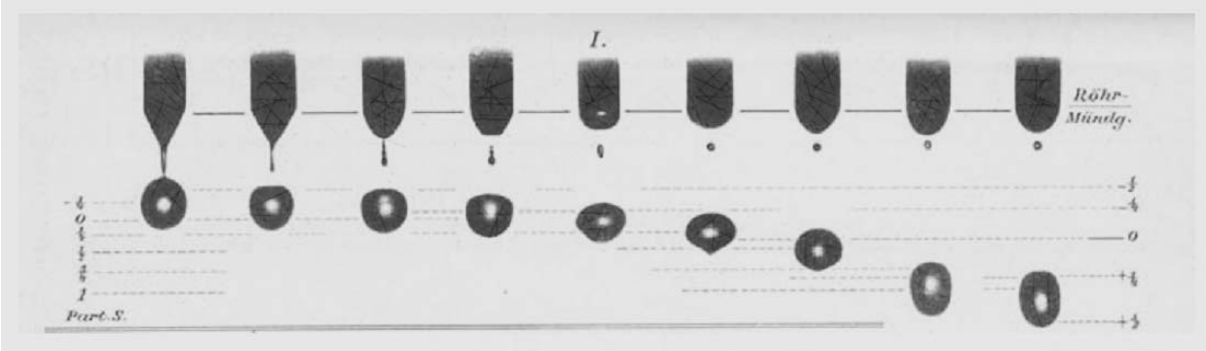

Figure 2-4: Water droplet falling form the pipette (Lenard 1887).

The cohesive forces between the fluid particles depends on the surface tension (Rowlinson 2002) and therefore research work on surface tension related phenomena saw an significant progress, both from a theoretical and experimental point of view, in the later part of 19th century. A research paper by Lenard (1887), who observed the drop oscillations that remain after break-up, which was already noted by Savart (1833). By measuring their frequency, the value of the surface tension can be deduced. Lenard (1887) employed a stroboscopic method and recorded sequences showing dynamics close to drop breakup and hence oscillations as shown in Figure 2-4. In addition, Lenard was able to record a sequence showing the dynamics close to breakup, leading to the separation of a drop. The author was able to see origin of satellite droplet formation. However, as noted before, dynamics close to the breakup was noted by only few people and still Rayleigh's linear stability analysis was only tool theoretically which does not include a mechanism for satellite drop formation.

Edgerton, Hauser et al. (1937) discovered that highly viscous fluid such as glycerol forms extremely long thread that breakup into multiple satellite droplets. Figure 2-5 shows a water and mixture of glycerol-alcohol falling from the nozzle in two different cases. Water jet breakup into main drop and several satellite drops. When measuring the quantity of water, main drop and satellite drop taking into account; some of the satellites drops are projected upward by comparing the satellite droplet formation with main droplet in the previous sequence and thus do not contribute to the volume of the main drop. Therefore the total weight depends on a very subtle dynamical balance that can hardly be a reliable measure of surface tension. Moreover, mixture of glycerol forms extremely long threads, which break up into

multiple satellite drops. In particular, the drop weight cannot be a function of surface tension alone, but also viscosity.

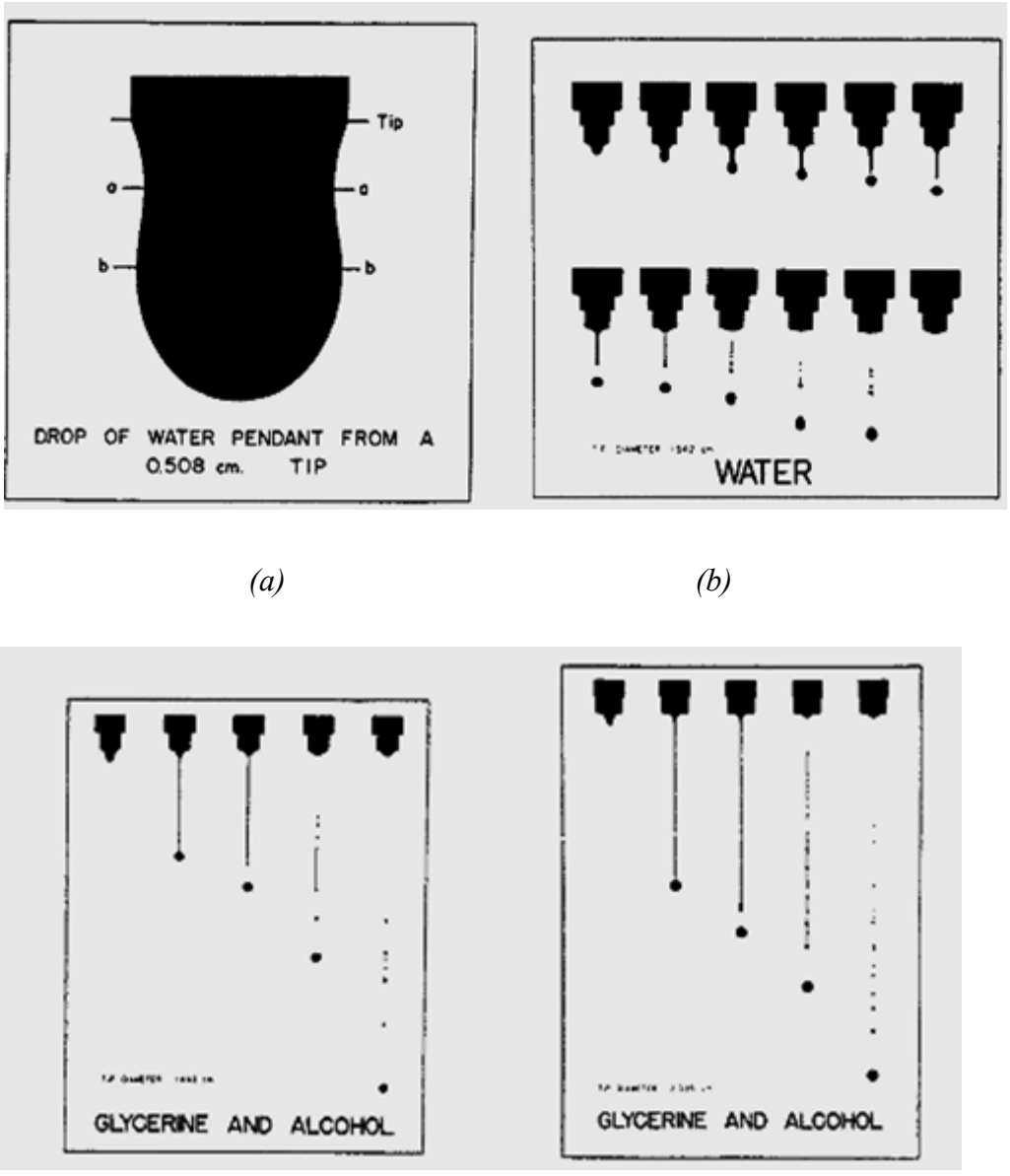

Figure 2-5: Drop of water (*a* and *b*) and drop of glycerol-alcohol mixture (*c* and *d*). (Edgerton, Hauser et al. 1937).

High speed digital photography and cinematography enables insight at the point of breakup and open up new horizons. Use of photographic method was introduced by Rayleigh (1891). However, his observations were qualitative in nature. There have been many quantitative experimental studies on liquid jet such as (Haenlein 1931,

Baird and Davidson 1962, Donnelly and Glaberson 1966, Goedde and Yuen 1970). Baird and Davidson (1962) analysed annular jet qualitatively and quantitatively and concluded that the jet behaviour primarily depends on weber number of the jet. Where Weber number is defined as (Equation 2.4)

$$We = {\rho U^2 a}/{\sigma} = \frac{Inertial\ force}{Surface\ tension\ force} \tag{2.4}$$

Where ρ is the density of the fluid, U is a jet exit velocity, a is the size of the orifice and σ is the surface tension. As shown in Figure 2-6, when Weber number is more than 1, long jets were obtained as shown in Figure 2-6 (*a*), (*b*) and round form of the jet were observed when it is less than 1 as shown in Figure 2-6 (*c*) and (*d*).

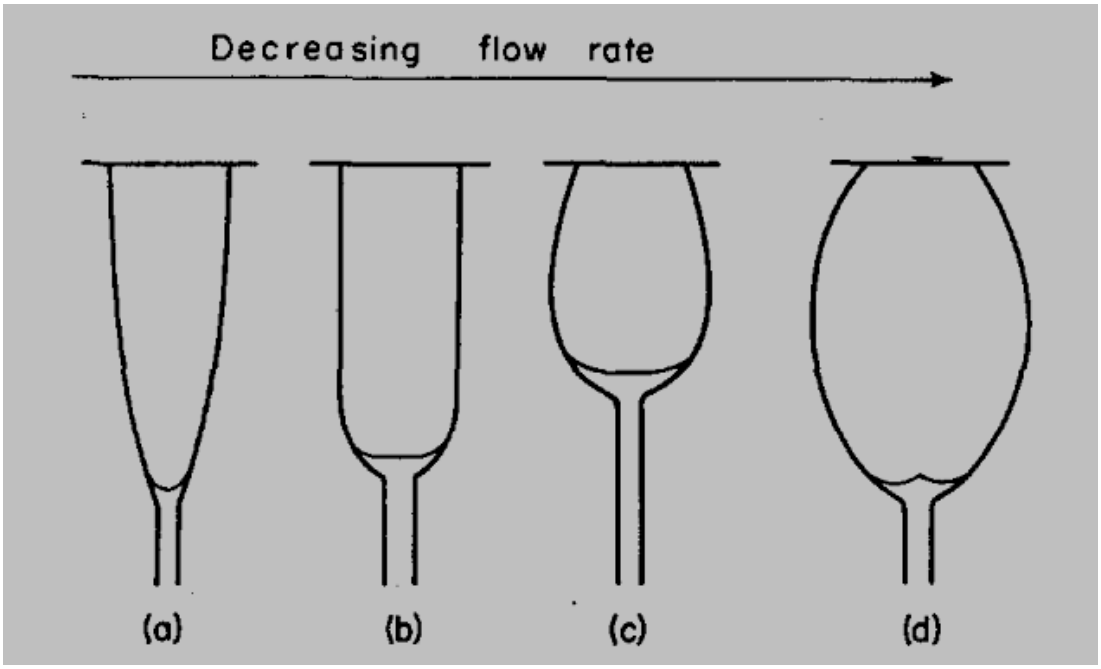

Figure 2-6: Effect of flow rate and hence weber number on annular jet profile (Baird and Davidson 1962).

Further photographic observations of the liquid jet instability was published by Donnelly and Glaberson (1966). A water jet was examined by imposing audio frequency disturbance. Stroboscopic flash pictures were taken which enabled a direct determination of the growth of disturbances. In addition to that, effect of viscosity on the stability were examined which could then be compared to the calculation of Chandrasekhar (1961).

Goedde and Yuen (1970) investigated capillary instability of jets, with different viscosities and under imposing audio frequency disturbances. Complex behaviour of satellite drop formation was observed and considered the non-linear effects of jet instability in detail. These results were contrasting to the satellite droplet formation at downstream of the thread, which was confirmed by Pimbley and Lee (1977). Pimbley and Lee (1977) further added the possibilities of thread breakup downstream, upstream or simultaneously from both ends. They were able to control the formation of satellite droplets by increasing the amplitude of the initial disturbance.

There have also been many studies that focus on finding methods to reduce the formation of satellites. The reduction/ elimination of satellite droplets was a significant challenge in 1970s for inkjet printers. Inkjet printers work by first charging a drop and then using an electric field to deflect the drop towards the desired position. A bimodal drop size distribution is a problem, as drops of different sizes are deflected differently in the electric field, leading to a reduction in quality. Chaudhary and Maxworthy (1980a) and Chaudhary and Maxworthy (1980b) performed extensive experimental investigations into satellite formation. The work of Chaudhary and Maxworthy (1980b) agrees qualitatively with that of Pimbley and Lee (1977), that there is a transition from rear merging to forward merging as the driving amplitude is increased, and that the critical amplitude that corresponds to the no-merge condition increases with wavenumber. The Weber number has also been shown to have a significant effect (Vassallo and Ashgriz 1991). With this, rear merging, no merging and forward merging satellites are shown in Figure 2-7. Moreover, Vassallo and Ashgriz (1991) observed different breakup regimes shown in Figure 2-7

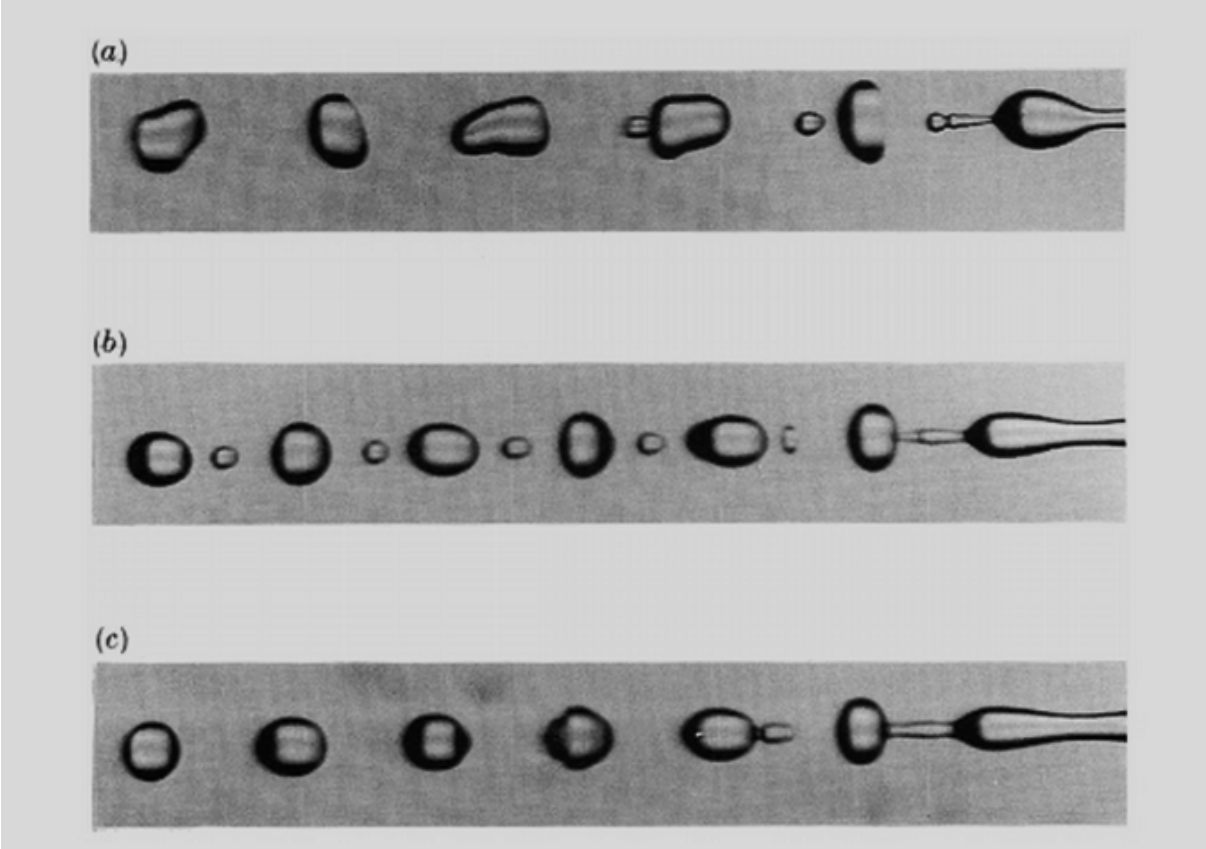

Figure 2-7: Experimental observations of Vassallo and Ashgriz (1991) for rear merging (*a*), no merging (*b*) and forward merging (*c*) satellite droplets respectively.

More subsequent studies (Peregrine, Shoker et al. 1990, Vassallo and Ashgriz 1991, Shi, Brenner et al. 1994, Zhang and Basaran 1995, Kowalewski 1996, Clanet and Lasheras 1999) on the necking and satellite drop formation at the time of jet breakup under both jetting and low velocity dripping. Peregrine, Shoker et al. (1990) work contained high resolution pictures of water falling from the nozzle. The author concluded that the last stage of the jet breakup is dominated by the properties of pinch singularity. This work was extended by Shi, Brenner et al. (1994) for high viscosity conditions. Kowalewski (1996) was detected satellite droplet formation as shown in Figure 2-8, during experimentation. Further, neck radius and neck length can be predicted with the help of picture taken by Zhang and Basaran (1995) and Brenner, Eggers et al. (1997).

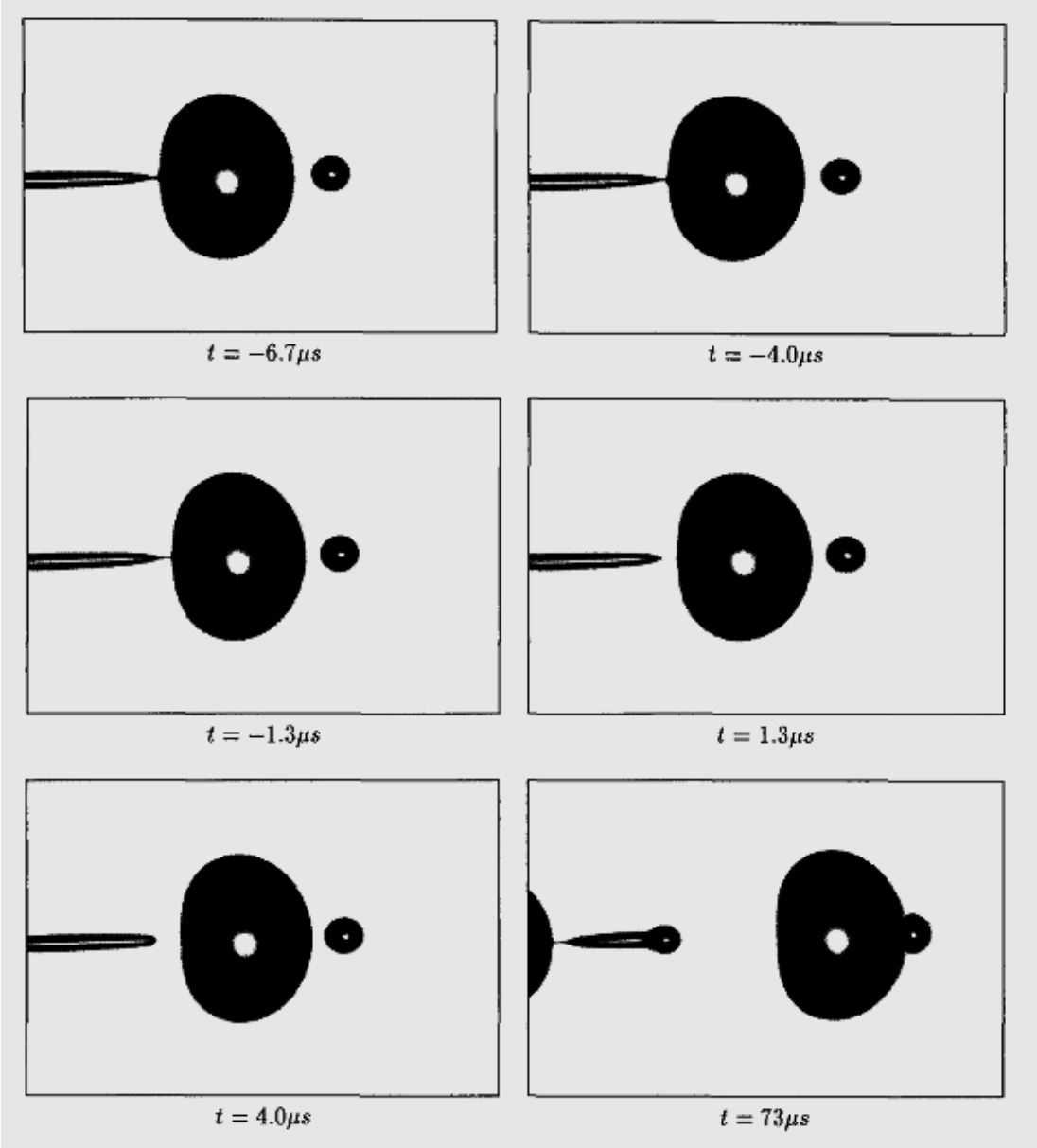

Figure 2-8: Separation of the droplet from liquid jet of Radius =98.5 μm (Kowalewski 1996).

Dynamic of drop formation on the nozzle tip of a vertical tube into ambient air was studied by Zhang and Basaran (1995). In the first stage, the drop profile changes from spherical to pear-shape right after previous drop detached. Throat of the peer shape takes the appearance of liquid thread as time progresses. This liquid thread connects to the bottom portion of the drop which is about to detach with rest of the liquid remaining on the nozzle tip. Effects of physical and geometric parameters on the drop formation process composed development, extension and breakup of liquid thread and the satellite droplet formation. Finite inertial, capillary, viscous and

gravitational forces were found responsible for different drop formation dynamics and satellite drop formation.

Linear stability analysis and Rayleigh's work is useful tool for the prediction of continuous length of the jet, it also permits a description of the initial growth of instabilities as they initiate near the nozzle. Non-linear effects close to break up point is more important and therefore, linear stability analysis fails to describe the details of the drop breakup which lead to formation of satellite drops. Theoretical research still focuses on extending Rayleigh's classical work with the help of mathematics even after hundred years. On the other hand, experimental work explored the dynamics of free surfaces which is beyond the validity of linear theory. Bogy (1979) reviewed all significant earlier work on drop formation. An extensive and detailed review on the work done on liquid jets is given by Eggers and Villermaux (2008).

Recent experimental studies of jet break up and drop formation fall into three different categories; (1) dripping (where liquid velocity is very low that jet cannot form and hence drop forms on the nozzle tip) (2) jetting where liquid jet emerge from the nozzle and breakup into droplets into droplet (3) Liquid bridge. Most of the early work focused on different stages of drop formation, size and number of the resulting drops. Further advancement of the technology brings computers and simulation softwares to predict and validate experimental results of the drop formation process. Moreover, immiscible liquid-liquid gained more importance during the first decade of the 21st century due to its applications in various disciplines.

2.2 Immiscible liquid jets

The formation of a liquid jet injected into other immiscible liquid and the breakup of the jet into droplets is fundamentally important in the industrial processes, such as emulsification, solvent extraction. The breakup of the jet increases the interfacial area, hence enhancing heat and mass transfer, and most importantly; chemical reactions. The jet formation, breakup and droplet formation has therefore been studied extensively (Taylor 1934, Tomotika 1935, Tomotika 1936, Meister and Scheele 1969a, Meister and Scheele 1969b, Kitamura, Mishima et al. 1982, Bright

1985, Das 1997, Lister and Stone 1998) in order to predict the length of the jet and the volume of the droplets.

In addition, several group of researchers studies immiscible fluids, which includes; Lister and Stone (1998), Cohen, Brenner et al. (1999), Zhang and Lister (1999), Longmire, Norman et al. (2001), Webster and Longmire (2001), Webster and Longmire (2001), Milosevic and Longmire (2002) . Hence the breakup of a liquid jet into droplets in immiscible liquids system is still an attractive phenomenon in science and engineering.

2.2.1 Droplet volume prediction and jetting regimes

While Rayleigh classic work focused on liquid jet in air, Tomotika (1935) first discussed the instability of a long cylindrical column of an incompressible viscous liquid surrounded by another viscous fluid. He employed experimental results from Taylor (1934) and expanded Rayleigh work of linear stability analysis to both phases. Tomotika (1935) developed a relationship between the growth rate of symmetrical disturbances and the dimensionless wave number ka for a general immiscible liquid-liquid system through linear analysis. In its most general form, the relation between q and ka is a fourth order determinantal equation,

$$\begin{vmatrix} I_1(ka) & I_1(k_1a) & R_1(ka) & R_1(k_1'a) \\ ka\, I_0(ka) & k_1a\, I_0(k_1a) & -kaR_0(ka) & -k_1'aR_0(k'_1a) \\ \frac{2\mu}{\mu'}k^2 I_1(ka) & \frac{\mu}{\mu'}(k^2+k_1^2)I_1(k_1a) & 2k^2R_1(ka) & \left(k^2+k_1'^2\right)R_1(k_1'a) \\ G_1 & G_2 & G_3 & G_4 \end{vmatrix} = 0 \quad (2.5)$$

Where,

$I_1'(x) = \frac{d}{dx}I_1(x)$

$k_1'^2 = k^2 + \frac{iq}{v'}$

$$k_1^2 = k^2 + \frac{iq}{v}$$

$$G_1 = 2i\ \frac{\mu}{\mu'} k^2 I_1(ka) - \frac{q\rho}{\mu'} I_0\ (ka) + \ \sigma \frac{(k^2a^2-1)kI_1(ka)}{a^2 q\mu'}$$

$$G_2 = 2i\ \frac{\mu}{\mu'} k k_1 I_1'(k_1 a) + \sigma \frac{(k^2a^2-1)kI_1(ka)}{a^2 q\mu'}$$

$$G_3 = 2ik^2 R_1'(ka) + \frac{q\rho'}{\mu'} R_0(ka)$$

$$G_4 = 2ikk_1' R_1'(k_1 a)$$

From (Equation 2.5) it is possible to deduce all the classical limiting cases, e.g. for a low viscosity liquid jet in a gas, jet and atmosphere viscosity and atmosphere density are neglected, thus reducing (Equation 2.5) to

$$q^2 = \sigma(1 - k^2a^2)ka \Big/ \frac{\rho a^3 I_0(ka)}{I_1(ka)} \tag{2.6}$$

which is the same equation as Rayleigh derived. Also, if the viscosity of the jet cannot be ignored, (Equation 2.6) reduces to,

$$q^2 + 3\frac{\mu k^2 q}{\rho} = \sigma \frac{(1-k^2a^2)k^2a^2}{2\rho a^3} \tag{2.7}$$

which is identical with the equation derived by Weber (1931).

Tomotika (1935) discussed two limiting cases where $\mu/\mu' \to \infty$ and where $\mu/\mu' \to 0$. In both case the inertia of both phases was neglected. it was found that the greatest value for q occurred when $ka\ (i.e.\ \gamma) = 0$, corresponding to varicose wavelengths which are very large compared with the jet diameter. For the general case where μ/μ' is finite (but inertial terms can still be neglected) Tomotika (1935) determined that the value of ka corresponding to maximum instability is 0.59 when $\mu/\mu' = 0.28$ and the corresponding wavelength is $5.33d$. Thus Tomotika's analysis would apply for the low speed injection of one liquid into another, where the liquid viscosity ratio assumes a finite value. Finally, he derived a general low velocity equation relating the growth rate of a disturbance to liquid properties, jet diameter, and wavelength of the disturbance by writing the equations of motions for an incompressible Newtonian fluid for both

phases and relating the two boundary conditions at the interface. It is noteworthy that the Rayleigh's classic work only focused on the growth of instabilities leading to break up of liquid jets in air. Tomotika extended that analysis to liquid jets in viscous fluid.

Several higher order analysis have been done to expand the work of Rayleigh (Rayleigh 1878, Rayleigh 1891) and Tomotika (Tomotika 1935, Tomotika 1936). For instance, Lafrance (1975) extended the model by including up to 3rd order. He made two conclusions: (i) nonlinear terms are responsible for the appearance of satellite droplets and (ii) inclusion of higher order term have less or no effect on overall jet length and primary droplet diameters. Further studies were accomplished by Geer and Strikwerda (1983) proposed a numerical solution of nonlinear 2-dimensional equation in the cross-sectional plane of the jet results in shape of the interface of a jet. Furthermore, Keller (1983) produced better agreement on velocity and radius variation of the falling jet with the experiments done by Rayleigh (1878).

Ranz and Dreier Jr (1964) carried out further investigation on instabilities in immiscible liquid systems. Ranz and Dreier Jr (1964) analysed the initial instability at a plane interface between two viscous fluids in relative motion, though the theory is claimed to be applicable to cylindrical jets of sufficiently large diameter. The correlation developed for the wave length of the fastest growing disturbance is based on three factors e.g. viscosity ratio, density ratio and a dimensionless viscosity number. The correlation is limited to high interfacial relative velocities where the disturbance wavelength is small compared with the jet diameter. Debye and Daen (1959) investigated the case of an inviscid jet in another inviscid liquid. At zero velocity, the jet was stable to asymmetrical disturbances became unstable when the jet velocity exceeds a critical value. This critical velocity was found to increase with increasing interfacial tension.

Drop formation in immiscible liquid-liquid system was experimentally studied by Hayworth and Treybal (1950) as a further extension of Harkins and Brown (1919). These workers studied drop formation as a function physical property such as nozzle diameter, velocity of dispersed phase through nozzle, interfacial tension, and viscosity of dispersed and continuous phase and density of both phases. Uniform

drop size was observed for velocity below 10 cm/sec. However, non-uniformity on drop size was observed for velocity between 10-30 cm/sec and at higher velocities. An empirical equation (2.8) and graphical solution was drawn to predict all drop size for velocities below 10 cm/sec and velocities between 10-30 cm/sec with 7.5% error. As mentioned above, they also presented a diagram from which the drop diameter could be obtained without long iteration. Tested with several liquid-liquid pairs, this correlation was found to apply up to 30 cm/sec of velocity.

$$V_F + 4.11(10^{-4})2V_F^{2/3}\left(\frac{\rho d_d v^2}{\Delta\rho}\right) = 21(10^{-4})\left(\frac{\rho d_0}{\Delta\rho}\right) + 1.069(10^{-2})\left(\frac{d_0^{0.747} v^{0.385} \mu_c^{0.188}}{\Delta\rho}\right)^{3/2} \quad (2.8)$$

Null and Johnson (1958) performed experiments with three different immiscible liquid-liquid systems and developed correlation(2.9) which describe drop formation and predict drop volume for flow rate range between $0 \leq \sqrt{d_0 v_N^2 \rho_D / g_c \rho} \leq 1.4$. Surface tension phenomena, which is the driving force for jet breakup, was explained by Rowlinson (2002) in term of cohesive force between fluid particles.

$$V = \frac{\pi}{6} d_0^3 \left(\frac{d_d}{d_0}\right)^3 \quad (2.9)$$

In a series of publications, Meister and Scheele (Meister and Scheele 1967, Scheele and Meister 1968a, Scheele and Meister 1968b, Meister and Scheele 1969a, Meister and Scheele 1969b) experimented 15 different liquid-liquid systems to develop an understating of the jet and drop formation. They described the general behaviour of the jet in case of low, critical and higher flow rates. For low flow rates; drop nucleates, grow and break off from the nozzle at regular intervals. For the cases where jet formed and elongated to a certain length from the nozzle; droplet breakup occurs. In the final behaviour, jet velocity is very high and jet disrupt into small droplets.

Meister and Scheele (1967) derived six correlations from (2.5) which are applicable to predict the growth rate and wave length of most unstable wave. In their following work, Scheele and Meister (1968a) developed a correlation to predict drop volume for immiscible liquid-liquid system at low velocities. Equation (2.10) is developed

for computations of drop volume by balancing four different forces and flow into drop during necking taking into account.

$$V_F = \frac{\pi\sigma d_0}{g\Delta\rho} + \frac{20\mu Q d_0}{D_F^2 g\Delta\rho} - \frac{4\rho' Q U_N}{3g\Delta\rho} + 4.5\left(\frac{Q^2 d_0^2 \rho'\sigma}{(g\Delta\rho)^2}\right) \quad (2.10)$$

Experimental results from 15 different systems were compared by these workers and in addition, these results were compared with (Harkins and Brown 1919, Hayworth and Treybal 1950) and (Null and Johnson 1958). It has been shown that the prediction of drop volume from the correlation is with good agreement with experiments.

Further, Scheele and Meister (1968b) derived set of equation for the prediction of jet velocity of dispersed jet in another immiscible liquid. There are two mechanisms considered and equations for both the mechanisms were developed. Experimental data from 15 different systems were compared with developed equations. First mechanism equation showing better agreement with experimental data which was developed based on the kinetic force of the liquid at the nozzles exit.

If the jet has a length less than twice the wavelength of the most unstable wave, drop formation is not always controlled by the instability mechanism but at times by a force balance mechanism similar to that which controls the formation of drops at velocities below that of initial jet formation. Meister and Scheele (1969a) improved their correlation (Scheele and Meister 1968a), based on instability mechanism, for predicting drop volume for higher velocity where jet length is higher than one wave length.

$$V_F = \frac{2\pi^2 (a^3) \lambda/2}{N(ka)_{max} \left(U_I / U_A\right)_{\lambda/2}} \quad (2.11)$$

$$V_F = F\left(\frac{2\pi\sigma d_0}{g\Delta\rho} - \frac{4\rho' Q U_N}{3\left(\frac{a}{a_n}\right)^2 g\Delta\rho} + \frac{40\mu Q\alpha}{D_F^2 g\Delta\rho} + 7.15\left(\frac{Q^2\alpha^2\rho'\sigma}{(g\Delta\rho)^2}\right)^{1/3}\right) \quad (2.12)$$

Equation (2.12) should be used when the jet is less than one wavelength long. If the jet (2.11) should be used when the jet is greater than two wavelengths long, and if

the jet is between one and two wavelengths long, the mechanisms will alternate to produce an equal number of each size drop.

Meister and Scheele (1969b) have developed stability curves for liquid jet into another liquid (Refer to Figure 1(Meister and Scheele 1969b)). There is a critical velocity (maximum) at which a sudden increase in jet length occurs. They developed a predictive equation for this critical velocity, which was claimed to show satisfactory agreement with experimental data. They also modified and extended Tomotika's theory to include relative phase motion. It is proposed that growth rates calculated from this theory can be used to predict jet breakup lengths beyond the critical point for sharp increase in jet length, i.e. in the vicinity of the jet breakup curve maximum. It is of interest to note that the jets used in the experimental work of this investigation were laminar and possessed a fully developed parabolic velocity profile at the nozzle exit. Therefore, the E of these jets would possess the maximum value of two. The effect of velocity profile relaxation(Scheele and Meister 1968b) on jet stability was not considered and further experimental work would be necessary to determine the significance of this effect in immiscible liquid systems.

Chazal and Ryan (1971) also analysed the drop formation process of organic compound in water. This analysis involves solution of equations with proper boundary conditions. These workers came up with the equation (2.13) to calculate drop volume and results were compared with (Scheele and Meister 1968a) and average error of 6.3% was found between the results. This equation is valid only when single drops are formed at higher flow rates. This equation is not valid for group of droplets. The upper limit of applicability is given by (2.14).

$$V_d = \frac{2\pi R_N \sigma}{g\Delta\rho}\left[\psi + 1.648\frac{g\Delta\rho R_N U_N V_D^{1/3}}{\sigma U_t} - 0.875\frac{\rho_D R_N U_N^2}{\sigma}(1+\beta)\right] \tag{2.13}$$

R_N *can be calculated from* $\rho_D \dfrac{(U^2)_{Ave}}{U_{Ave}}$

$$= \frac{4\rho d_d Q^2}{3\pi R_N^2}\left[1 + 2C_2\sqrt{\frac{\Delta\rho g R_N^2}{\sigma}} + \frac{C_2^2 \Delta\rho g R_N^2}{\sigma}\right]$$

$$U_N = \frac{0.82\Delta\rho}{\rho_D}(gR_N)^{1/2}\left(\frac{\sigma}{g\Delta\rho R_N^2}\right)^{0.95} \quad (2.14)$$

Perrut and Loutaty (1972) employed photographic technique to measure mean droplet size in spray column.15 different pairs of liquid-liquid systems, chosen in order to obtain large range of physical properties, were used. These workers manage to conclude that the ratio of $d/\emptyset$ decreased linearly from 2.07 to 1.44 whilst the Eőtvős number (Bond number) ($E_0 = B_0 = \frac{\Delta\rho\ g\ LL^2}{\sigma}$) varies from 0 to 1.70 and there was no mass transfer between two phases.

Kitamura, Mishima et al. (1982) carried out experiments by varying the motion of continuous phase. Shortened jet was observed when the absolute value of the continuous phase velocity relative to the jet increased from zero. These co-workers measured jet length and drop size. These results found to have the best agreement with Tomotika's stationary jet solution which is further translated at the average velocity of the jet. Further, Kitamura, Mishima et al. (1982) employed analysis form Tyler (1933) and Tomotika (1935) for drop size and wavelength calculation respectively. They found best agreement when the relative velocity of the phases was zero. However, 40% largest error was found when (2.15) applied to immiscible liquid-liquid system. This error was mainly due the hydrodynamics resistance of surrounding liquid on the jet stability.

$$d_d = (1.5\ \pi\ D^3/x^*)^{1/3} \quad (2.15)$$

Walters and Marschall (1988) performed experiments on immiscible liquid-liquid systems. They explained reasons for inconsistency in calculation of drop volume from past literatures. Their results commented on the past result that the variation of drop volume with flow rate is maxima and minima rather than a smooth curve.

Teng, Kinoshita et al. (1995) performed instability analysis and developed an simplified equation to predict the size of the droplet formed by the breakup of the cylindrical liquid jets:

$$\frac{d_d}{d_0} = \left(\frac{3\pi}{\sqrt{2}}\right)^{\frac{1}{3}}(1 + Z^*)^{\frac{1}{2}} \quad (2.16)$$

Where $Z^* = (3\mu + \mu')/(d_0\sigma\rho)^{1/2}$ is Ohnesorge number and μ,μ', $d_{0,}\sigma, \rho$ is viscosity of continuous phase, viscosity of dispersed phase, orifice diameter, interfacial tension and density of dispersed phase respectively.

From the equation, the primary drop sizes were dependant on Ohnesorge number. As viscosity increases, viscous forces act to damp out surface perturbations on the jet and retard wave growth. This allows the jet to remain intact for longer, increasing break-up length and eventually breaking up into droplets that are smaller in size.

This droplet-size equation applies to wide range of parameters and conditions like low-velocity, liquid-in-liquid and liquid-in-gas jets involving Newtonian or non-Newtonian fluids that follow power-law shear stress versus deformation rate relationships. Moreover, Teng, Kinoshita et al. (1995) tested this equation by comparing the resultant theoretical predictions for droplet size with experimental data for seventeen Newtonian liquid systems and five power-law non-Newtonian/Newtonian liquid systems (power-law liquid jet in Newtonian liquid and Newtonian liquid jet in power-law liquid), as well as with the full numerical solutions of Tomotika's equation. Good agreement is observed. The present analysis demonstrates clearly the dependence of droplet size on a modified Ohnesorge number.

All the corelations for the drop volume predition have been mentioned in this section is summarized in Table 2-1.

Table 2-1: Summary of drop volume prediction correlations.

No.	Equations	Reference	Comments
1	$V_F + 4.11(10^{-4})2V_F^{2/3}\left(\frac{\rho d_d v^2}{\Delta\rho}\right) = 21(10^{-4})\left(\frac{\rho d_0}{\Delta\rho}\right) + 1.069(10^{-2})\left(\frac{d_0^{0.747} v^{0.385} \mu_c^{0.188}}{\Delta\rho}\right)^{3/2}$	(Hayworth and Treybal 1950)	Uniform drop size was observed for velocity below 10 cm/sec. However, non-uniformity on drop size was observed for velocity between 10-30 cm/sec and at higher velocities. An empirical equation (2.7) and graphical solution was drawn to predict all drop size for velocities below 10 cm/sec and velocities between 10-30 cm/sec with 7.5% error.
2	$V = \frac{\pi}{6} d_0^3 \left(\frac{d_d}{d_0}\right)^3$	(Null and Johnson 1958)	performed experiments with three different immiscible liquid-liquid systems and developed correlation which describe drop formation and predict drop volume for flow rate range between $0 \leq \sqrt{d_0 v_N^2 \rho_D / g_c \rho} \leq 1.4$.

3	$V_F = \frac{\pi\sigma d_0}{g\Delta\rho} + \frac{20\mu Q d_0}{D_F^2 g\Delta\rho} - \frac{4\rho' Q U_N}{3g\Delta\rho} + 4.5(\frac{Q^2 d_0^2 \rho'\sigma}{(g\Delta\rho)^2})$	(Scheele and Meister 1968a)	(2.9) is developed for computations of drop volume by balancing four different forces and flow into drop during necking taking into account.
4	$V_F = F\left(\frac{2\pi\sigma d_0}{g\Delta\rho} - \frac{4\rho' Q U_N}{3\left(\frac{a}{a_n}\right)^2 g\Delta\rho} + \frac{40\mu Q\alpha}{D_F^2 g\Delta\rho} + 7.15\left(\frac{Q^2\alpha^2\rho'\sigma}{(g\Delta\rho)^2}\right)^{1/3}\right)$	(Meister and Scheele 1969a)	(2.11) should be used when the jet is less than one wavelength long. If the jet (2.10) should be used when the jet is greater than two wavelengths long, and if the jet is between one and two wavelengths long, the mechanisms will alternate to produce an equal number of each size drop.
5	$V_d = \frac{2\pi R_N\sigma}{g\Delta\rho}\left[\psi + 1.648\frac{g\Delta\rho R_N U_N V_D^{1/3}}{\sigma U_t} - 0.875\frac{\rho_D R_N U_N^2}{\sigma}(1+\beta)\right]$	(Chazal and Ryan 1971)	This analysis involve solution of Navier stoke equations with proper boundary conditions. These workers came up with the equation (2.12) to calculate drop volume and results were compared with (Scheele and Meister 1968a) and average error of 6.3% was found between the results. This equation is valid only

			when single drops are formed at higher flow rates. This equation is not valid for group of droplets. The upper limit of applicability is given by (2.13).
6	Photographic technique	(Perrut and Loutaty 1972)	A photographic technique was used to measure drop size. Illumination from the backside of the column via electronic provide contrast between continuous and dispersed phase and made possible to measure a great number of drops and to obtain their size distribution. Photographs also showed that drops were quite spherical but in order to prevent any distortion error only the vertical diameter was considered
7	$d_d = (1.5\,\pi\,D^3/x^*)^{1/3}$	(Kitamura, Mishima et al. 1982)	Effects of hydrodynamics resistance of surrounding liquid on the jet stability have significant effect on the error for the immiscible liquid-liquid system.

8	$\frac{d_d}{d_0} = \left(\frac{3\pi}{\sqrt{2}}\right)^{\frac{1}{3}} (1 + Z^*)^{\frac{1}{2}}$	(Teng, Kinoshita et al. 1995)	The present analysis demonstrates clearly the dependence of droplet size on a modified Ohnesorge number.

2.2.2 Jet interactions in stationary liquid jets

For a liquid jet (dispersed phase) moving within another liquid (continuous phase), the disturbance on the liquid/liquid surface can be described by following form;

$$\delta(t, y) = \delta_i e^{nt+iky} \tag{2.17}$$

Where δ and δ_i are the dynamic and initial magnitude of the disturbances, respectively; n is the growth rate of disturbance; and k is the wave number which is related to the wavelength, λ, by;

$$k = (2\,\pi)/\Lambda \tag{2.18}$$

The infinitesimal disturbances can either grow or decay depending on the system properties, including viscosities and densities of both liquids, interfacial tension, and jet radius, a. If there is a maximum value of n, then the corresponding disturbance would grow fastest and dominate jet breakup. This maximum value of n, which is denoted as n^*, can be found by linear instability analysis. Consequently, the resultant droplet size can be calculated from the corresponding wave number.

The linear analysis includes 3 steps: (i) determining the fluid motions causing the interfacial disturbances in both phases; (ii) matching the motions at the interface (stresses and velocities in both normal and tangent directions) to find the characteristic equation; and (iii) solving the characteristic equation to find n^* (Phan and Evans 2008).

More recently, the interaction between interfacial waves of neighboring jets has been experimentally observed (Elemans, Van Wunnik et al. 1997) to follow either on-phase or out-of-phase effects (Figure 2-9). Subsequently, a qualitative analysis (Knops, Slot et al. 2001) was carried out to describe dissipation between two interfacial disturbances and consequently predict the critical distance between jets.

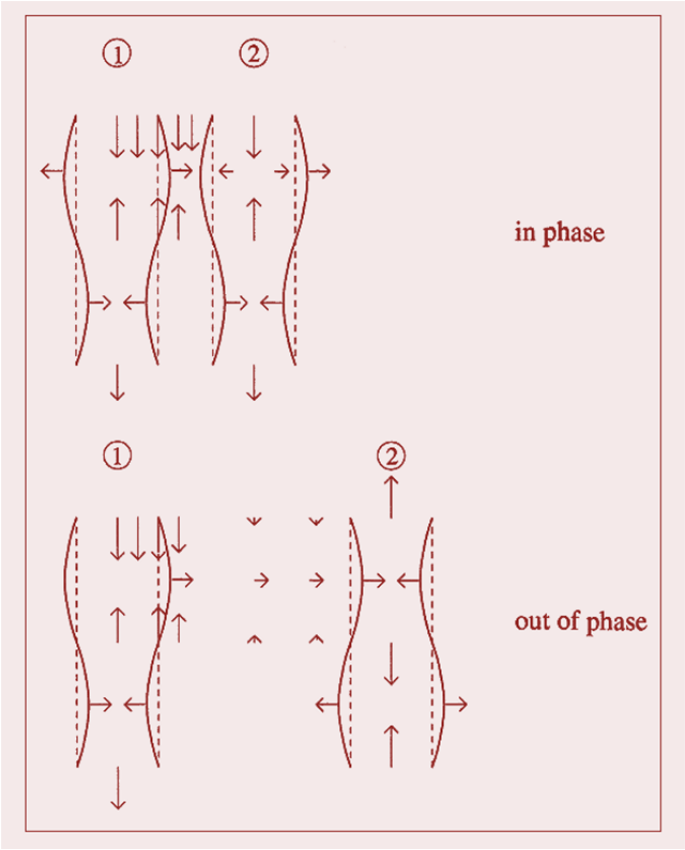

Figure 2-9: In-phase and out-of-phase deformation observed by Knops, Slot et al. (2001).

For engineering processes, the stationary jets are almost impractical. Instead, most industrial processes, such as micro reactors, employ moving jets (Hessel, Löwe et al. 2005). In these cases, jet moving velocity is much higher than rotational and axial component of the jet velocity created by interfacial disturbance ($v_{jet} >> v_r, v_z$). Therefore, the approximation approach is no longer applicable. Most likely moving jets are broken up in the out-of-phase arrangement (Pennemann, Hardt et al. 2005). It should be noted that the CFD simulation (Pennemann, Hardt et al. 2005) was done for a single jet only and then mirroring for multiple jets. As the results, the jets are inherently in-phase and the jet-jet interaction was not included.

On the other hand, one more important phenomenon, interaction between two jets and its breakup, was studied by various researchers (Elemans, Van Wunnik et al. 1997, Knops, Slot et al. 2001, Gunawan, Molenaar et al. 2002, Gunawan, Molenaar et al. 2004). Elemans, Van Wunnik et al. (1997) performed experimental study on polymeric blend in another molten polymer described interactions between two

adjacent jets. The sinusoidal distortions at the surfaces of two adjacent jets develop out of phase phenomena. The development of these out of phase modes is delayed due to the fact that the distortions of the threads have to fit into one another. Once this fit has been reached, the distortions develop just as fast as in the case of a single thread. Figure 2-10 shown out of phenomena up to 510 seconds.

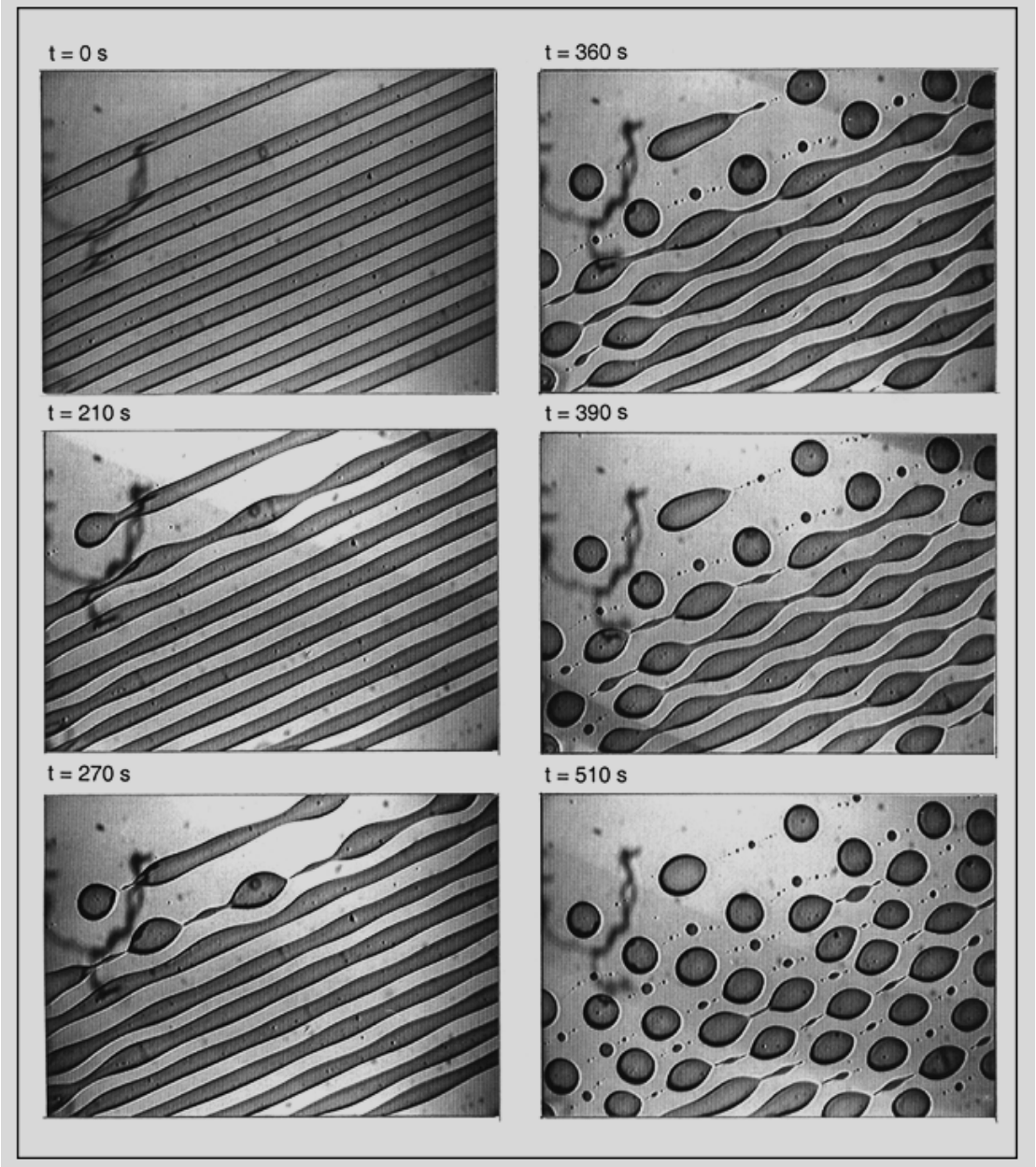

Figure 2-10: Out of phase deformation observed by Elemans, Van Wunnik et al. (1997). The jet diameter is 70 micron and measurement was performed at 230 °C.

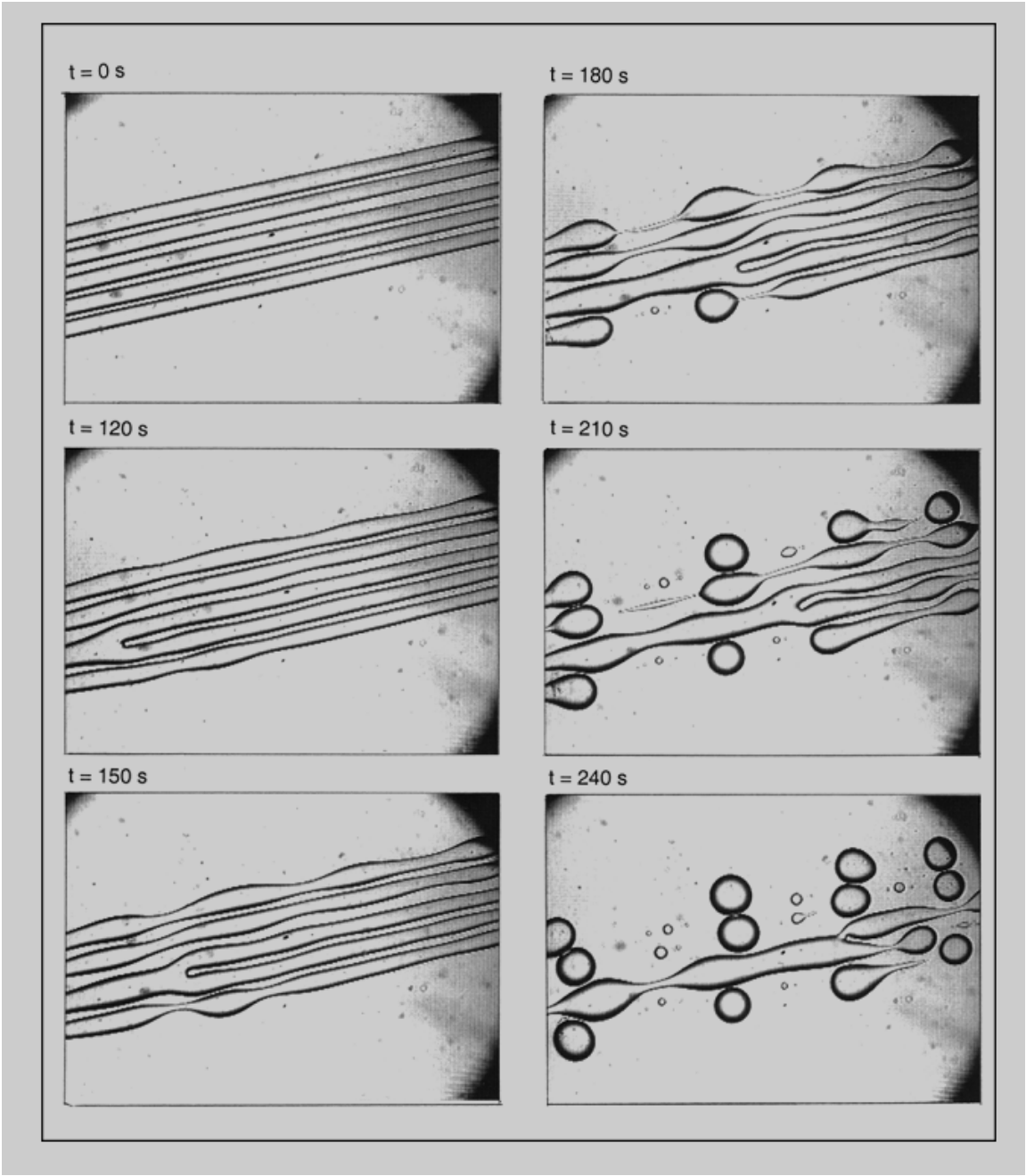

Figure 2-11: In-phase deformation observed by Knops, Slot et al. (2001).The jet diameter is 70 micron and measurement was performed at 230 °C.

In experimental observation, Knops, Slot et al. (2001) observed that neighbouring threads may break up in-phase or out-of-phase. Figure 2-11 shows both phenomena observed in the series of experiments. They employed principle of minimal dissipation of energy to approach the problem and found that the dissipation term due to the interaction of the thread depends on the relative distance $\hat{b} = b/a$

between the threads. Critical distance between two jets were calculated as $\hat{b} = 3.4$ where viscosity ratio between two immiscible liquid was taken as 0.91. There are two cases were concluded:

- $\hat{b} < 3.4$ Dissipation is minimal for $\alpha=\pi$ and jet will breakup out-of-phase mode.
- $\hat{b} > 3.4$ Dissipation is minimal for $\alpha=0$ and jet will breakup in-phase mode.

Viscosity ratio between both phase (dispersed and continuous) and distance between two jets are the defining factors whether jet breakup in-phase mode or out-of-phase mode. Further,Gunawan, Molenaar et al. (2002) extended the work by solving Navier Stoke equation with the help of Fourier series. Their conclusion agree with the experimental findings of Knops, Slot et al. (2001). However, they seem to disagree with the principle of dissipation of energy and the value of critical distance between two jets.

2.2.3 Emulsion formation and stability

An emulsion is a mixture of two immiscible liquids where one liquid is dispersed in the form of small drops in another liquid that forms a continuous phase (Becher 1965, Leal-Calderon, Schmitt et al. 2007). Emulsions are important for a variety of applications such as macromolecular delivery (Okochi and Nakano 2000, Vasiljevic, Parojcic et al. 2006, Degim and Çelebi 2007), enhanced oil recovery (Taylor and Hawkins 1992, Huang and Varadaraj 1996), food processing (Muschiolik 2007), hazardous material handling (Ouyang, Mansell et al. 1995), mining explosives (Oxley 1998), and cosmetics (Schramm 2005). The presence of a surfactant is one of the factors for the long-term stability of emulsions: the surfactant molecules migrate to the liquid-liquid interface, inhibit droplet coalescence (Becher 1965) and can be used in the wide variety of applications. Conventionally, emulsions are produced by mixers, in which droplets are formed by shear force.

Shear mixing technique was used by Mason and Bibette (1997) to produce emulsions. Their experiments have roughly identified three broad classes of rupturing scenarios when the shear is initiated very gradually.

- Tip Streaming: Droplet elongates and rotates under the shear, developing pointed ends that eject tiny droplets of the dispersed phase.
- Droplet rupture into two: the droplet is ruptured into two droplets of almost equal volume (sometimes accompanied by much smaller "satellite" droplets created during the neck down).
- Liquid thread: the droplet is stretched into an extremely elongated "liquid thread" that undergoes a capillary (Rayleigh) instability and breaks into a chain of many droplets.

They discovered that the effective viscosity of the emulsion is responsible for droplet size when fracturing is eliminated and leads to a high degree of monodispersity. Micro reactor technology gained more importance in the field of chemical engineering and biotechnology during 20^{th} and 21^{st} century for achieving large interface to volume ration to enhance reaction rate. Haverkamp, Ehrfeld et al. (1999) performed experimental study on micro mixer for the production of oil in water emulsions. They noted that the droplet size found to decrease with flow-rate range employed the study as shown in Figure 2-12.

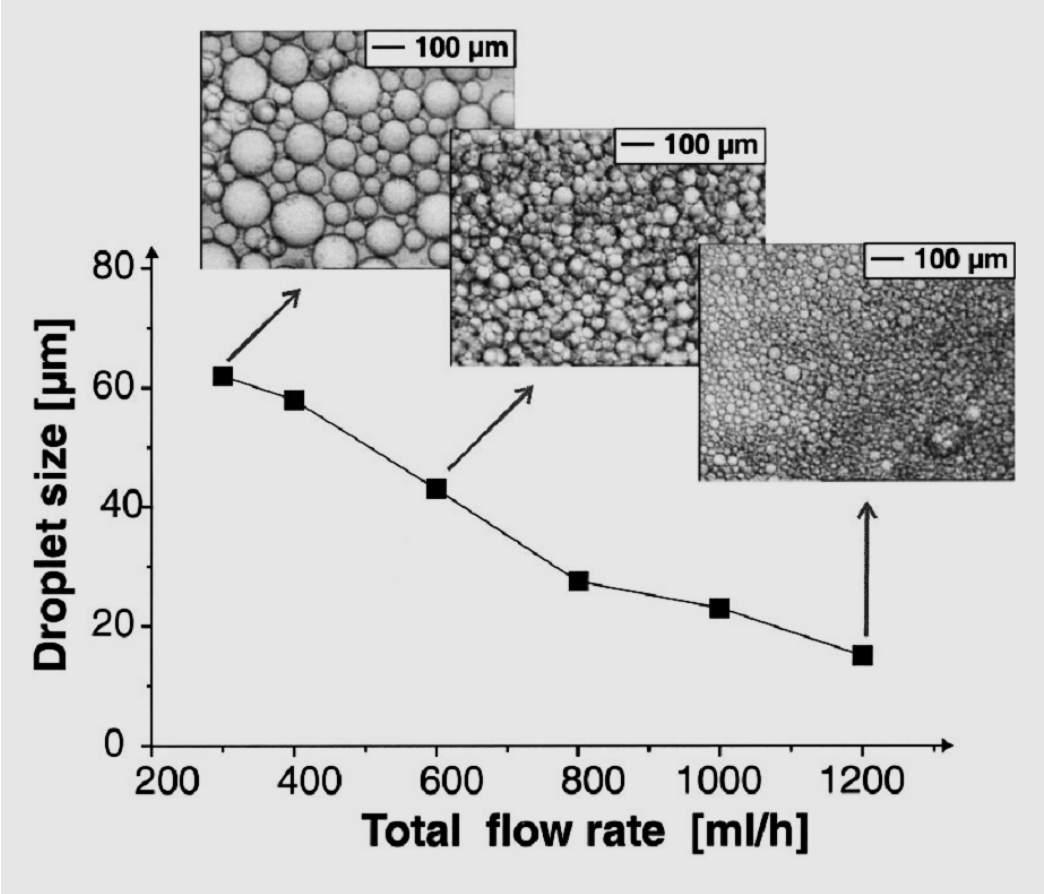

Figure 2-12: Photographs of dispersed oil-in-water phases generated from silicon oil and dyed water fed into the micro mixer with a channel width of 25 µm at various total flow rates. The droplet size of the dispersed phases decrease when increasing the total flow rate (Haverkamp, Ehrfeld et al. 1999).

Webster and Longmire (2001) studied the effects of viscosity ratio between dispersed and continuous phase, where two immiscible liquid-liquid system perturbed, and found that the viscosity ratio affects the stability of the jet, pinch off angle and droplet size. These co-workers studied two different combination of fluid in which they observed effect of forcing frequency on pinch-off dynamics. Jet instability called "*Erratic helical motion*" of the jet observed at higher flow rates (*Re*=43 and *Fr*=2.4).

Use of microfluidic devices are one of the important techniques for the formation of emulsion under controlled environment. Thorsen, Roberts et al. (2001) produced emulsions in a microfluidic device by pumping oil stream from one end and water stream from another at a T-shaped junction. They observed instability as results of shear forces and surface tension inside the microfluidic device. Further, Sugiura,

Nakajima et al. (2002) performed micro channel emulsification with different channel widths and lengths. They measured droplet diameters and detachment times at different flow velocities of the dispersed phase. The experimental results show that the droplet diameters were almost independent of the channel width, channel length, and the flow velocity in lower flow velocity ranges, as interpreted from the viewpoint of the droplet formation mechanism. Cramer, Berüter et al. (2002) performed experiments on various silicon oil as dispersed and mixture of PEG (Polyethylene glycol), water and ethanol. They observed unstable jet breakup process even after maintaining the flow conditions. Although, breakup mechanism was irregular, the jet length follows linear relationship with the flow rate at given viscosity and viscosity ratio. They also observed different droplet formation pattern as a function of viscosity ratio. Cramer, Fischer et al. (2004) further studied drop formation at a capillary tip in laminar flow. The focus of the study was on dripping. The drop breakup is affected by the flow dynamics of both disperse and the continuous phase. Consequently, the effect of flow rates, fluid viscosities and interfacial tension on the droplet size was investigated and observed the dynamics of satellite drop generation.

Flow focusing technique for the production of emulsions was also employed by Gañán-Calvo and Gordillo (2001) and Anna, Bontoux et al. (2003). Anna, Bontoux et al. (2003) summarised that the drop size is a function of flow rate and flow rate ratios explains regimes with monodisperse and polydisperse droplets. The smallest droplets produced can be much smaller than the orifice radius, in which case the drop size depends on the flow rates, and also there is a range of flow conditions where drops with diameters comparable to the orifice width are formed independent of the flow rates. Recently,Nie, Seo et al. (2008) studied emulsification via flow focusing. Their results suggested that the break-up dynamics of the lower viscosity fluids resembles the rate-of-flow-controlled break-up. An extensive review by Hessel et al (Hessel, Löwe et al. 2005) and Nisisako (2008) was done on the micro structure devices for the formation of emulsions.

Wang W. and co-workers (Wang, Ngan et al. 2009) performed experiments at flow rate range (50-500 µl/min) on the formation of organic drops from a capillary into a

stationary water using a high-speed video camera. Geometric parameters such as current contact angle (angle of the interface with the top capillary wall), drop height, neck length, mean drop growth velocity and drop wetted diameter on the top capillary wall are measured experimentally. Current contact angle found to change during the formation process which is identified as four different stages of drop formation.

2.3 CFD study on immiscible liquid jets and droplets

It was in the early 19th century Navier (1827), Poisson (1831) and Stokes (1845) derived the fluid flow equation commonly known as Navier-Stokes equation. This Navier-Stokes equation is the basis for computational fluid dynamics calculations. It was not possible to attain numerical solution of this equation without the powerful computer. A broad over generalisation of exact solutions of the NS equations with numerical descriptions of fluid flow have been obtained for years e.g. Hagen Poiseuille for laminar pipe flow, others for concentric cylinders, parrallel plates. Solutions for turbulent flow also exist e.g. Prandtl, Karman although they require assumptions about the so called Reynolds stresses. Numerical solutions of the Navier-Stokes equation equations involving both time and space, called Numerical simulations (NS), that describe turbulence without empirical modelling require very powerful main frame computers. CFD's are coarser solutions often for steady state flow only. Their main advantage is the ease of dealing with complex geometries.

Computational fluid dynamics is the analysis of the systems involving fluid flow, heat transfer and associated phenomena such as the chemical reactions by means of computer-based simulation(Versteeg 1995). “Computational Fluid Dynamics (CFD) is a discipline that encompasses the numerical solution of the equations of motion (mass, momentum and energy) in a flow geometry of interest, together with subsidiary sets of equations reflecting the problem at hand. Harris, Roekaerts et al. (1996) further detailed three sets of equations incorporated with the CFD flow modelling

- Equation describing turbulence quantity
- Equation describing chemical species
- Equation describing multiphase flow

In the last decade of the 20th century, Zhang and co-workers (Zhang and Stone 1997, Zhang 1999a, Zhang 1999b) extensively studied dynamics of drop formation from the nozzle at low Reynolds numbers in immiscible liquid-liquid system. Zhang and Stone (1997) numerically modelled drop formation at nozzle tip vertically immersed in another immiscible liquid at low Reynolds number using boundary integral method. Dimensionless number such as Bond number and capillary number as well as viscosity ration between dispersed and continuous phase were considered for the drop formation process. Numerical study includes formation of boundary integral equations and calculations are performed by varying one dimensionless quantity at a time. They were able to demonstrate entire drop formation process as shown in Figure 2-13.

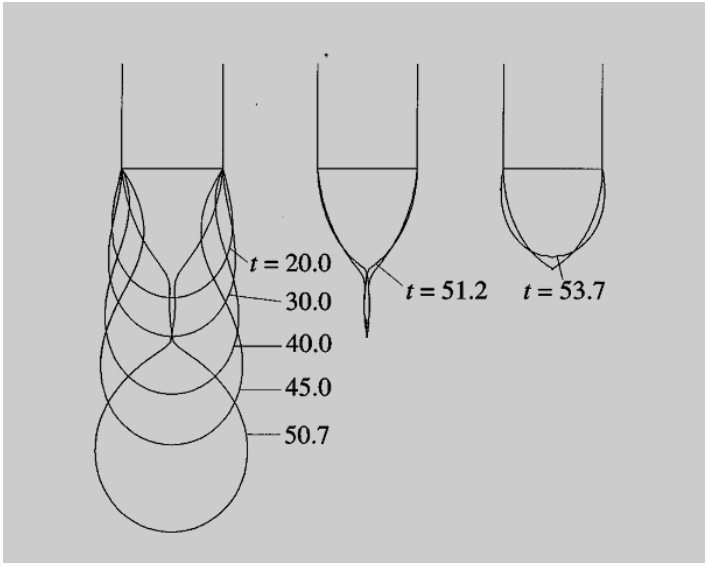

Figure 2-13: Sequence of drop formation process for viscosity ratio=0.1 Bond number=0.5 and Capillary number=0.1.

This work was further extended Zhang (1999b) to a condition where viscous liquid drips from the circular nozzle and breakup into droplet inside another immiscible liquid and how ambient fluid affect the dynamics of the droplet formation. Zhang (1999b) extended work of Richards, Beris et al. (1995) which used VOF/CSF numerical technique of investigation on droplet formation. Free surfaces can smoothly cross the computational mesh in VOF/CSF methods which ensures that the calculations pass the point of necking followed by natural breakup of drops without interruption and capable of detecting satellite droplet generation. These numerical results were validated with experimental data of 2-ethyl-1-hexanol (2EH) drops forming in distilled water system. In addition, their conclusion suggested that the jet length and drop volume increase significantly with increased Reynolds and capillary numbers and with decreased Bond number of dispersed liquid. Wall effect of fluid container can alter the satellite droplet formation by increase in volume of drop and reduction of jet length. Kobayashi and co-workers (Kobayashi, Mukataka et al. 2004, Kobayashi, Mukataka et al. 2005, Kobayashi, Mukataka et al. 2005, Kobayashi, Mukataka et al. 2005, Kobayashi and Nakajima 2006, Kobayashi, Uemura et al. 2007, Kobayashi, Hirose et al. 2008, Kobayashi, Takano et al. 2008, Kobayashi, Vladisavljević et al. 2011)proposed the technique to produce monodisperse emulsion of micro meter size via straight through micro channels and associated with CFD simulation results.

Kobayashi and co-workers (Kobayashi, Mukataka et al. 2004) performed CFD simulation of oil in water through oblong micro channels (Figure 2-14) and compared with experimental results. The droplet formed from the micro channel considerably depends on the aspect ratio of the channel. Pressure and velocity in the region around neck and channel exit are important in the drop formation process. CFD simulations were in the good agreement with the experimental findings.

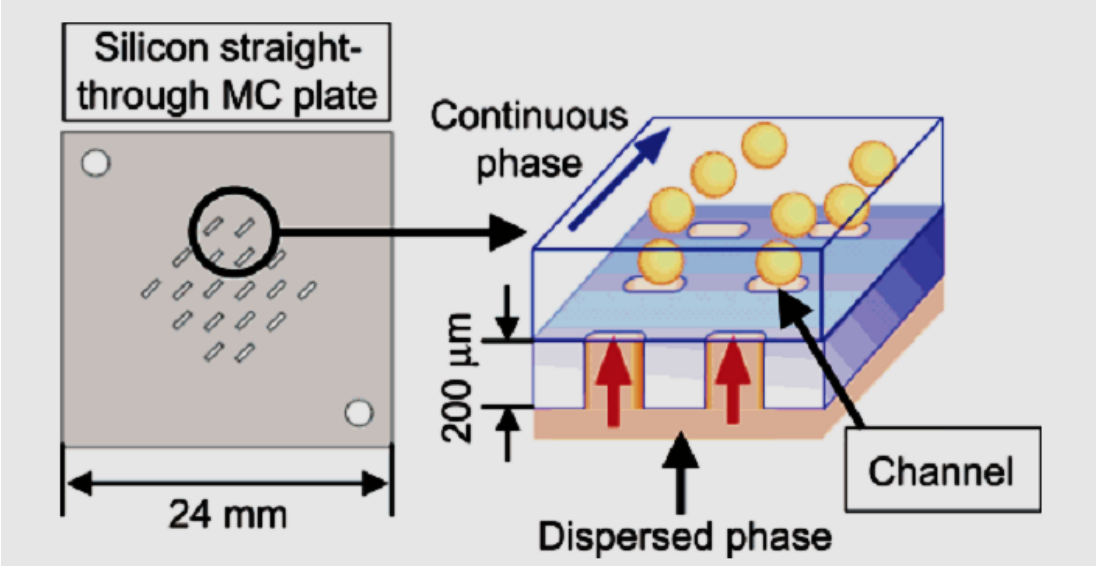

Figure 2-14: Schematic illustration of a silicon straight-through micro plate and the droplet formation process from a channel (Kobayashi, Mukataka et al. 2004).

Kobayshi and his colleagues (Kobayashi, Mukataka et al. 2005) further performed experiments and CFD simulations with different oils as dispersed phase with varying physical properties to study the effect of type and properties on the droplet formation process. Droplet diameter was gradually decreasing with increasing oil viscosity below threshold value of 100 mPa s. However, diameter of droplet was found to increasing with oil viscosity above threshold value. Moreover, droplet diameter was not affected by surfactant concentration below threshold value of oil viscosity. Conversely, surfactant concentration has considerable effect on droplet diameter above threshold value of oil viscosity. Significant decrease in dynamic interfacial tension triggered its importance in the droplet formation in straight through micro channel. Later, they (Kobayashi, Mukataka et al. 2005, Kobayashi, Mukataka et al. 2005) developed an array of straight through micro channel plate for higher throughput and simulated using CFD. Droplet diameter of 18 to 53 µm can be generated with aspect ratio between 3 and 3.25 with channel of shorter line of 5 to 15 µm. Their following publications (Kobayashi, Uemura et al. 2007, Kobayashi, Hirose et al. 2008, Kobayashi, Takano et al. 2008, Kobayashi, Vladisavljević et al. 2011) reflect further experiments and CFD analysis on the straight through micro channel and effect of size on the droplet size. Overall, Kobayashi and co-workers

developed novel technique, which can be used in the food and pharmaceuticals industries, of droplet formation via straight micro channels.

Homma, Koga et al. (2006) numerically studied the breakup of an axisymmetric liquid jet, injected vertically upward from a nozzle into another immiscible liquid, into droplets. They identified three different breakup modes, dripping, jetting with uniform droplets, and jetting with non-uniform droplets, on the basis of Weber number and viscosity ratio.

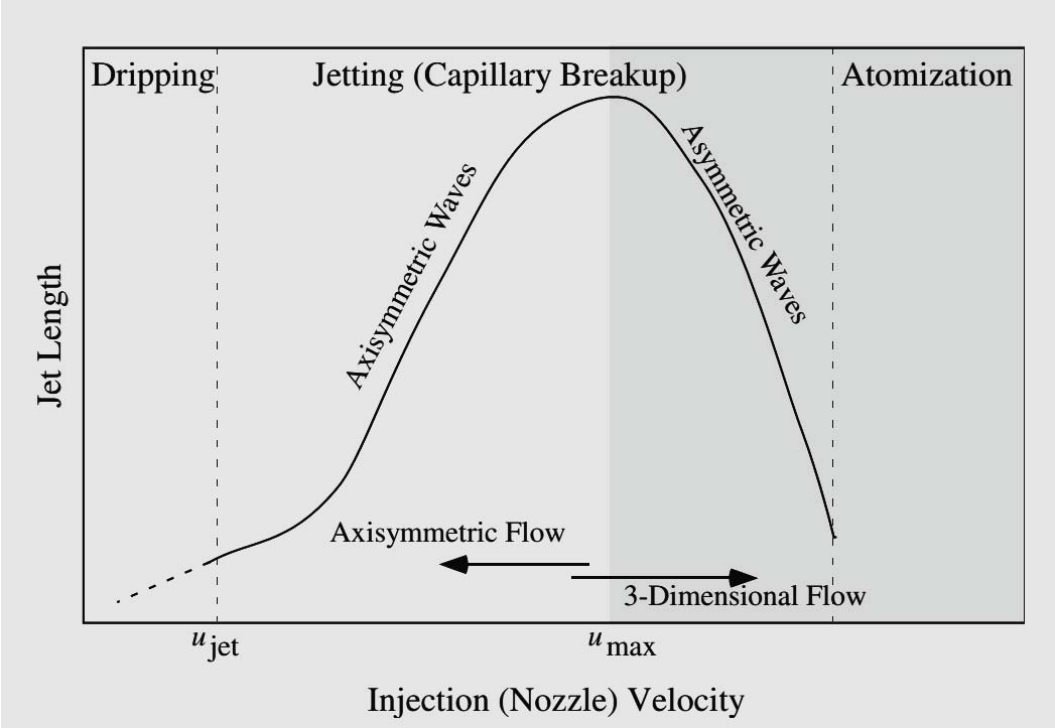

Figure 2-15: Schematic diagram of breakup modes when a liquid injected into another immiscible liquid (Homma, Koga et al. 2006).

Subsequently, Homma, Yokotsuka et al. (2010) found good agreement between numerical simulations and experiments. Moreover, non-Newtonian effects are discussed by visualizing the distribution of viscosity. The breakup length of the jet becomes large while shear thinning occurs inside the jet, while the jet becomes short when shear thinning occurs in continuous phase.

Tiemgren and his colleagues (Gun and Martin 2007) modelled drop formation in immiscible liquid-liquid system in co-flowing continuous phase. In the co-flowing liquid, they measured pressure and shear stress around the drop during drop

detachment and maximum and minimum pressure were found in the continuous phase near the stagnation point and behind the top of the drop respectively. Higher shear stress was found at the top of the forming drop. The shear stress outside the drop causes a drag which, together with the drag originated from the pressure field around the drop, promotes drop detachment. Further, Tiemgren and co-workers (Timgren, Trägårdh et al. 2010) developed a model for the drop size prediction in cross flow emulsification. The model has also been compared with experimental results on drop formation using various membranes, cross-flow velocities and surfactants. The difference between the model and experimental results is mainly due to the adsorption of surfactants onto the drop interface and the shape of the membrane pores. In the following publication, Tiemgren and colleagues (Timgren, Trägårdh et al. 2009) mentioned about the effect of cross flow velocity on the size of drops. Droplet size decreased with increased cross flow velocity. An increase in cross-flow, oil viscosity and capillary pressure displace the position of necking and drop detachment away from the capillary opening, which will have a decreasing effect on the final size of the drop.

In a cross flow emulsification, it is more important to control the droplet size to produce monodisperse emulsions. Hong and Wang (2007) developed numerical model for the co flowing phenomena in a microfluidic. Droplet size was independent of the flow rate ratio of $\geq$ 0.1 between dispersed and continuous phase. Moreover, Capillary number (*Ca*) had linear relationship with droplet size, which makes droplet control more convenient. In the second case where flow rate ratio (Q_d/Q_c) *is* < 0.1 and the droplet size is greatly dependent on the flow rates. Four different patterns of droplet formation occurred with flow rate ratio < 0.1. Importantly, monodisperse droplets are formed in the last pattern where value of capillary number was used as *Ca*=0.221 and hence increasing the capillary number of the continuous fluid, viscous stress exerted by the external fluid becomes so large that it squeezes the disperse fluid to form a very narrow thread, which allows formation of monodisperse droplets with diameters much smaller than the tube width.

In a series of different studies (Hua, Zhang et al. 2007, Chen, Wu et al. 2013)was investigated on micro droplet formation in co flowing liquid. These studies focused

on the effect of flow rate of co-flowing stream on the drop formation process. Hua, Zhang et al. (2007) developed correlations for the dimensional droplet size r_d^* for the dripping and jetting mode with the continuous flow parameters such as the Reynolds number (Re_o), Weber number (We_o), Capillary number (Ca_o), and viscosity ratios (μ^*) as

- $r_d^* \propto {Ca_o}^{-1/2} {Re_o}^{-1/6}$ For the dripping mode
- $r_d^* \propto {Ca_o}^{1/3} {We_o}^{-1/2} {\mu^*}^{-1/2}$ For the jetting mode

Apparently, much of the work was performed on the immiscible liquid-liquid system to predict jet breakup length and resultant droplet size prediction. An interfacial phenomenon between multiple jets inside another immiscible liquid is still a topic of importance for higher production rate and micro reactor designing.

Chen, Wu et al. (2013) performed simulations and reproduced dripping, widening jetting and narrowing jetting simultaneously with the help of VOF simulations. In addition, the capillary number of the outer fluid and the Weber number of the inner fluid not only determine the drop diameter and generation rate but also the regime of emulsification. More specifically, dropping regime, rather than jetting regime, is a favourable way to produce monodisperse emulsions.

Soleymani, Laari et al. (2008) simulated solvent extraction process using VOF and noticed the effects of size and shape of the hole on the size of the resultant droplet. The shape of the hole has considerable effect on the size of the resultant droplets. The simulation results were verified with experimental observations obtained using high-speed video technology and the numerical results for the drop sizes, shapes and formation times were found to be consistent with images of experimental drops across a wide range of solvent volumetric flow rates.

Phan and Evans(Phan and Evans 2008) performed experiments of water jet inside the canola oil filled and stationary column to quantify influence of jet velocity on the jet breakup inside continuous phase.

Delteil, Vincent et al. (2011) carried-out simulations to quantify the growth rate of the instability at jet breakup. Brackbill (Brackbill, Kothe et al. 1992) surface tension

model employed to carry out further simulations using water as injected liquid and compressed carbon dioxide as surrounding medium. Breakup length and the droplet size were accurately predicted as evidenced in literature. These above studies have contributed significantly to the understanding of the formation of a jet and the breakup of the jet into droplets in immiscible liquids systems.

2.4 Summary

An overview of the previous experimental and computational fluid dynamics work starting from single droplet in an air to complex system of immiscible liquids have been reviewed in this chapter. Immiscible liquid-liquid interaction was a topic of research with the introduction of micro fluidic devices for experimentation and modelling. It is important to understand the dripping, jetting and jet breakup phenomena for the design of micro reactor. The theoretical understanding can provide modern chemical and pharmaceutical industries with vital insights improve production rate and quality of produced emulsions.

The dripping, jetting and jet breakup analysis has been carried out for single jet system and CFD simulations have been further used to analyse the effects of aspect ratio and volumetric flow rate on resultant droplet size for rectangular nozzle. This immiscible liquid system has been examined experimentally and computationally for instability during emulsification and hence the effect of instability on emulsion quality. In contrast, the interaction between moving jets in liquid-liquid system remains unknown experimentally and theoretically. Consequently, this study intends to fill the knowledge gap by investigating the jet breakup for single and multiple laminar axisymmetric water jets into canola oil. An extensive series of experiments and simulations of water in canola oil have been performed to understand mechanism and dynamics of jet interactions and instability and the critical distance between multiple jets on jet formation, jet breakup length and droplet size. It should be noted that the canola oil was selected for the practical application of mining emulsions explosives.

Chapter 3. Experimental and Simulation methodology

This chapter describes laboratory scale setup, materials and methodologies used to carry out experiments. In addition, computational domain configuration, grid/mesh configuration and simulation methodologies are described in this chapter. The processing of immiscible liquids is common and experiments have been performed using water and canola oil. A high speed camera has been used to capture jet formation, breakup and droplet formation during emulsification. Simulations have been carried out to validate the aforementioned phenomenon.

3.1 Experimental methodology

3.1.1 Experimental setup

The experimental setup consists of a vertical column filled with canola oil. Dispersed phase jets from two different sizes of nozzles have been introduced from the top of the column. Detailed dimensions of the column and size of the nozzle are given in Table 3-1 and sketch of experimental setup is shown in Figure 3-1.

Table 3-1: Detailed dimensions of experimental setup.

Column Dimensions	300 X 300 X 1000 mm
Nozzle Dimensions	ID : 1.59512 mm OD : 1.68910 mm ID : 0.80264 mm OD : 0.85598 mm
Distance between two nozzle	Case : 1 3 mm Case : 2 5 mm Case : 3 7 mm
Material of construction	Column: Perspex Acrylic Nozzle : Polyimide Piping : Flexible silicon rubber

The nozzles have been sufficiently long (length to diameter ratio greater than 20) and submerged 5 mm below the free surface of the continuous liquid inside the column to assure a fully developed velocity profile at the nozzle exits The nozzles were attached to a plenum chamber which was fed by a pump and volumetric flow rate controlled by a valve from a chamber containing the dispersed phase liquid. High speed camera was used along with computer to visualize jet and droplet behaviour inside the column during the experiment. Vertical and horizontal ruler has been attached on the face of the column toward camera to exactly measure the characteristic length such as jet breakup length and jet size of the jet. Jetting phenomena and droplets formation process have been captured at 125 frames per second. Jet breakup length, jet size and droplet size have been measured continuously during the experiments. All experiments were carried out at 22.5°C (room temperature).

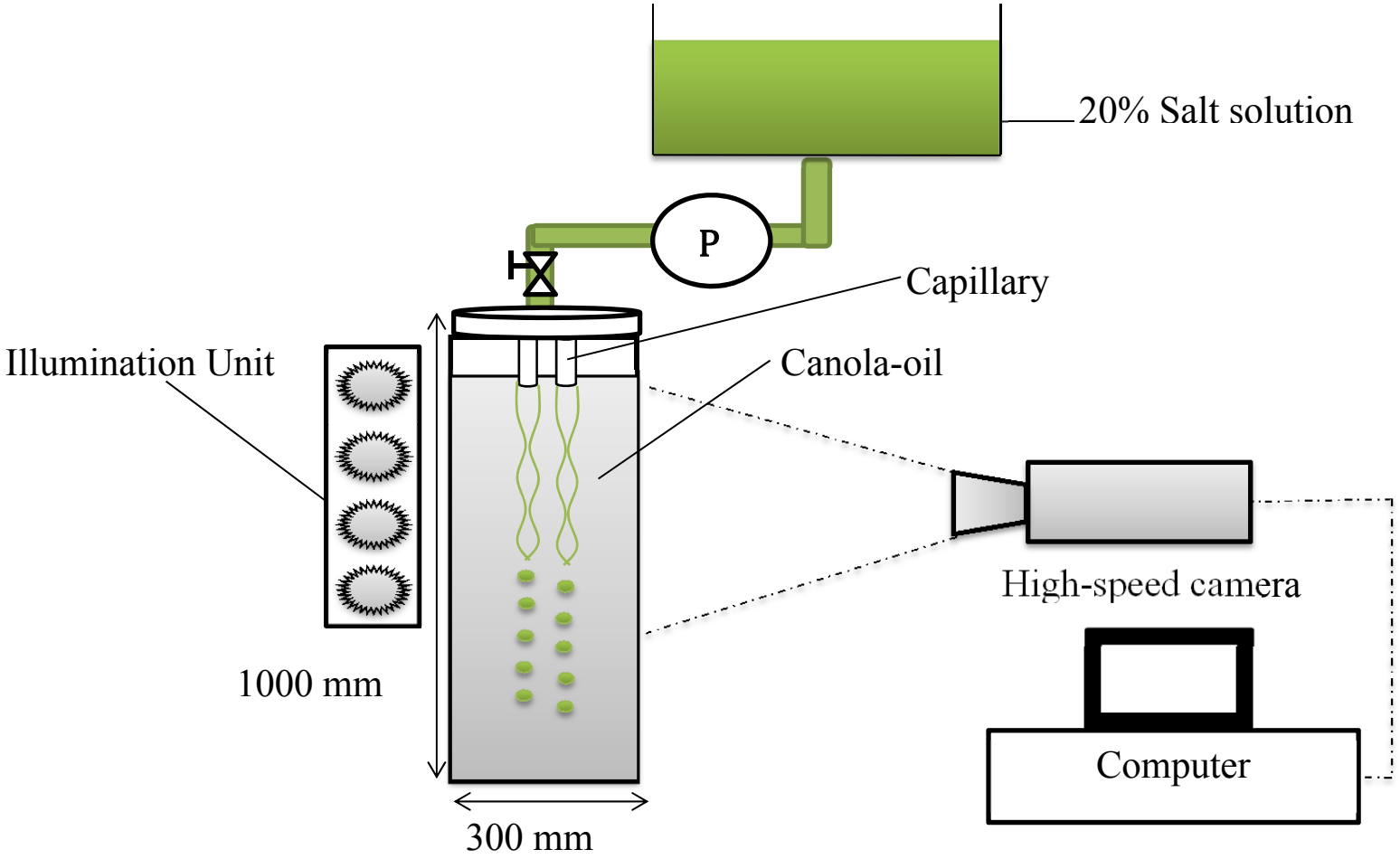

Figure 3-1: Graphical representation of the experimental setup.

3.1.2 Determination of jet breakup length (L_3) and jet diameter (D_j) and average volumetric flow rate (Q_{av})

High-speed camera from Fastec Imaging™ has been employed for all video capturing and analysis of these video recordings has been done on FIMS software V 3.0 (Figure 3-2) and PAC player V 2.31 (Figure 3-3) supplied with the camera. Video recordings have been taken over a period of approximately two seconds and then run into PAC player. Droplet breakup phenomena during the breakup of 20 droplets have been taken into consideration for the jet breakup length L_3 analysis for each run of 1-2 seconds. Jet diameter (D_j) has been continuously measured during drop breakup and average volumetric flow rate (Q_{av}) was calculated from each volume of droplet and divided by total time taken for the formation of 20 droplets. These calculations were repeated for all single and multiple jet system and finally averaged to calculate average value for the system.

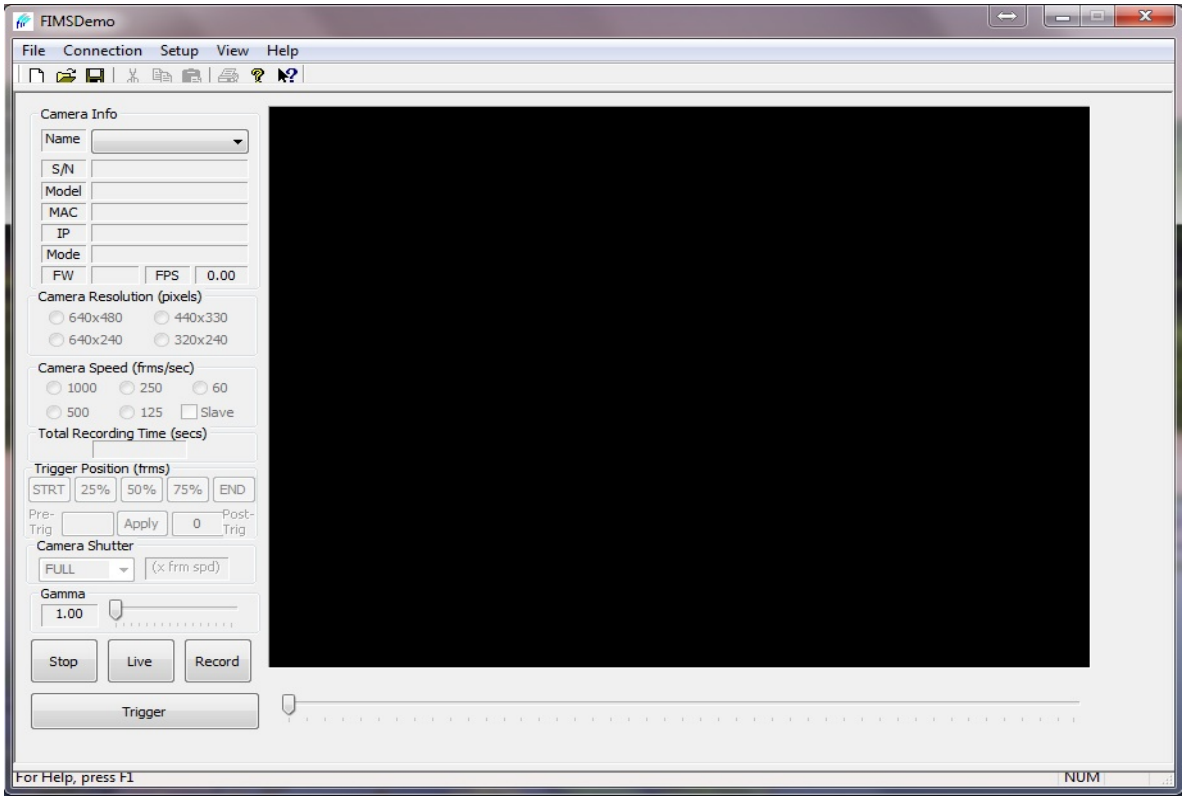

Figure 3-2: FIMS software graphical user interface (GUI).

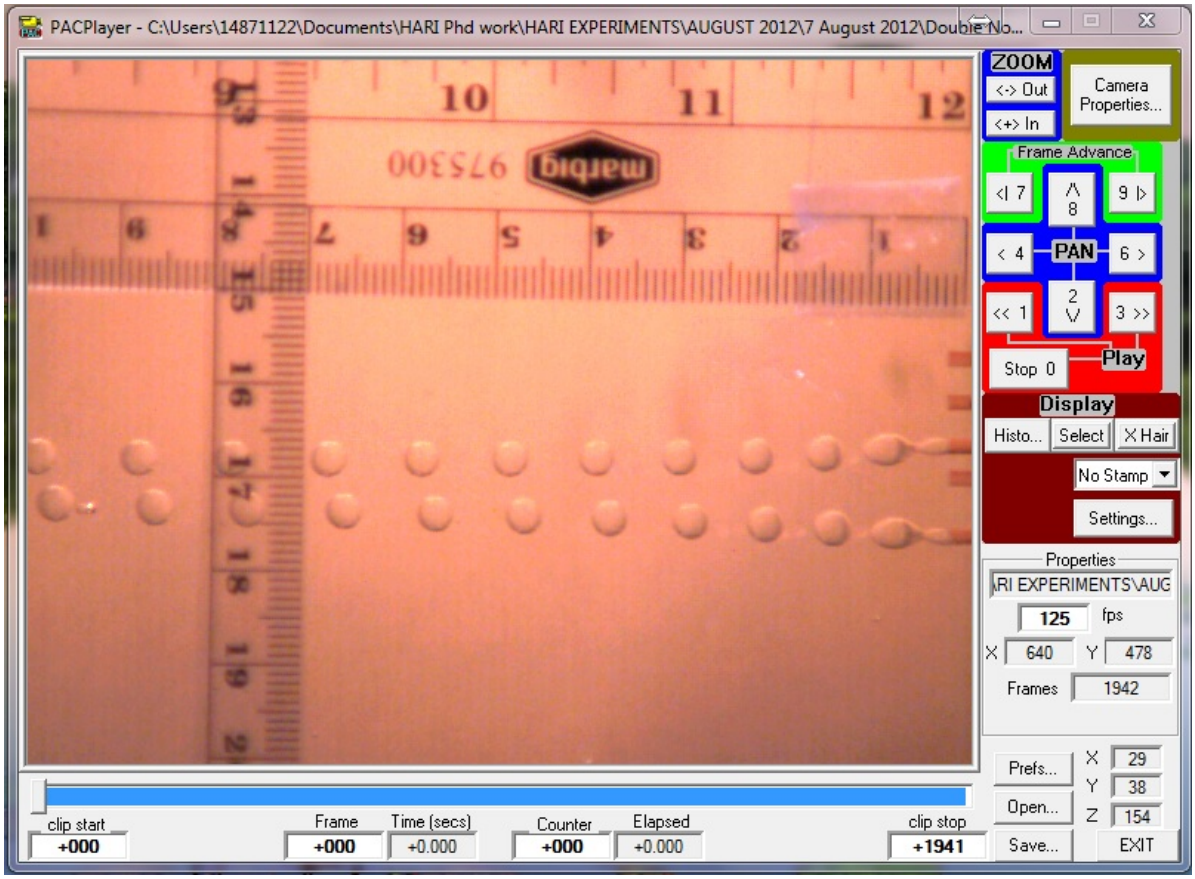

Figure 3-3: PAC player graphical user interface (GUI).

3.1.3 Determination of droplet volume and size

High speed video recording was analysed in PAC player to determine the number of droplets produced. Volume of each droplet was calculated from equivalent droplet diameter, d_d, of the droplet and the data was further averaged with number of droplets. This information was then used calculate the cumulative total volume, V.

3.1.4 Determination of surface tension

Surface tension and contact angle measurement of liquid is a very essential for insight of fluid dynamics and rheological behaviour of liquids. The pendant and sessile drop shape analysis methods have become the most widely used techniques for this measurement and it is used for measurement of interfacial tension and contact angles of pendant drops, sessile drops, and bubbles. Axisymmetric Drop Shape Analysis (ADSA) is the most powerful among these techniques. Complicated

numerical methods are involved and therefore developed (Bashforth and Adams 1883, Maze and Burnet 1969, Maze and Burnet 1971, Hartland and Hartley 1976) for determination of interfacial properties using drop shape analysis. Basically, an efficient numerical scheme is employed to fit a theoretical Laplacian curve with known surface tension values to an experimental profile obtained from a digital image of the drop(Hoorfar and Neumann 2004, Zuo, Ding et al. 2004, Hoorfar, Kurz et al. 2005, Hoorfar and W. Neumann 2006).

There are three major steps are involved in the determination of interfacial properties from sessile and pendant drops.

1. Image acquisition: Video recordings were acquired from the PAC player and converted into the Windows media player compatible format. Window movie maker was used to convert video into several images in order to measure surface tension of the droplet.
2. Image processing: Image J^{TM} (www.imagej.net) was used to process all the images to make it compatible for the ADSA to measure surface tension of the droplet. Image were cropped and rotated if necessary. Images are converted into binary images (black/white) using Image J thresholding.
3. Numerical computation: These binary images were process for calculation in ADSA for the determination of surface tension values. A brief discussion of the computation is given below:

The image of the drop is acquired and transferred to a host computer directly from microscopic camera. Evaporation rate is negligible or none as drop is surrounded by continuous phase. A spot light source is used to illuminate the drop, and a heavily frosted diffuser is used in front of the light source to provide a uniformly lit background and to minimize heat emission to the drop during image acquisition. An image analysis has been employed to detect the coordinates of the drop profile. Finally, the measured profile of the drop is fitted to a Laplacian curve using an optimization method. The latter uses an objective function that specifies the discrepancy between the theoretical Laplacian curve and the actual profile as the sum of the squares of the normal distances between the measured points and the calculated curve. This objective function is minimized numerically to obtain the

interfacial tension and contact angle values (Hoorfar and Neumann 2004). Figure 3-4(a) shows drop profile used to measure interfacial surface tension and Figure 3-4 (b) smoothed edge for final surface tension measurement.

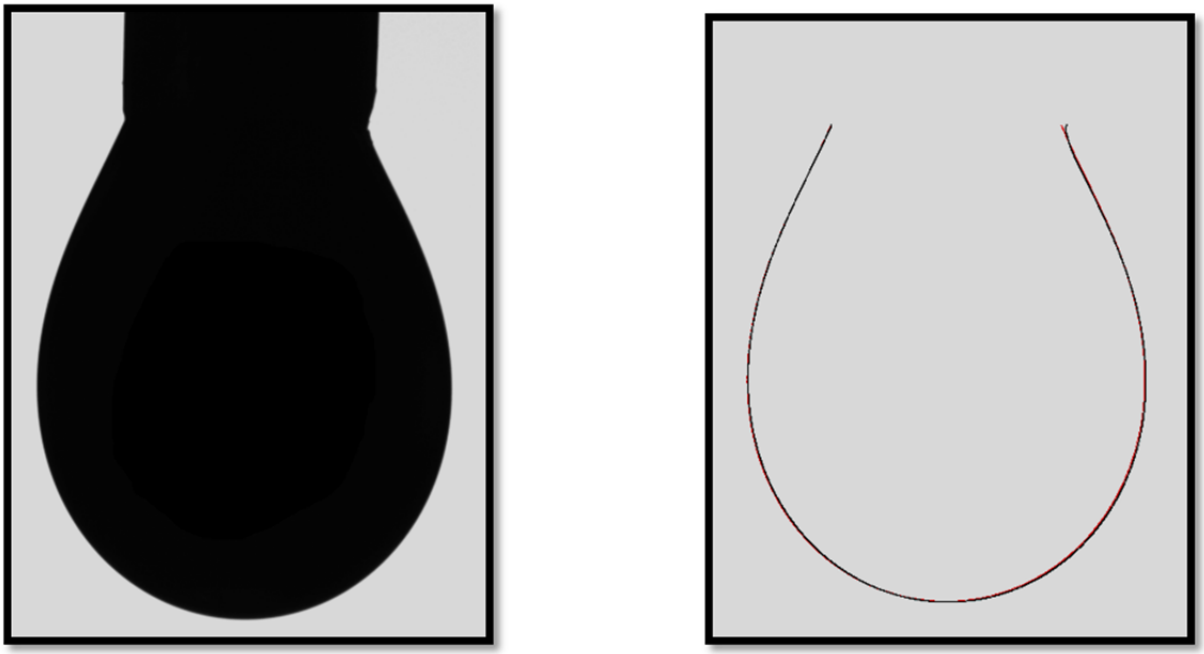

(a) *(b)*

Figure 3-4: Droplet profile and smoothed edges for ADSA method of surface tension measurement (*a*) Drop profile (*b*) Smoothed edges for final surface tension measurement.

3.1.5 Determination of density and viscosity

Densities and viscosities of the salt solution and the canola oil were measured using Antone Paar Density meter (DMA 4100) and Vibro Viscometer (SV-10), A&D Co. Ltd. at 22.5 °C respectively. Table 3-2 below shows physical properties of continuous and dispersed phase.

Table 3-2: Physical properties of continuous and dispersed phases.

Property	**Continuous phase**	**Dispersed phase**	**Interfacial Tension**
μ (Pas)	0.0603	0.0039	
ρ (kg/m^3)	913	1147	
σ (N/m)			0.021

3.2 Simulation methodology

Pre-analysing the problem prior to the CFD simulations is critical for the quality of results obtained from the CFD simulations. Pre-analysing include ground work to reduce the complexity of the problem and can be reduced by making appropriate assumptions. However, these assumptions should be made to a level that it should not affect the accuracy and adequacy of the results. In addition, user needs to decide whether the geometry of the problem can be resolved in two or three dimensions, keeping in mind that three dimensional simulations are computational power intensive. The next step is to discretise flow field into a computational domain which is generally known as the grid/mesh. According to Nigel and Joe (1998), mesh is a set of points distributed over a calculation field for a numerical solution of a set of partial differential equations (PDEs). Mesh is generally generated using CAD based software such as GAMBIT. It is vital to generate appropriate mesh to facilitate accurate numerical solution. While generating a mesh there are various factors that needs to be considered such as:

- Mesh should be sufficiently dense but practically computable.
- Grid spacing should be smooth.
- Discontinuities or skewness should be avoided.
- Appropriate choice of the grid should be made.
- Well organised grid is desirable

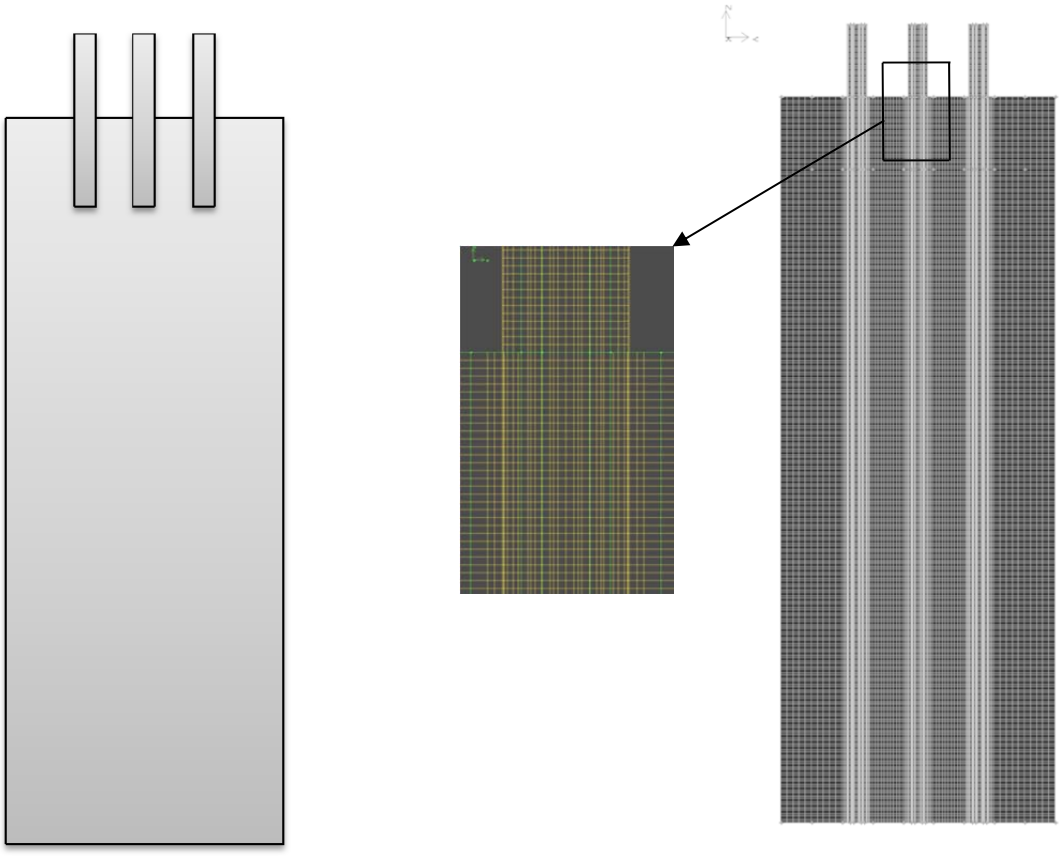

(a) *(b)*

Figure 3-5: (*a*) Computational domain (*b*) Details of grid configurations and refinement throughout the jet pathway.

3.2.1 Grid independency

Grid size is critical in properly resolving distinct interfaces involving small dimensions. In the VOF model at any given instance, a cell in the computational domain has either of three conditions; completely filled, completely empty or interface. The governing equations for the VOF model are shown in (Figure 3-8). Hence an initial estimate of the expected minimum drop size or jet diameter must be made to decide the grid size. In order to study the effect of grid size three different grid configurations was compared and the final grid, a uniform grid of 1mm using map scheme was developed, thereafter a refinement was performed near the inlet regions of the three channels respectively. A rectangular cube of dimensions 2.4 mm wide, 2.4 mm deep and 100 mm height was meshed with uniform grid of 0.1 mm

and aspect ratio with the largest grid size of 1mm was used in the remaining cross-section. The hexahedral mesh type and Cooper type scheme was used in fine mesh areas. 1.8 million cells taken into simulation. Computational domain and grid configuration details are shown in Figure 3-5 and Figure 3-6. The physics of the system do suggest the later refined grids would produce near to physical results. It was observed that the finest grid of the three configurations used, provided the smoothest interface tracking as expected. Thus, this configuration was chosen to carry out further investigations.

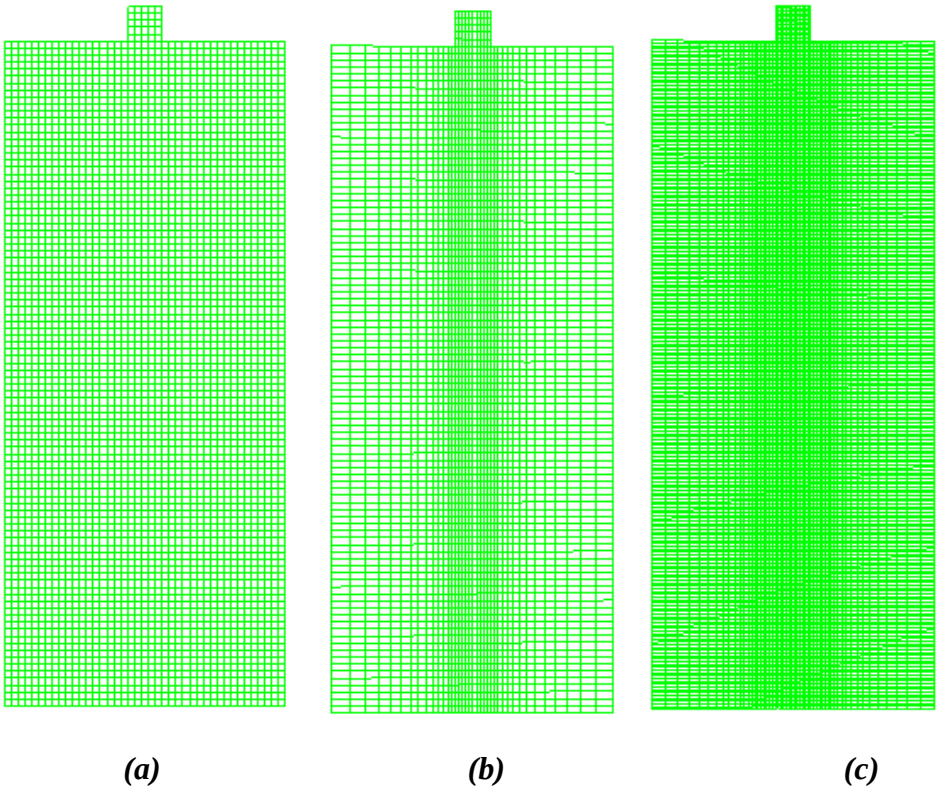

Figure 3-6 Grid configuration to study the effect of grid size

3.2.2 Boundary conditions

Transient simulations were carried out using Fluent (Fluent Inc., http://www.arc.vt.edu/ansys_help/flu_ug/flu_ug.html) to track the interface between the disperse phase and the continuous phase (Figure 3-7). Instability in the jet during the breakup process is tracked by the Interface tracking. Momentum equation can describe the wave disturbance coming through the nozzle.

The VOF model (Figure 3-8) is a surface-tracking technique that is useful when studying the position of the interface between two immiscible fluids (Table 3-3). A single set of momentum equations is shared by the fluids, and the volume fraction of each of the fluids in each computational cell is tracked throughout the domain (Figure 3-9). The flow was assumed to be incompressible laminar, dominated by the surface tension and viscous forces. The VOF model uses phase averaging to define the amount of continuous and dispersed phase in each cell. More information on VOF model can be found in (Harvie and Fletcher 2000)

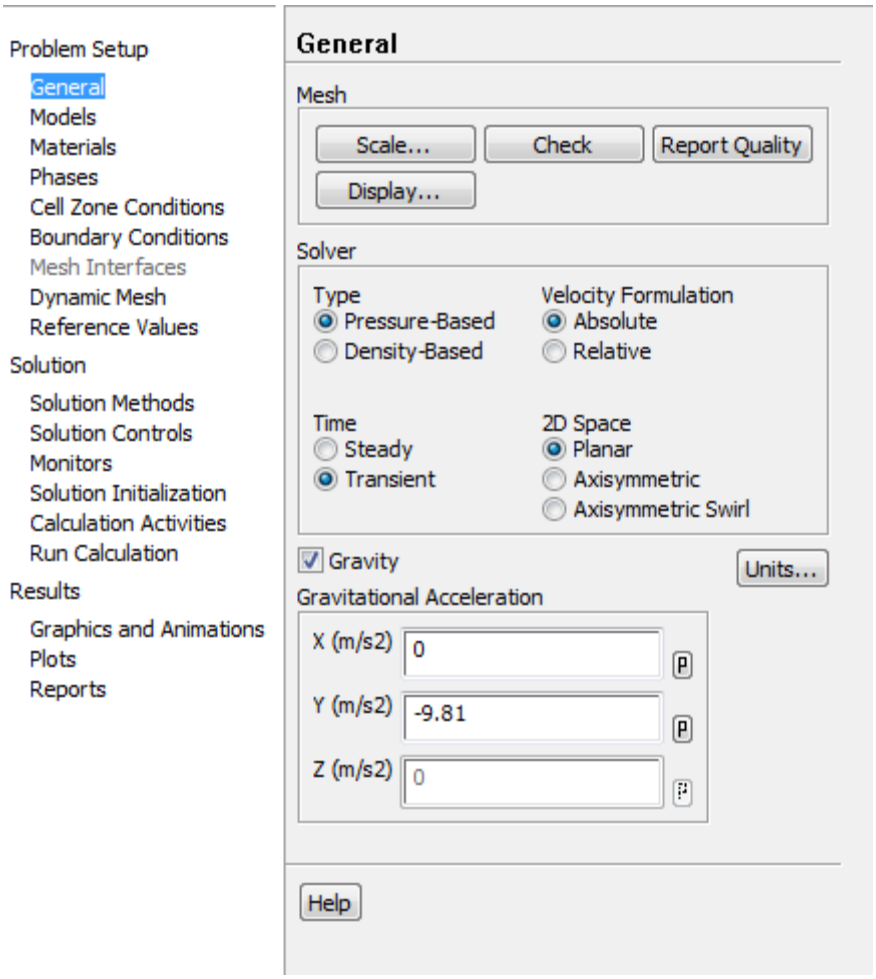

Figure 3-7 Problem setup in ANSYS Fluent V 14.0

The PRESTO (pressure staggering option) scheme was used for pressure interpolation. The pressure-velocity coupling was done using the SIMPLE scheme.

A second order upwind discretization was applied for the momentum equation. For interpolating the gas-liquid interface the geometric reconstruction scheme was used. An adequate time step (usually 1x 10^{-5} Seconds) was used to limit global Courant number to 0.25. Courant number value of 0.25 or below can avoid the divergence in the simulation. The results were considered to attain steady state and converged when global mass fluxes were balanced and all the residuals were maintained below 1×10^{-3}. QUICK scheme was used for volume fraction equation. A double precision solver was used to minimize truncation errors (Figure 3-10).

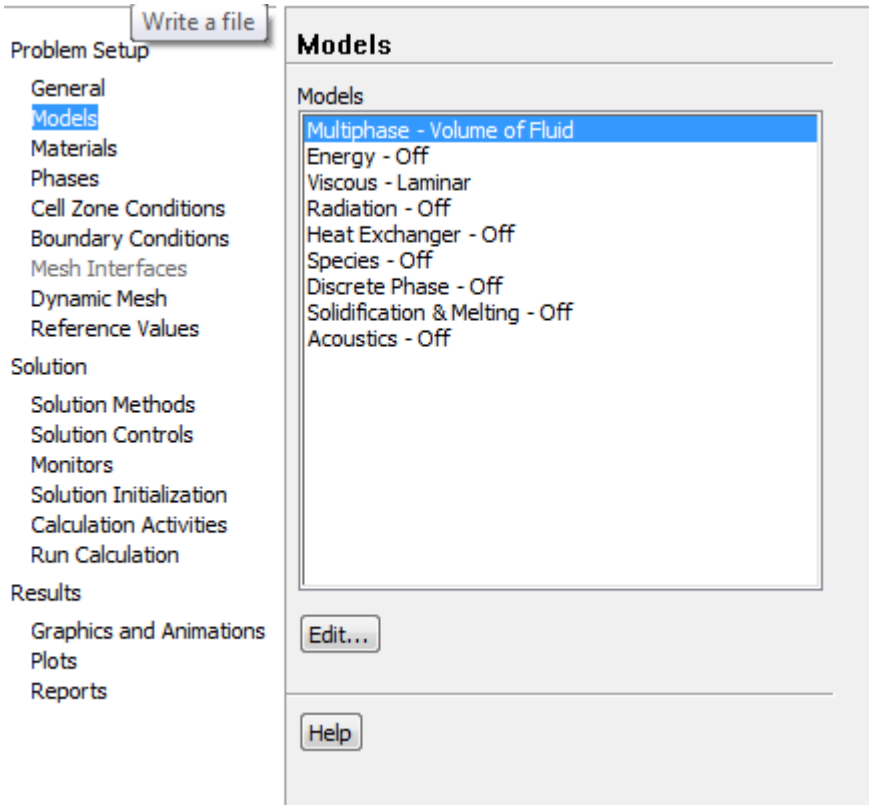

Figure 3-8 Model selection in ANSYS Fluent V14.0

Table 3-3: Governing equations of VOF model.

Equation Name	Equation
Equation of Continuity	$$\frac{\partial \rho}{\partial t} + \nabla \cdot (\rho \vec{v}) = 0 \quad (3.1)$$
Momentum Equation	$$\frac{\partial (\rho \vec{v})}{\partial t} + \nabla \cdot (\rho \vec{v} \vec{v}) = -\nabla p + \nabla \cdot \left[\mu \left(\nabla \vec{v} + \nabla \vec{v}^{\,t}\right)\right] + \rho \vec{g} + \vec{F} \quad (3.3)$$
Volume Fraction Equation; If for q^{th} fluids volume fraction is αq then; For $\varepsilon_q = 0$; cell is empty (for q^{th} fluid) For $\varepsilon_q = 1$; cell is full (for q^{th} fluid) For $0 < \varepsilon_q < 1$; cell contains interface between q^{th} fluid and other fluids.	$$\frac{1}{\rho_q}\left[\frac{\partial}{\partial t}(\varepsilon_q \rho_q) + \nabla \cdot \varepsilon(\alpha_q \rho_q \vec{v}_q) = s_{\varepsilon_q} + \sum_{q=1}^{n}(\dot{m}_{pq} - \dot{m}_{qp})\right] \quad (3.3)$$ $$\sum_{q=1}^{n} \varepsilon_q = 1 \quad (3.4)$$ $$\frac{\varepsilon_q^{n+1}\rho_q^{n+1} - \varepsilon_q^{n}\rho_q^{n}}{\Delta t} V + \sum_f \left(\rho_q^{n+1} u_f^{n+1} \varepsilon_{q,f}^{n+1}\right) = \left[\sum_{p=1}^{n}(\dot{m}_{pq} - \dot{m}_{qp})\right] V \quad (3.5)$$
Continuum surface force (CSF) Model; Surface Tension	$$F_{vol} = \sigma_{ij} \frac{\rho K_s \nabla \varepsilon_i}{\frac{1}{2}(\rho_i + \rho_j)} \quad (3.6)$$
Courant number	$$Co = \frac{\Delta t}{\Delta x_{cell} / v_{fluid}} \quad (3.7)$$

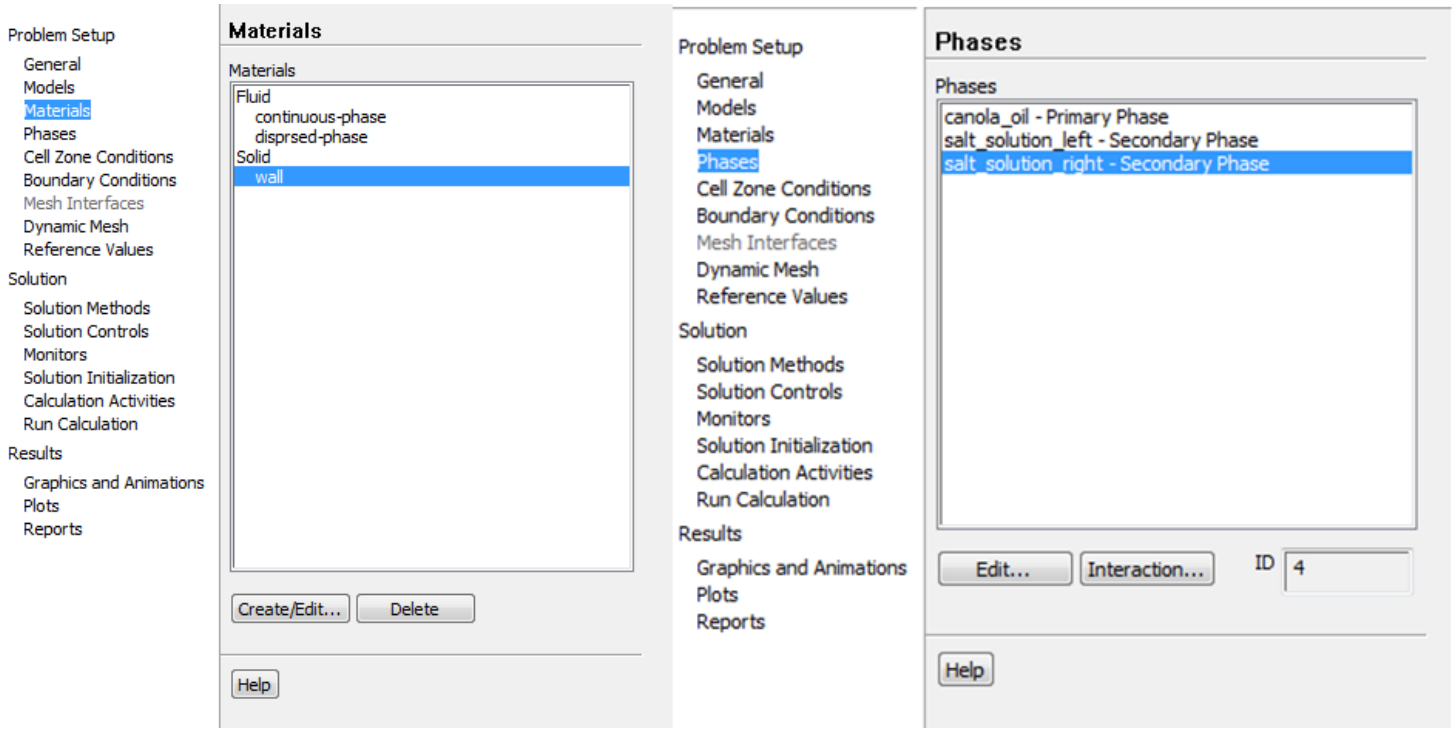

Figure 3-9 Phase selection and setup in ANSYS Fluent V 14.0

3.2.3 Selection of multiphase model

Several methods such as the front tracking, level set, marker particle, shock capturing and volume of fluid (VOF) (Hirt and Nichols 1981) are available for dynamics characterisation of free surfaces involved in the study of chemical engineering equipment. Table 3-4 shows their comparison on the basis of their merits and weaknesses. VOF method is selected for analysing breakup mode of jet and resulting droplets throughout all simulations.

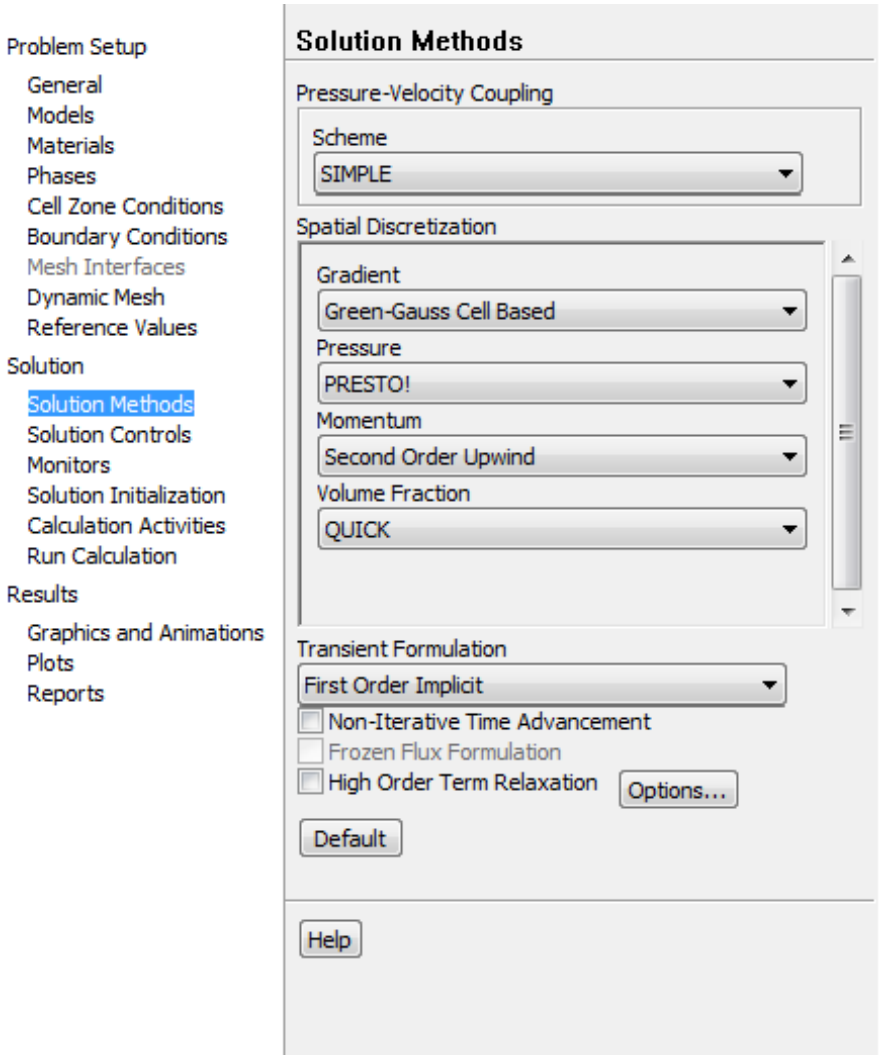

Figure 3-10 Solution methods selection in ANSYS Fluent V 14.0

Table 3-4: Overview of interface tracking techniques (Gopala and van Wachem 2008).

No.	Method	Advantages	Disadvantages
1	Front tracking	• Extremely accurate • Robust • Accounts for substantial topology changes in interface	• Mapping of interface mesh onto Eulerian mesh • Dynamic re-meshing required • Merging and breakage of interfaces requires sub-grid model
2	Level set	• Conceptually simple • Easy to implement	• Limited accuracy • Loss of mass (volume)
3	Shock capturing	• Straightforward implementation • Abundance of advection schemes is available	• Numerically diffusive • Fine grids required • Limited or small discontinuities
4	Marker particle	• Extremely accurate • Robust • Accounts for substantial topology changes in interface	• Computationally expensive • Re-distribution of marker particles required

5	VOF	• Conceptually simple • Straightforward extension to three dimensions • Merging and breakage of interfaces occurs automatically	• Numerically diffusive • Limited accuracy
6	PLIC VOF	• Relatively simple and accurate • Merging and breakage of interface occurs automatically	• Difficult to implement in three dimensions • Extension to boundary fitted grids very difficult
7	Compressive VOF	• Relatively simple and accurate • Easily adaptable to boundary fitted grids • Merging and breakage of interface occurs automatically	• Requires very low Courant numbers else becomes inaccurate or unstable

There have been two series of simulations run during the course of the project.

(1) Rectangular shaped single jet simulations.
(2) Circular shaped single jet and multiple jet simulations.

Table 3-5: Physical properties of continuous and dispersed phases for CFD simulations.

Property	**Continuous phase (Canola Oil)**	**Dispersed phase**	**Interfacial Tension**
System -1 (dispersed phase :20% salt solution)			
μ (Pas)	0.0603	0.0039	
ρ (kg/m3)	913	1147	
γ (N/m)			0.021
System -2 (dispersed phase :glucose solution)			
μ (Pas)	0.26	0.08	
ρ (kg/m^3)	915	1220	
γ (N/m)			0.022

Physical properties for continuous and dispersed phase were taken from (Phan and Evans 2008) for the rectangular shaped single jet simulations. Table 3-5 show physical properties of the continuous and dispersed phases for the experiments performed with rectangular nozzles and with circular nozzles respectively.

Table 3-6: Nozzle dimensions used for simulations.

Nozzle No.	X (mm)	Y (mm)	AR(--)	D_H (mm)	A_0 (mm^2)
1	3.00	3.33	1.11	3.16	10.0
2	2.00	5.00	2.50	2.86	10.0
3	1.30	7.70	5.92	2.22	10.0
4	1.00	10.00	10.00	1.82	10.0

Four different size of rectangular nozzle (Table 3-6) were employed in the simulation to study effect of aspect ratio on the jet breakup and droplet formation and also Table 3-7 shows inlet configurations for the rectangular nozzle in the simulations.

Table 3-7: Inlet configurations for rectangular nozzles.

Width	Depth	Schematic	Aspect ratio
3 mm	3.33 mm	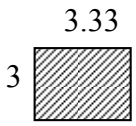	1.11
2 mm	5 mm	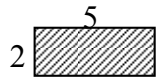	2.5
1.30 mm	7.70 mm	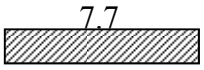	5.92
1 mm	10 mm	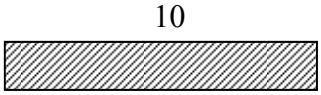	10

3.3 Summary

The experimental and simulation methodologies have been presented in this chapter. Step by step methods have been carried out to acquire experimental data from all the experiments. Simulations methodologies have also been discussed in details to describe primary methods of computational domain and selection of model to carry to study emulsification process simulations. In addition, Grid independency and boundary conditions for the simulations are critical for the analysis. The VOF method emerged as the model of choice for the numerical study over other numerical methods. As mentioned in the Table 3-4 that merging and breakage of interface occurs automatically as interfacial tracking is the focus of our study.

Chapter 4. Single Jet

Experiments on single jet have been carried out to study dripping, jetting and jet breakup phenomena of water jet in canola oil for single jet system and analysis of the results have been discussed in this chapter. Single jet breakup have been captured using high speed camera at 125 frames per second. Moreover, CFD simulations have been use for dripping, jetting and jet breakup analysis has been carried out for single jet system. In the second part of this chapter, CFD simulations have been further used to analyse the effects of aspect ratio and volumetric flow rate on resultant droplet size for rectangular nozzle. Single jet immiscible liquid system has been examined for instability during emulsification and hence the effect of instability on emulsion quality has been discussed in the final part of this chapter. The CFD simulation results have been analysed to study the effects of instability on jet breakup, droplet formation and size of resultant droplets.

4.1 Experiments on jet and drop formation

Droplet formation process at low flow rates were carried out to study the effect dimensionless numbers on the jet breakup length and size of the droplet. Reynolds number and Weber numbers were calculated for the single jet experiments and plotted against dimensionless droplet diameter and dimensionless jet breakup length. Steep increment in the size of mean droplet diameter was observed for higher Reynolds numbers.

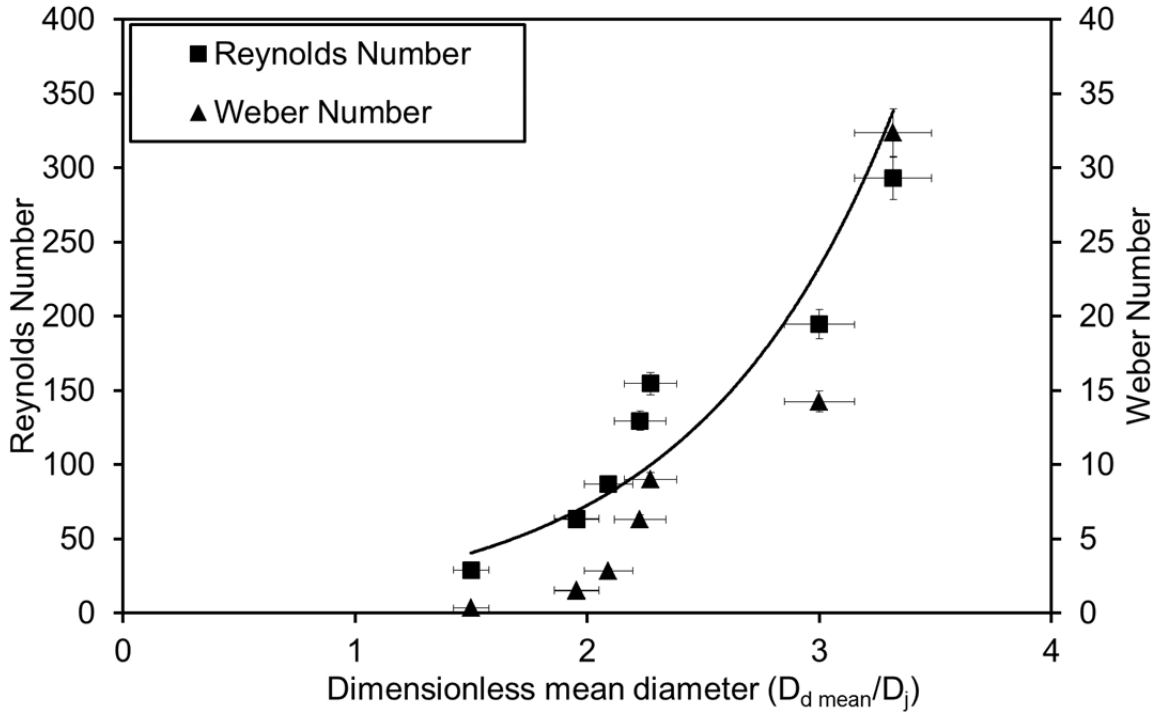

Figure 4-1: Effect of dimensionless number (Reynolds Number and Weber Number) on the dimensionless mean droplet diameter (Normalised by initial jet diameter D_j). 20 droplets were averaged for each condition.

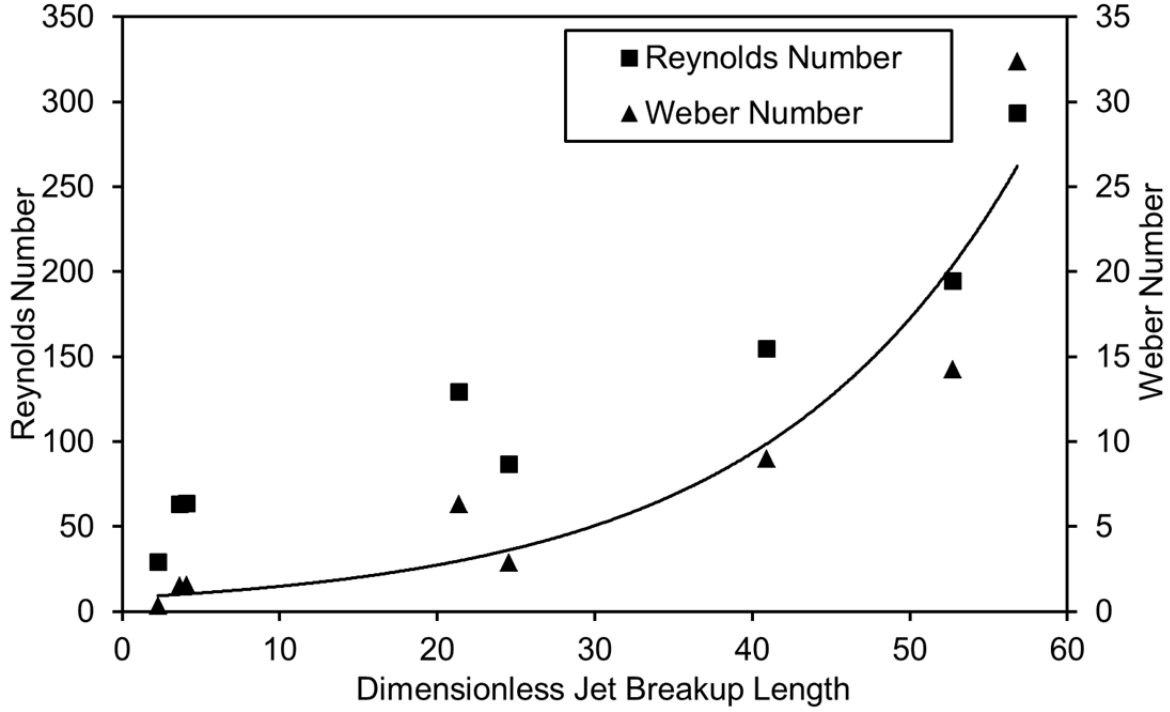

Figure 4-2: Effect of dimensionless number (Reynolds number and Weber number) on the dimensionless jet breakup length (Normalised by initial jet diameter D_j). 20 droplets were averaged for each condition.

Figure 4-1 shows that increasing Reynolds and Weber numbers leads to increment in dimensionless mean droplet diameter. Steep increment in the size of mean droplet diameter was observed for higher Reynolds and Weber number (specifically after Reynolds number >200 and Weber number> 20). Moreover, Figure 4-2 shows increment in jet breakup length with Reynolds and Weber number increase. The CFD simulations results for single jet system were compared to the data obtained from the experiments to validate the simulation method. Figure 4-3 show regular droplet formation directly at nozzle tip and Figure 4-4 demonstrates the step-by-step sequence of the drop formation for the dispersed phase used in the simulations. Good agreement was evidenced (Figure 4-4) between the results obtained from the CFD simulations and the experimental results for the drop formation sizes in different heights of the column.

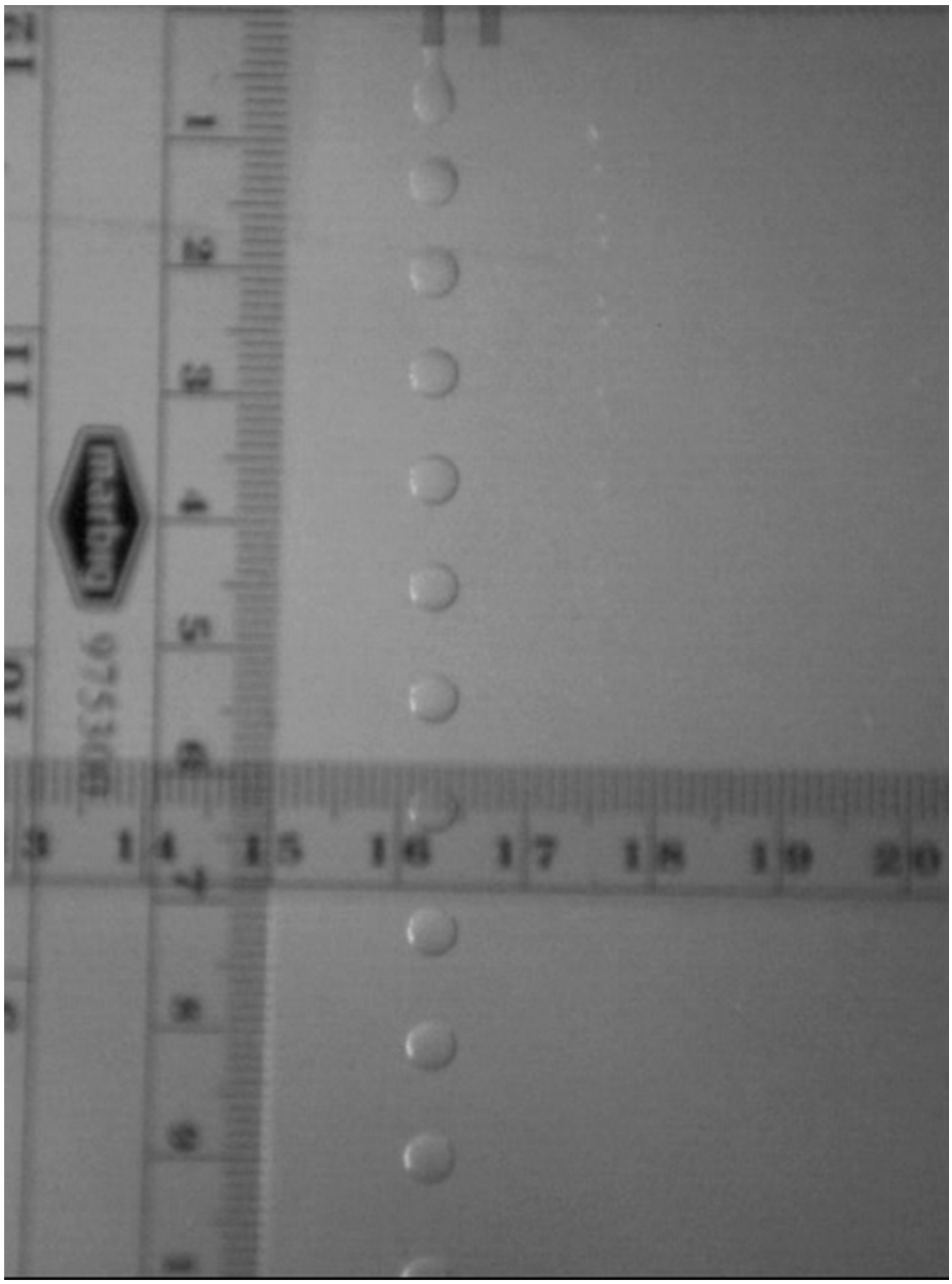

Figure 4-3: Droplet formation from nozzle tip at low flow rate.

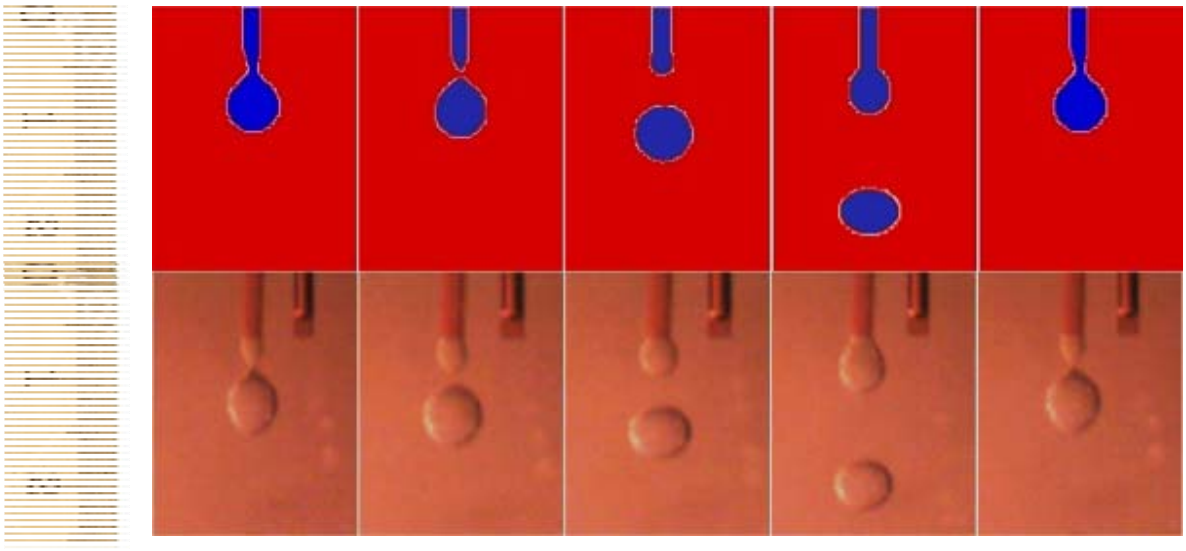

Figure 4-4: Sequence of drop formation for the single jet system, CFD simulation (top row) experimental observations (bottom row) at Q_{av}=124 mm^3/s.

4.1.1 Jet breakup and droplet formation

Single dispersed jet inside the continuous canola oil phase was further studied by increasing flow rate. Regular jet breakup was observed at flow rates below 831 $\pm$ 50 mm^3/s. Irregularity in droplet breakup were experienced at higher flow rates. The irregularity in break up phenomena and droplet formation was investigated for the water and canola oil system.

Phan and Evans (Phan and Evans 2008) performed experiments on immiscible liquid-liquid system of glucose-water solution and canola oil. Computation fluid dynamics simulation of the same system was carried out for the understating of jetting and jet breakup phenomena as well as droplet formation. Initially, droplets were formed at the nozzle tip and no jet was observed as seen in Figure 4-5 (a). As shown in Figure 4-5(b-c), jet was formed and transformed from rectangular to circular shape as travelling downwards. Jet diameter remained stable until it breakup into droplets. Jet length increased with increasing flow rate in Figure 4-5 (*b*) and (*c*). Figure 4-5 (d) was taken 150 mm below the nozzle opening as jet length is higher than all cases.

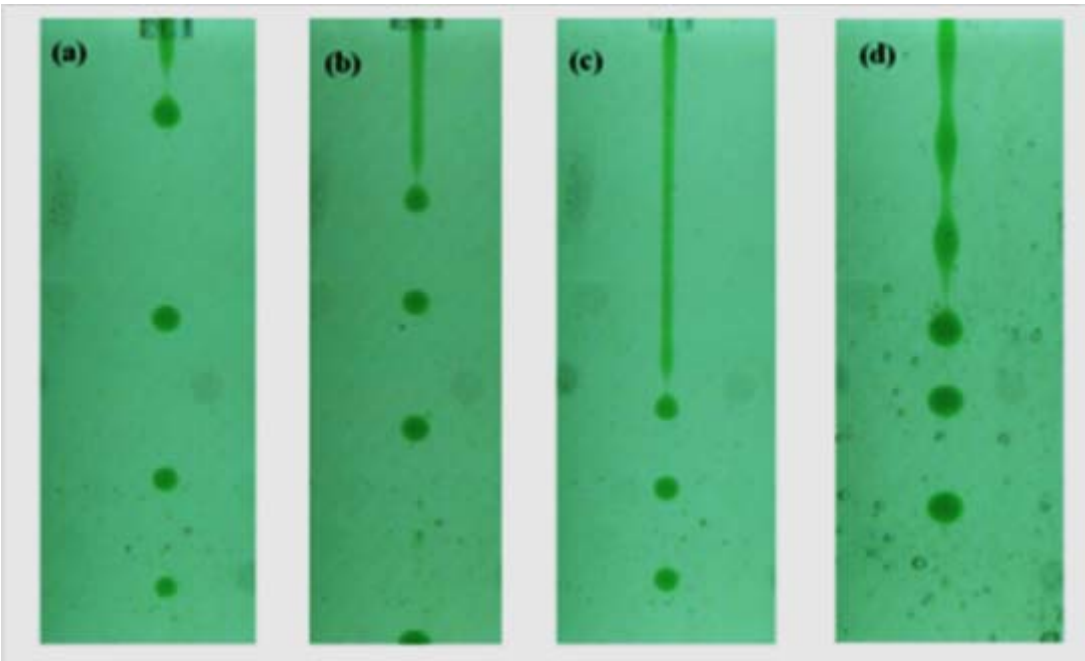

(a) *(b)* *(c)* *(d)*

Figure 4-5: Droplet formation at different flow rates (Q_{av}>831 mm^3/s) (Phan and Evans 2008).

4.1.2 Influence of pressure gradient and jet flow rate on instability, jet breakup and droplet size

There were two different types of instabilities found during jet breakup at high flow rates range (Q_{av}>1252 mm^3/s). First, axisymmetric instability and the other one was asymmetric (non-symmetric) growth, i.e. "swinging phenomena of the jet", before breaking up into droplets. It is noteworthy that the breakup mode for the phenomena has not been reported in the literature. Moreover, droplet diameter and jet breakup length were greatly influenced by these instabilities, higher droplet size was observed during single jet breakup. In Figure 4-6 droplet diameter for single were plotted against average volumetric flow rate. For single jet, droplet diameter was found to increase linearly until 800 mm^3/s. Further, nonlinear escalation in droplet diameter had become evident for average volumetric flow rate above 800 mm^3/s. Also shown is the theoretical (Teng, Kinoshita et al. 1995) droplet size of 4.33 mm for a stationary jet (based on an observed jet diameter of 2.2 mm and physical properties given in (Table 4-1); which is smaller than droplet diameter for single jet. Thus it can be concluded that the single jet cannot produce smaller droplet size.

Equation 2.16 was used to calculate theoretical droplet diameter of 4.33 mm. The origin of surface deformation (wave like formation as a horizontal component) taken place before the break-up, which is consistent with theory. The breakup is governed by exponential growth of this wave formation.

The existence of swinging phenomena can be explained by pressure gradient generated around the jet during the jet formation process and droplet breakup process inside the continuous phase. Induced pressure gradient between neck and swell region of the jet cause fluid to flow from neck to swell region of the jet which generate instability along the jet (Goedde and Yuen 1970). Magnitude of these instabilities was further amplified by interfacial properties of continuous phase liquid together with higher volumetric flow rate resulted in jet swing. As shown in Figure 4-9 (a), instability was not evidenced at lower flow rate. However, jet observed instability at higher flow rate which is shown in Figure 4-9 (*b*). Jet breakup length and droplet diameter against average jet flow rate for single jet are reported in Table 4-1.Experimental data can be found in Appendix 7.1.

Table 4-1: Jet breakup length, droplet diameter versus average jet flow rate for single jet.

Q_{av} (mm^3/s)	d_d (mm)	L_3 (mm)
124	**3.3**	**5**
270	**4.3**	**8**
272	**4.3**	**9**
514	**4.6**	**54**
553	**4.9**	**47**
660	**5**	**90**
831	**6.6**	**116**
1252	**7.3**	**125**

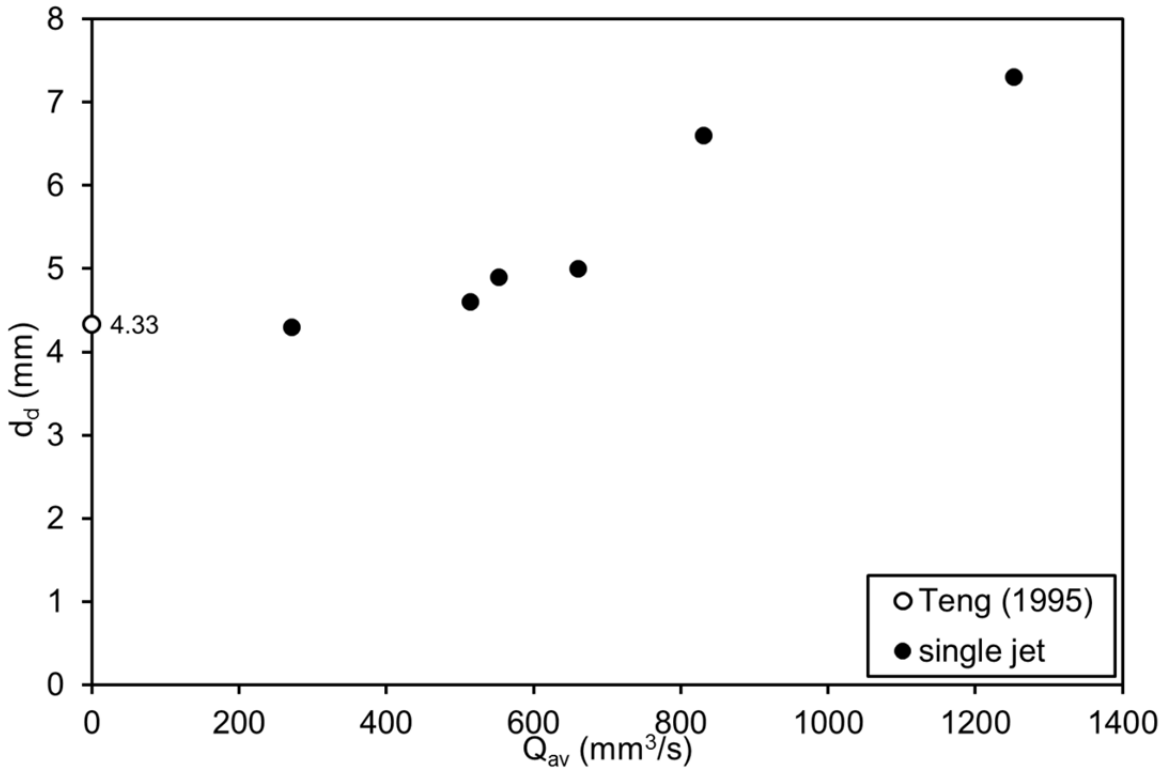

Figure 4-6: Droplet diameter versus jet flow rate for the single jet.

4.1.3 Influence of jet flow rate on jet breakup length

Jet breakup length, L_3, versus jet flow rate, Q_{av}, is shown in Figure 4-7 for the single jet. Single jet analysis was done and results are shown as filled circles in Figure 4-7. Jet breakup length found to increase with jet flow rate for all measured flow rates. However, breakup length was not increasing rapidly at higher flow rate which can be seen as plateau of the breakup length for single jet system. Further increasing the flow rate may give more information regarding this plateau.

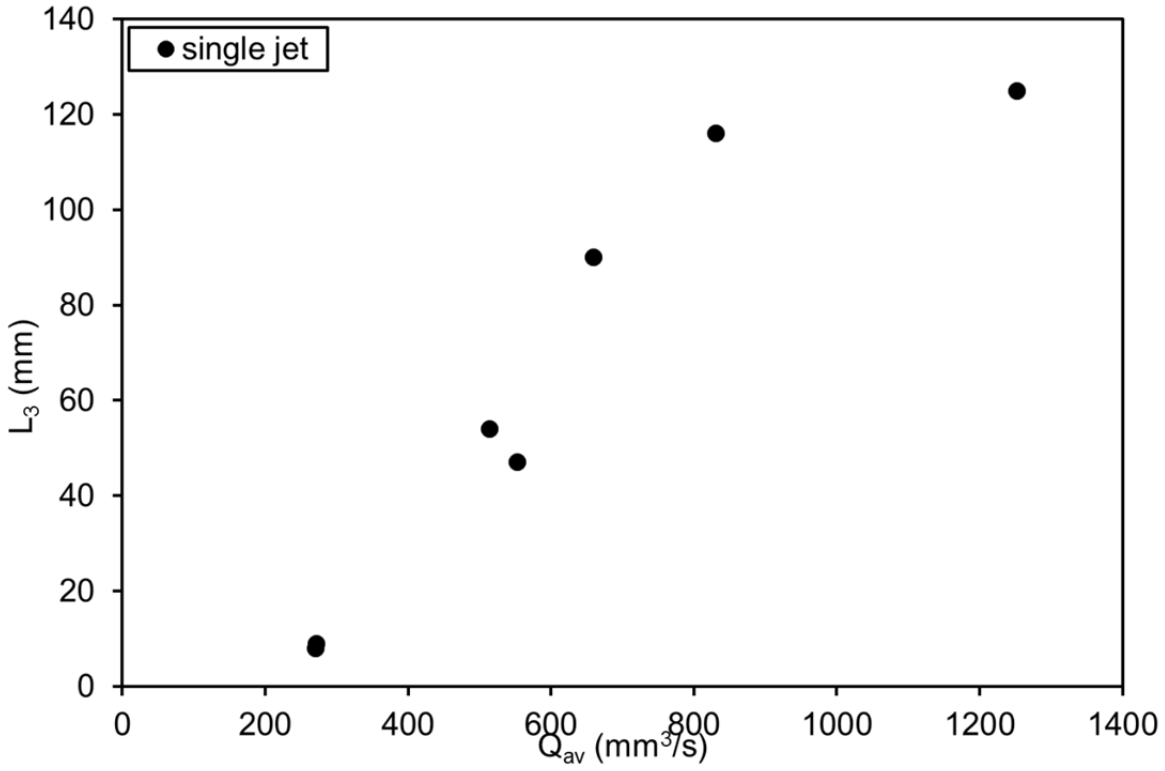

Figure 4-7: Jet breakup length versus jet flow rate for the single jet.

4.1.4 Influence of jet breakup length on droplet diameter

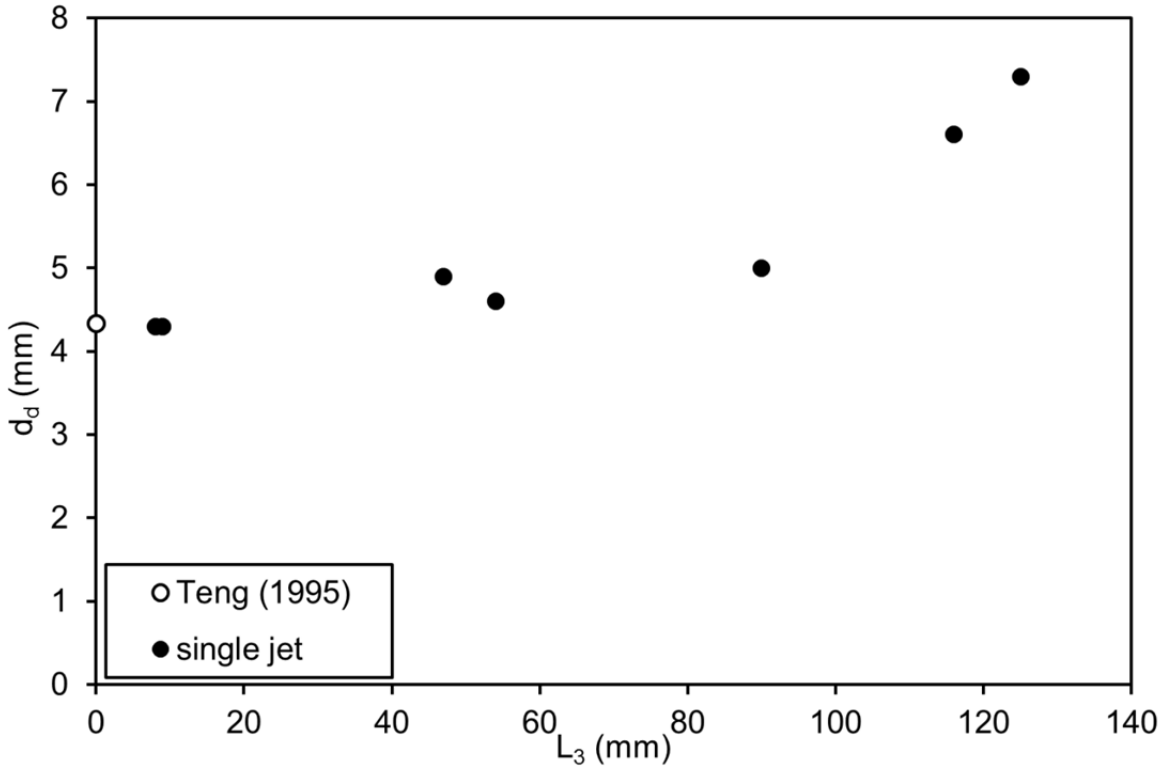

Figure 4-8: Droplet diameter versus jet breakup length.

In Figure 4-8, it was indicated that both the breakup length and resultant droplet diameter varied as a function of flow rate Q_{av}. In Figure 4-8, droplet diameter has been plotted as a function of the jet breakup length. It can be seen that, for the range of experimental conditions examined at least, d_d exhibited a linear relationship with L_3. Moreover, the measurements were consistent with the theoretical droplet size of Teng, Kinoshita et al. (1995) at zero jet breakup length. For single jet analysis, linear relationship is observed for lower jet breakup length (lower flow rates). However, non-linearity observed at higher breakup length (higher flow rates).

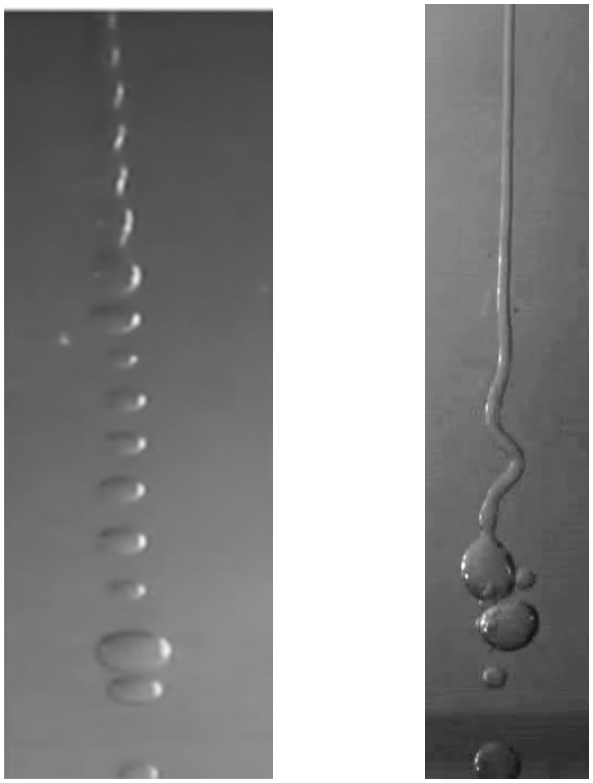

(a) *(b)*

Figure 4-9: Single jet experiments at different flow rates (*a*) Single jet (Q_{av} =831 $\pm$ 50 mm^3/s) (*b*) Single jet experiencing swing (Q_{av} ~ 1252 ± 50 mm^3/s).

4.2 Simulation results and discussions

Computational fluid dynamics simulations were run for various types of nozzles and parameters as follows:

1. Two dimensional simulations for rectangular nozzle with different aspect ratio at lower *Q*.
2. Three dimensional simulations for the above system
3. Three dimensional simulations for circular nozzles at higher *Q*'s.

Rectangular and circular nozzles with different sizes and aspect ratios (for rectangular nozzle) were simulated using computational fluid dynamics. Moreover, *2d* simulation were run initially and compared with *3d* simulations. As jet transformed from rectangular to circular at the point of jet breakup and droplet

formation at higher flow rates, only circular nozzles were simulated to quantify asymmetric instability. Single jet asymmetric deformation at higher volumetric flow rate was under microscope while running simulations and special attention was given to understand these phenomena with the help of hydrodynamics simulations.

4.2.1 Comparison of 2d, 3d model with experimental observation on rectangular nozzle

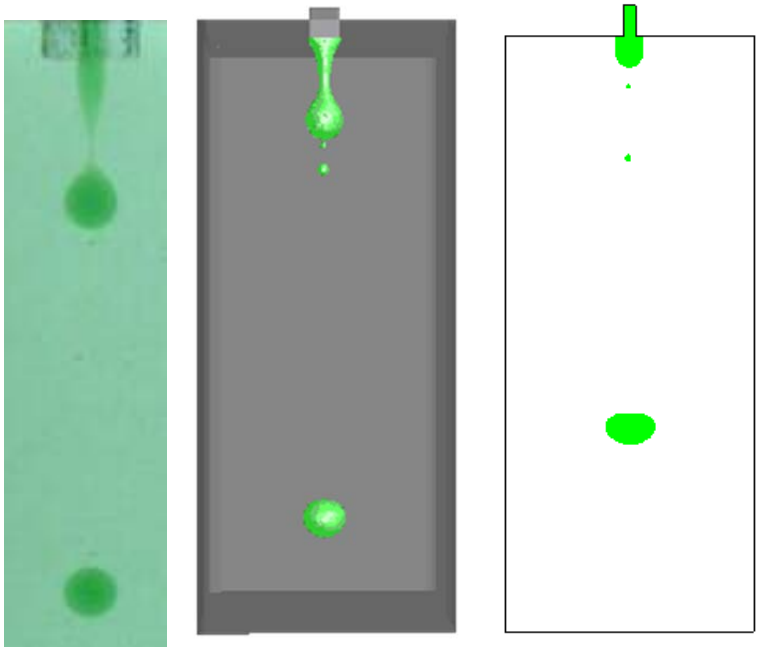

(a) *(b)* *(c)*

Figure 4-10: Instantaneous volume fraction of dispersed phase in continuous phase [*AR*=2.5, *Q*=100 mm^3/s] (*a*) experimental (*b*) *3d* model and (*c*) *2d* model.

Comparison of droplet formation between experimental observations and contours produced from CFD simulation are vitally important for the modelling perspective. Phan C. et al (Phan and Evans 2008) performed experiments on the water-canola oil system and CFD simulations were performed on the same system. Figure 4-10 represent and compares experimental observations (*AR* 2.5 Q 100 mm^3/s) with *2d* and *3d* simulations. It can be clearly seen that even qualitatively the *3d* model gave a better agreement to experimental results. In addition, it is worth noting that the jet formed from the rectangular inlet transforms to a circular shape thus, the shape of the droplet formed would be compromised if the *2d* model were used. Furthermore, it

was observed during the course of the simulations that with a given set of boundary conditions, the trajectories of droplets of the dispersed phase in *2d* simulations were inconsistent when compared with the experimental data. Although, this condition was overcome by using a wall boundary condition on the side but this assumption would compromise the physics of the system. Thus, it can be concluded that the *2d* model would not appropriately represent the current experimental system, and it is only appropriate to use the *3d* model for further investigations.

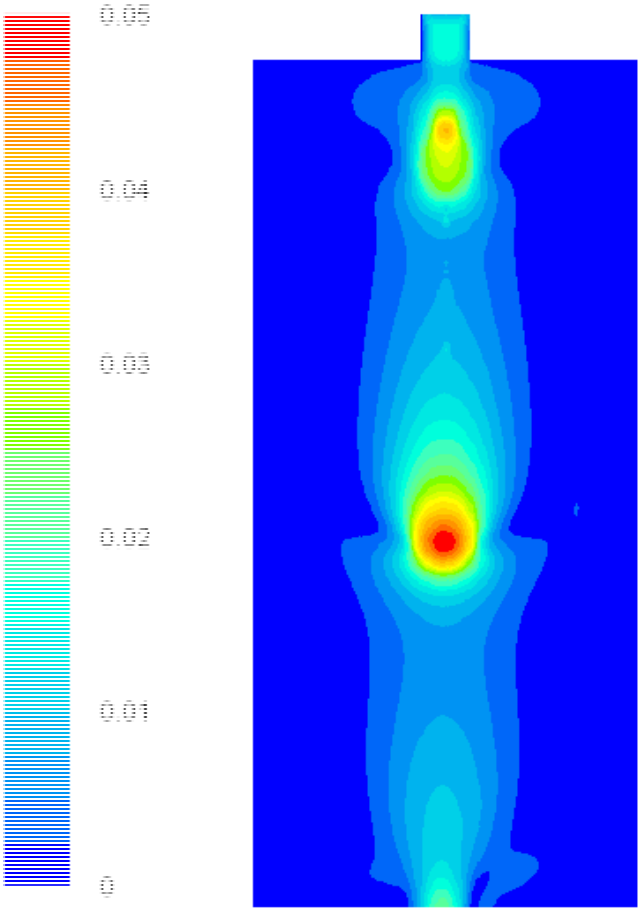

Figure 4-11: Contours of velocity magnitude for the flow pattern visualisation around broken droplets [AR=2.5, Q=100 mm^3/s].

Vertical component of velocity was dominant at the breakup. Therefore, previous approaches (e.g., Homma et al., 2006 (Homma, Koga et al. 2006); Richards et al., 1995(Richards, Beris et al. 1995)) of using *2d* axisymmetric models in order to

reduce the computational costs are not appropriate for noncircular jets and only the *3d* model simulations were used for the remainder of the study.

3d model of jet breakup into droplets can be further explained for flow pattern around the broken droplet. As shown in Figure 4-11 , flow pattern is shown as velocity contours.

4.2.2 Effect of volumetric flow rate on equilibrium jet diameter

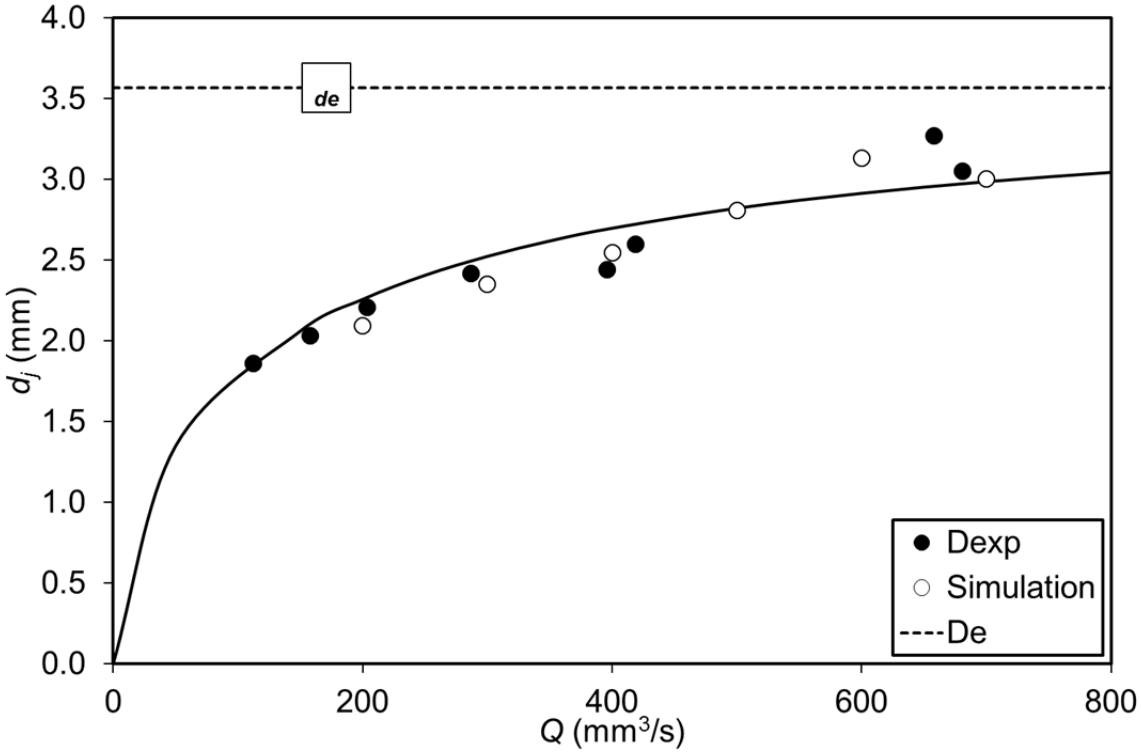

Figure 4-12: Equilibrium jet diameter versus liquid volumetric flow rate.

As discussed above, *3d* model simulations were utilised to determine the influence of volumetric flow rate on the equilibrium jet diameter. Once the liquid was discharged from the nozzle, the jet underwent a transformation from a rectangular to a circular shape before eventually reaching a constant or equilibrium diameter. The time (length from the nozzle) it took to reach this value increased with increasing volumetric flow rate. Consequently, the simulated equilibrium jet diameter (open circles) reported in Figure 4-12 are values taken at different axial distances from the

nozzle, in the region where the diameter remained constant. Also shown in Figure 4-12 are the time-averaged experimental measurements (closed circles). It can be seen that the simulations were within 10% of the experimental measurements, which is within the expected variance given that the grid size was 400 μm.

Ideally, it would be useful to predict the equilibrium diameter as a function of volumetric flow rate. A simple approach is to assume that the jet superficial velocity, V_2, at the equilibrium diameter is given by the sum of the initial superficial velocity, V_0, plus some slip velocity, V_2, between the jet and the surrounding liquid, that is:

$$v_2 = v_0 + \Delta v_2 = \frac{Q}{A_0 + \Delta v_2} \tag{4.1}$$

Where, A_0 is the cross-sectional area of the jet at the nozzle. Applying continuity, the equilibrium jet diameter, d_e, can be related to the volumetric flow rate, that is:

$$Q = v_2 A = \left(\frac{Q}{A_0 + \Delta v_2}\right)\left(\frac{\pi d_e^2}{4}\right) \tag{4.2}$$

$$d_j = \sqrt{\frac{4QA_0}{\pi Q + \pi A_0 \Delta v_2}} \tag{4.3}$$

Equation 4.3 has been fitted to the experimental measurements and simulated results given in Figure 4-12, using a constant V_2 value of 0.03 m/s. It can be seen that there is good agreement over the range of measured diameters; and if Equation (4.3) can be extrapolated to very high volumetric flow rates then the jet diameter will approach the equivalent circular diameter of the nozzle, d_e, of 3.568 mm as the slip velocity becomes negligible when compared with the superficial velocity of the jet.

4.2.3 Effect of nozzle aspect ratio on equilibrium jet diameter

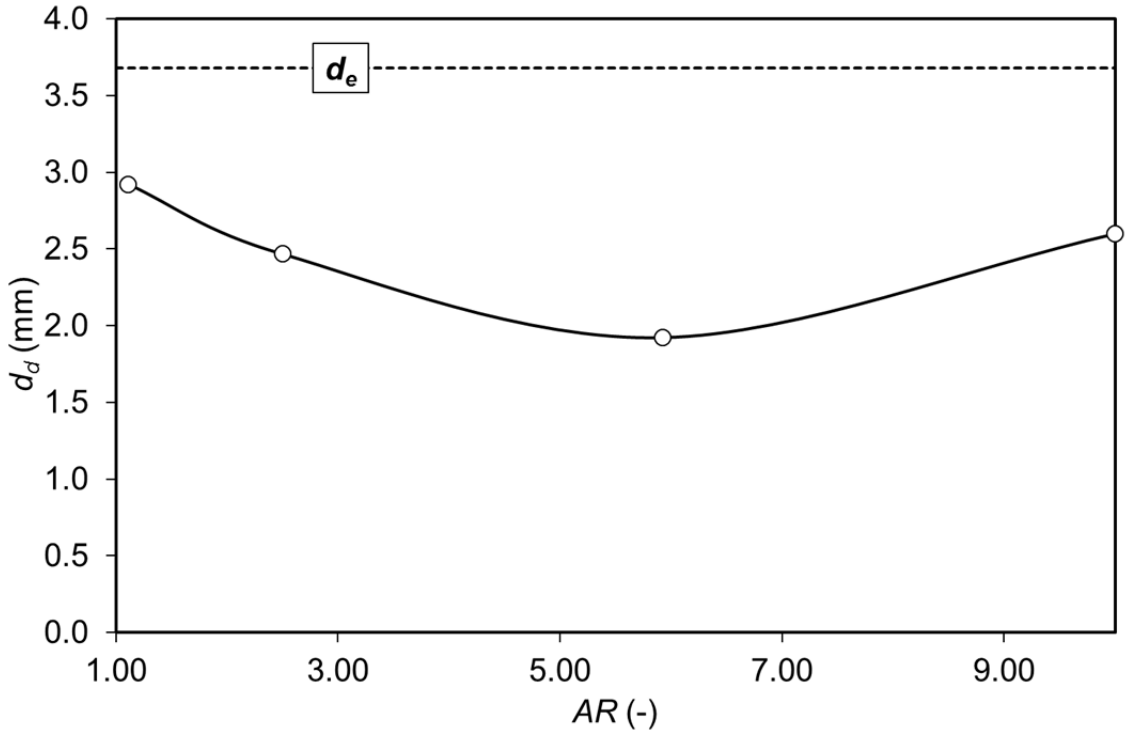

Figure 4-13: Equilibrium jet diameter versus nozzle aspect ratio.

Simulations were carried out to determine the equilibrium jet diameter as a function of nozzle aspect ratio, *AR,* at volumetric flow rate Q=400 mm^3/s. The results are shown in Figure 4-13.

It can be seen that the equilibrium jet diameter varied with *AR*, exhibiting a minimum equilibrium diameter in the range 5<*AR*<7. The reasons for the minimum are unclear. However, its existence raises the possibility that the geometry of a rectangular nozzle can be manipulated to minimise the resultant jet diameter, which according to Teng, Kinoshita et al. (1995) will result in a minimum droplet diameter, that is:

$$d_d = d_e \left(\frac{3\pi}{\sqrt{2}}\right)^{1/3} \left(1 + \frac{3\mu_2 + \mu_1}{\sqrt{d_e \sigma \rho_2}}\right)^{1/6} \quad (4.4)$$

Or

$$d \quad = d_e(1.882)\ \left(1 + \frac{0.167}{\sqrt{d_e}}\right)^{1/6} \tag{4.5}$$

Equation 4.4 has been used to estimate the breakup droplet diameter for the different nozzles, including circular nozzle, at Q=400 mm^3/s and using the measured equilibrium jet diameters given in Figure 4-13. The results in Table 4-2 show that for the same volumetric flow rate and cross-sectional flow area the droplet diameter can be reduced from about 8.4 mm to 4.7 mm, simply by changing from a circular to a rectangular nozzle. The analysis has shown that rectangular nozzles are indeed desirable as they can produce optimally smaller droplets with careful selection of the aspect ratio, typically in the range 5–7. Whilst there is increased pressure drop associated with the use of high aspect ratio rectangular nozzles, relative to circular nozzles, the disadvantage is balanced by the fact it is much easier to produce an array of rectangular nozzles than circular ones, especially for micro-devices (Hessel, Löwe et al. 2005)

Table 4-2: Estimated Droplet Diameter.

Nozzle No.	***AR(--)***	***d_d (mm)***
1	1.11	6.95
2	2.50	5.95
3	5.92	4.70
4	10.00	6.23
Circular	(D_0=3.57mm)	8.39

In summary, the *3d* CFD analysis was in good agreement with the experimental observations and showed that for given nozzle dimensions the equilibrium jet diameter increased with increasing volumetric flow rate. For each case, the jet underwent a transformation from a rectangular to circular cross-section prior to droplet breakup. It was also found that for a given liquid flow rate the equilibrium jet diameter was a function of aspect ratio. There appears to be an optimum aspect ratio of between 5 and 7 for generating minimum sized droplets that are approximately 30% less than for a circular nozzle with the same cross-sectional area.

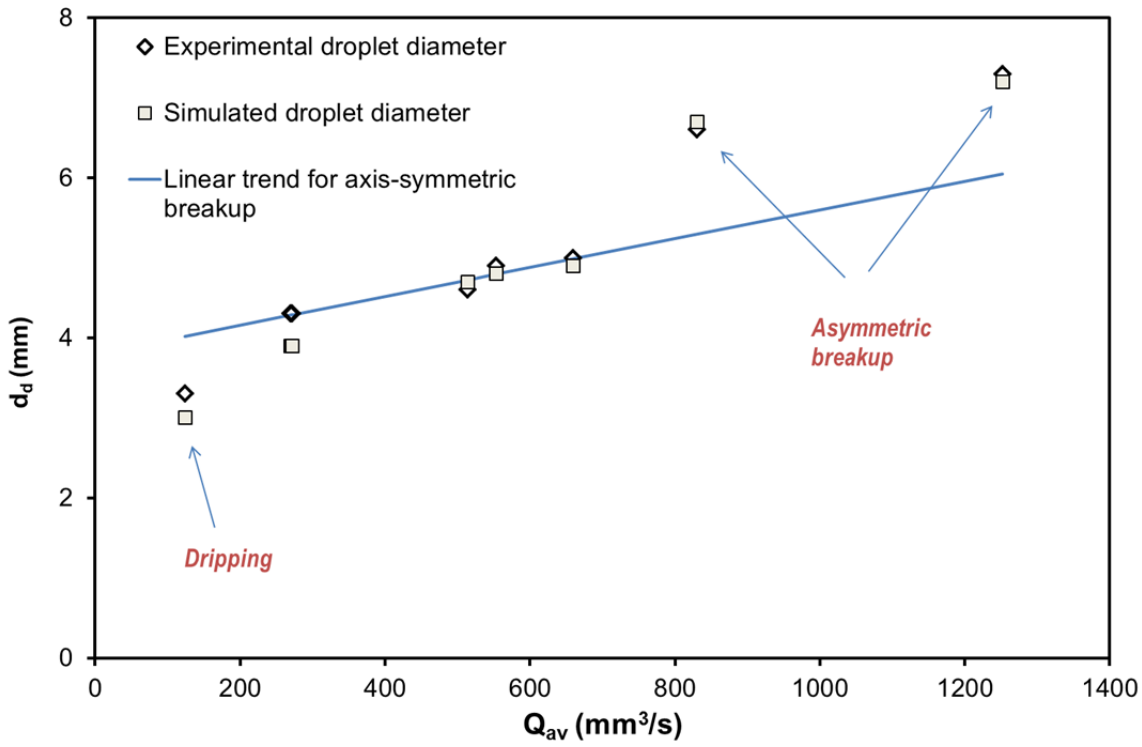

Figure 4-14 Comparison of droplet diameter obtained from experiments and CFD versus Qav for a single jet.

Figure 4-14 shows comparison of resultant droplet diameter from experiments and simulation as a function of volumetric flow rate. For the single jet, the experimental and CFD observations are in good agreement for all three regimes: dripping, axis-symmetric and asymmetric jet breakup.

4.2.4 Single jet instability

Computational fluid dynamics simulations were employed to validate asymmetric deformation for single systems. Instability was observed at the same flow rate range in single jet system. Simulation on single jet system was carried out and jet instability (swinging) was observed before the break up and this resulting into irregular breakup and non-uniform droplet size. A *XZ* plane in Figure 4-15 (A) shows "S" shaped instability on single jet at higher flow rate range. Slice plane was created along the jet length to observe instability. Mean volume fraction contours

Figure 4-15 (B)-(*a-d*) were taken to quantify the swing of jet along jet length. As shown in Figure 4-15, mean volume fraction was increased from 0 to 1, this means

the interface between continuous and dispersed phase is continuously moving. As "*a*" had no swing movement and there is no moving interface detected near the nozzle opening (40 mm from the continuous phase inlet). Subsequently, interface became evident further downward on the jet and hence instability was experience along the jet.

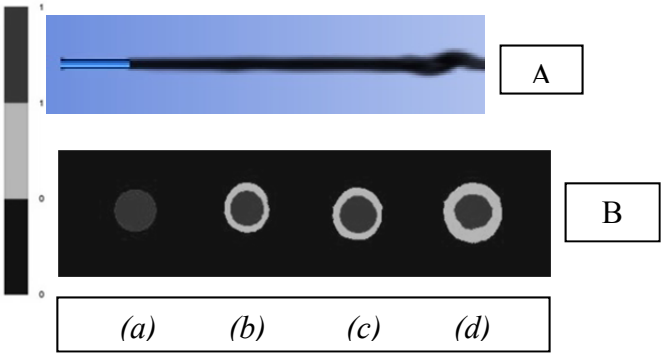

Figure 4-15: Single jet mean volume fraction on a *XZ* plane at (*a*) z = 40 mm (*b*) z = 55 mm (*c*) z = 70 (*d*) z = 85 mm.

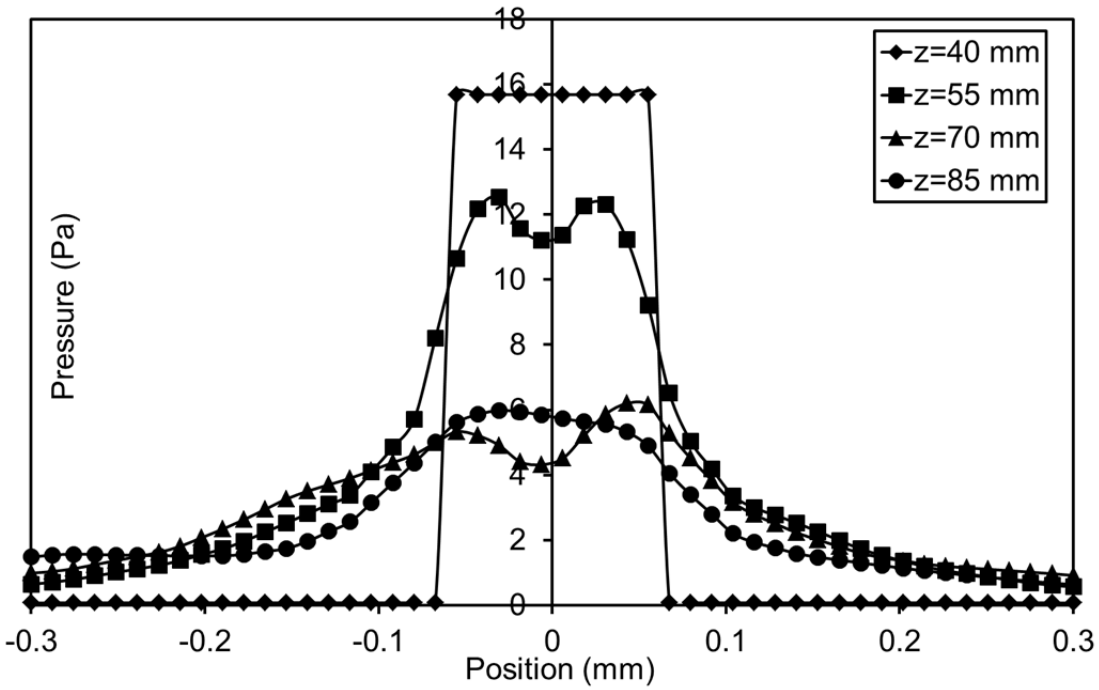

Figure 4-16: Single jet system pressure at 4 slice planes along the jet length.

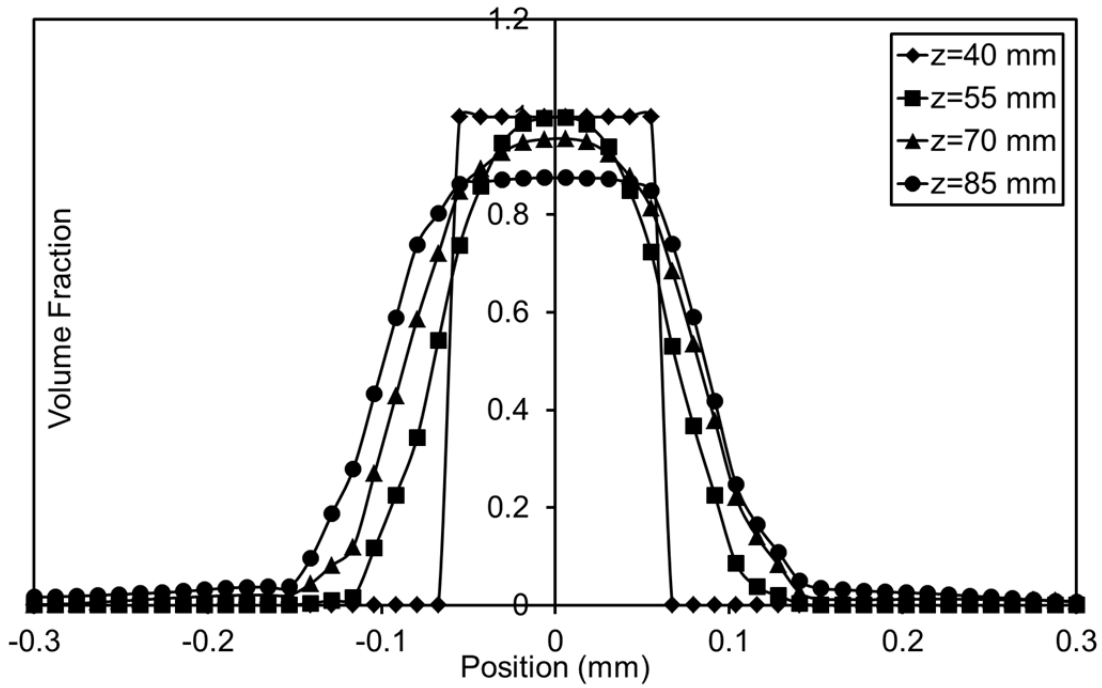

Figure 4-17: Single jet system mean volume fraction at 4 slice planes along the jet length.

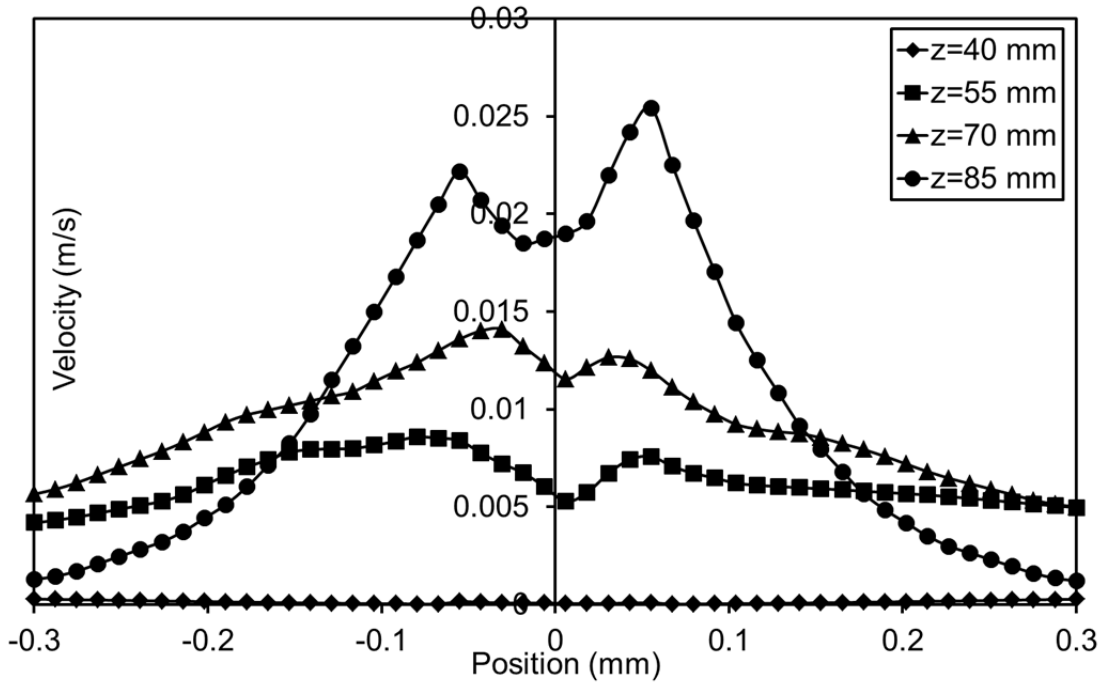

Figure 4-18: Single jet system u-velocity at 4 slice planes along the jet length.

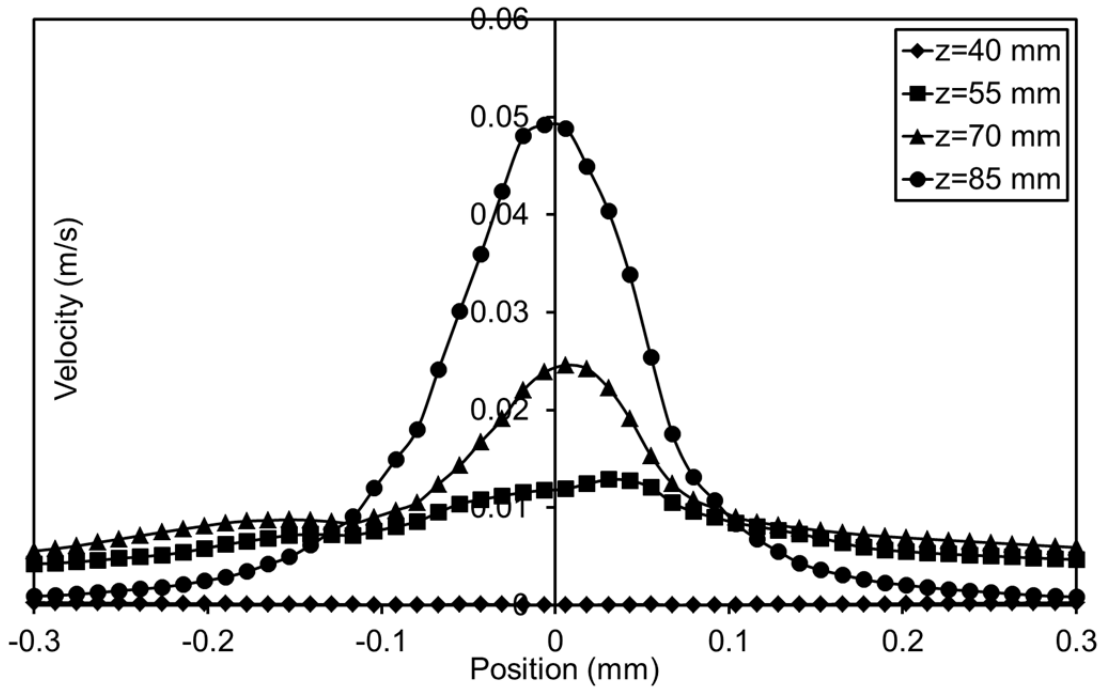

Figure 4-19: Single jet system *v-velocity* at 4 slice planes along the jet length.

Single jet system was further investigated to quantify swing jet behaviour. Four slice planes were employed to quantify the instability for single jet system. In Figure 4-16, Figure 4-17, Figure 4-18 and Figure 4-19 jet center position were displayed as position on the plane in order to visualise pressure, velocity and volume fraction distribution on the plane effectively. Pressure around the jet was plotted in Figure 4-16. It can be seen at 40 mm plane that there is narrow pressure distribution along the jets and hence no instability was observed at this plane. However, broader pressure distribution at 55 mm plane indicates the beginning of instability in the system. Further pressure distribution broadening observed at 70 mm and 85 mm plane indicates highest instability of the jet. Droplet size was negatively affected with this instability behaviour of the system and not desirable for smaller and uniform size of emulsion droplets. In double jet system, however, the pressure difference between in and outside of the interface tends to grow but overshadowed by jet-jet interaction forces.

Figure 4-17 shows the mean volume fraction of salt solution. Volume fraction contour are showing instability on planes at 55mm, 70 mm and 85 mm as contour for

at these planes are showing broader distribution. Jet movement at different slice planes which are corresponds to volume fraction contour in Figure 4-15 (B). These volume fraction contours showing stable jet at Figure 4-15 (B) (*a*). Instability was observed and shown in Figure 4-15 (B) (*b*), (*c*) and (*d*) as outer ring of the jet (grey colour). Figure 4-18 and Figure 4-19 shows horizontal and vertical velocity component named *u* and *v* velocities at different slice planes respectively. There is no instability observed on 40 mm plane. However, both *u* and *v* velocities experienced more fluctuations at when jet appears to be instable. Highest fluctuations were observed at 85 mm slice plane where jet became highly instable and these velocities and pressure fluctuations demonstrate jet asymmetric instability. The relative vertical movement between the jet and surround phase that give a rise to interfacial disturbance on the horizontal component. While the origin of the disturbance is not observable, the simulation verifies the breaking-up phenomena was governed by the growth of interfacial disturbance. The interfacial disturbance itself is influenced by the jet-jet interaction which is the focus of the next chapter.

4.3 Summary

Single jet droplet formation and jet breakup was studied experimentally and computationally for rectangular and circular nozzles. Moreover, single jet asymmetric instability was quantified computationally. Regular jet breakup was observed at flow rate below 831 $\pm$ 50 mm^3/s. Axisymmetric instability was observed at lower flow rate and produce regular breakup. On contrast, asymmetric or swing observed at higher flow rate. This produces irregular breakup with average droplet size larger than these from axisymmetric. The swings are not reported previously in the literature. This is unfavourable for any industrial operations involving emulsification. Jet deformations were observed as flow of the fluid from neck to swell region due to induced pressure gradient.

Magnitude of these instabilities was further amplified by interfacial properties of continuous phase together with higher volumetric flow rate resulted in jet swing. Computational fluid dynamic study of rectangular nozzle was in good agreement with the experimental observations and showed that for given nozzle dimensions the

equilibrium jet diameter increased with increasing volumetric flow rate. The experimental and simulation results in this Chapter confirm the hydrodynamics of the moving single jet and provide a foundation for multiple jets system.

Chapter 5. Multiple Jets

Multiple jet emulsifications, jet interaction phenomena, implication of jet interaction on jet breakup and droplet formation are vitally important area of study to understand emulsification process and achieve uniform size of droplets. In this chapter, the influence of jet interactions on multiple jets inside the continuous phase has been investigated by varying dispersed phase flow rate, nozzle diameter and number of nozzles. Experimental observations (Appendix 7.2) and computational fluid dynamics simulations have been performed and discussed to understand these phenomena in detail. The effects of critical distance between multiple jets on jet formation, jet breakup length and droplet size were also studied.

5.1 Experimental results

Typical interaction observed experimentally between two jets is shown in Figure 5-1 (*a*) in order to describe, several characteristics distance are defined as in Figure 5-1 (*b*). Initially, the jets are at a separation, X_1, equal to the spacing between the two nozzles. The surfaces of the two jets is relatively smooth and without any observable instabilities. Following the initial region of parallel motion the separation between the two jets appears to decrease. Additionally, at a distance, L_1, from the nozzle exit instabilities appear on the jet surface. The jets continue to move closer together until a relatively constant minimum separation, X_2, is reached at a distance, L_2. Beyond this distance the two jets moved in parallel and out-of-phase with the surface instabilities on each jet. At a distance, L_3, the breakup of both jets into droplets, with equivalent spherical diameter, d, was observed. Consequently, these characteristics distances were measured for different jet velocity (v) and different flow rate (Q).The characteristic lengths described in Figure 5-1 were determined for three jet average volumetric flow rates, Q_{av}. High-speed video recordings were taken over a period of approximately two seconds. The characteristic lengths were obtained from the video recordings. The images were also analysed to determine the number of droplets produced. This information was then used in conjunction with the equivalent spherical diameter, d, values to calculate the cumulative total volume, V. The slope of V versus time was used to calculate Q_{av}.

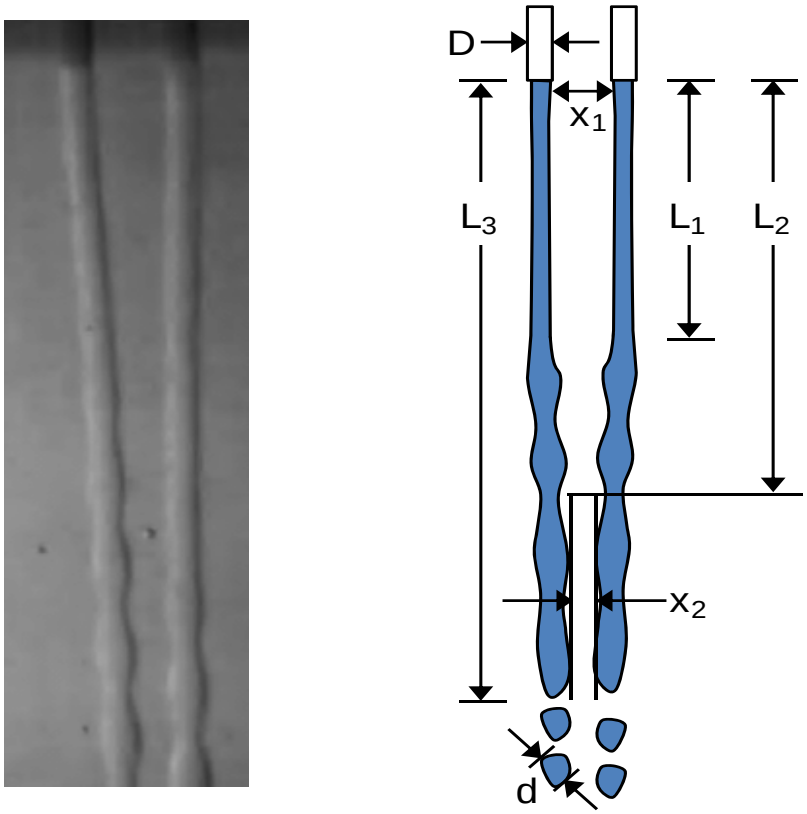

(a) *(b)*

Figure 5-1: Double jets system interaction and characteristic length.

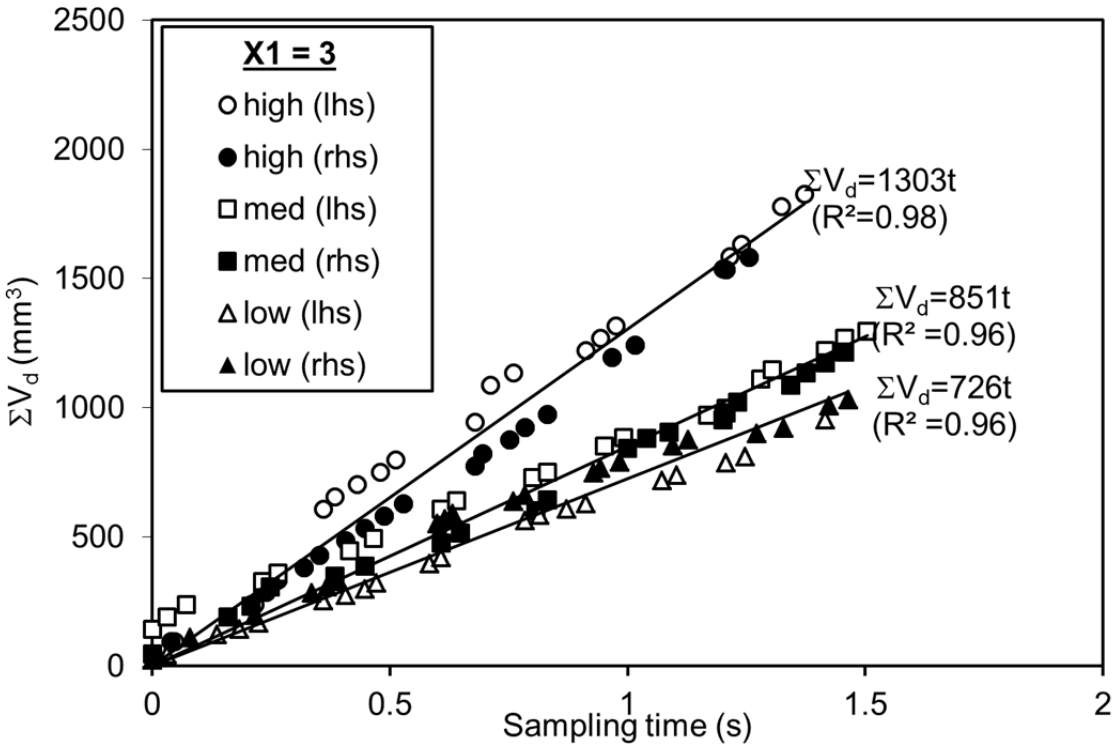
X1 = 3
high (lhs)
high (rhs)
med (lhs)
med (rhs)
low (lhs)
low (rhs)
ΣVd=1303t
(R²=0.98)
ΣVd=851t
(R² =0.96)
ΣVd=726t
(R² =0.96)
ΣVd (mm3)
Sampling time (s)
0
500
1000
1500
2000
2500
0
0.5
1
1.5
2

(a)

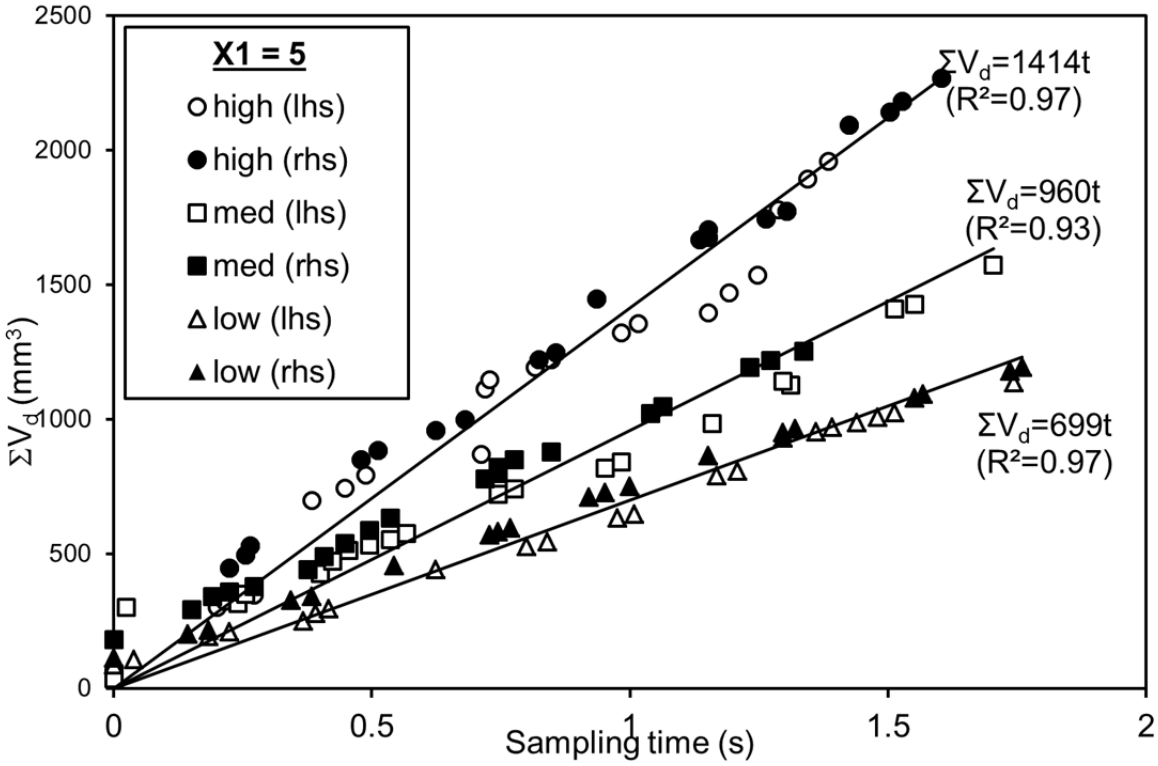
X1 = 5
high (lhs)
high (rhs)
med (lhs)
med (rhs)
low (lhs)
low (rhs)
ΣVd=1414t
(R²=0.97)
ΣVd=960t
(R²=0.93)
ΣVd=699t
(R²=0.97)
ΣVd (mm3)
Sampling time (s)
0
500
1000
1500
2000
2500
0
0.5
1
1.5
2

(b)

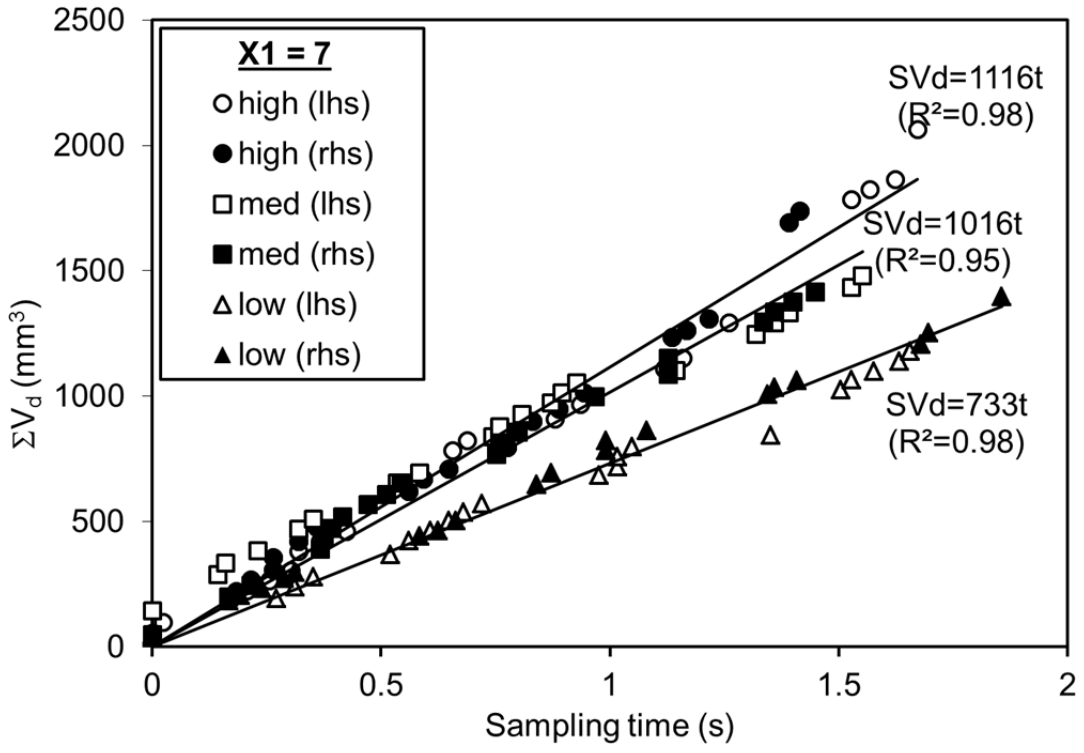

(c)

Figure 5-2: Cumulative droplet volume versus sampling time for different spacing between two jets *(a)* X_1=3 mm *(b)* X_1=5 mm *(c)* X_1= 7mm.

A typical result showing cumulative droplet volume for all three spacing between two jets and is shown in Figure 5-2 *(a) (b)* and *(c)* for two jets at three different average Q_{av} settings for X_1=3, X_1=5 and X_1=7 respectively. The two jets are nominally labelled as left (*lhs*) and right hand side (*rhs*), respectively; with supposedly the same constant jet flow rate for each jet attached to the common plenum chamber. In this analysis, droplet volumes were determined as an individual droplet. Subsequently, the accumulated volume of jet and all detached droplets were calculated as a function of time. The linear regression was then applied to quantify the flow rate (straight line in Figure 5-2 (*a*) (*b*) and (*c*)). Data was collected on both right hand side (*rhs*) and left hand side (*lhs*) jets to quantify symmetry of the system. Jet remained symmetric as shown in Figure 5-2 (*a*) (*b*) and (*c*) for all flow rates.

Table 5-1: Characteristic lengths versus average jet flow rate.

Q_{av} (mm^3/s)	X_1 (mm)	X_2 (mm)	d_d (mm)	L_1 (mm)	L_2 (mm)	L_3 (mm)
1303	3.0	2.0	5.5	65	15	99
851	3.0	2.0	4.9	11	21	59
726	3.0	2.0	4.6	11	13	41
1414	5.0	3.5	5.9	55	33	133
960	5.0	3.5	5.1	28	32	68
699	5.0	3.3	4.8	13	26	42
1116	7.0	5.0	5.7	50	40	148
1016	7.0	5.0	5.2	29	40	69
733	7.0	5.0	5.0	14	32	35

It can be seen that a linear relationship between cumulative volume and time was obtained (R^2>0.93) for each jet, indicating a constant volumetric flow rate. Differences of less than 10 per cent in the measured volume were observed between the two jets. The corresponding measured characteristic lengths, as shown in Figure 5-1 (b) are reported in Table 5-1 for each of the Q_{av} flow rates. It can be seen that for every experiment the spacing between the two jets, X_2, decreased from the initial separation distance. The jet length, L_2, at which the constant separation distance was attained increased with increasing initial (nozzle) separation distance, X_1, and largely independent of flow rate, Q_{av}. Both droplet diameter, d_d, and breakup length, L_3, decreased with decreasing Q_{av}.

5.1.1 Influence of jet flow rate and spacing on droplet diameter

Droplet diameter versus jet flow rate is shown on Figure 5-3 for the three different nozzle spacing. It can be seen that d_d is influenced by both Q_{av} and X_1. The droplet size increased with increasing Q_{av} for all three spacing; and is similar to that observed previously with a single jet(Phan and Evans 2008). Also shown is the theoretical (Teng, Kinoshita et al. 1995) droplet size of 4.33 mm for a stationary jet (based on an observed jet diameter of 2.2 mm and physical properties given in Table 3-2; which is greater than the extrapolated droplet diameter at Q_{av} = 0 for each of the

three nozzle spacing. Moreover, droplet diameter was higher for single jet analysis than two nozzle experiment. It appears that the jet-jet interaction resulted in a reduction in the droplet size, with the greatest reduction at the closest jet spacing of 3 mm.

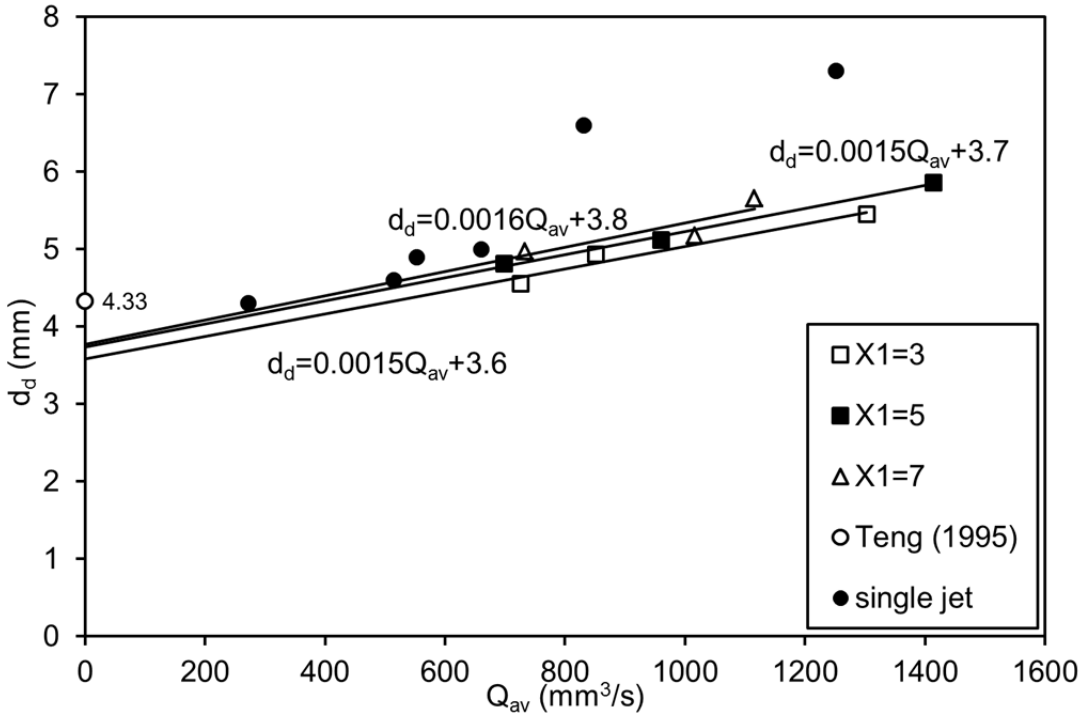

Figure 5-3: Droplet diameter versus jet flow rate and spacing between two nozzles.

5.1.2 Influence of jet flow rate and spacing on jet breakup length

Jet breakup length, L_3, versus jet flow rate, Q_{av}, is shown in Figure 5-4 for the three different nozzle spacing, X_1. For Q_{av} below 1000 mm^3/s it can be seen that L_3 for each of the nozzle separation distances was similar and exhibited a linear relationship, which is consistent with the single jet breakup length (Kitamura, Mishima et al. 1982) At higher flow rates, however, L_3 appeared to vary as a function of X_1, with L_3 increasing with increasing nozzle spacing. Single jet analysis was done and results are shown as filled circles in Figure 5-4. For flow rate below 1000 mm^3/s, Breakup length was found to decrease for two jets system when compared to the breakup length of single jet. Moreover, similar phenomena were observed at higher flow rates except for nozzle spacing X_1 = 7 mm. This is an

advantage for designing multi jet device as breakup length is reduced by placing multiple jets closer and higher number of droplets can be produced.

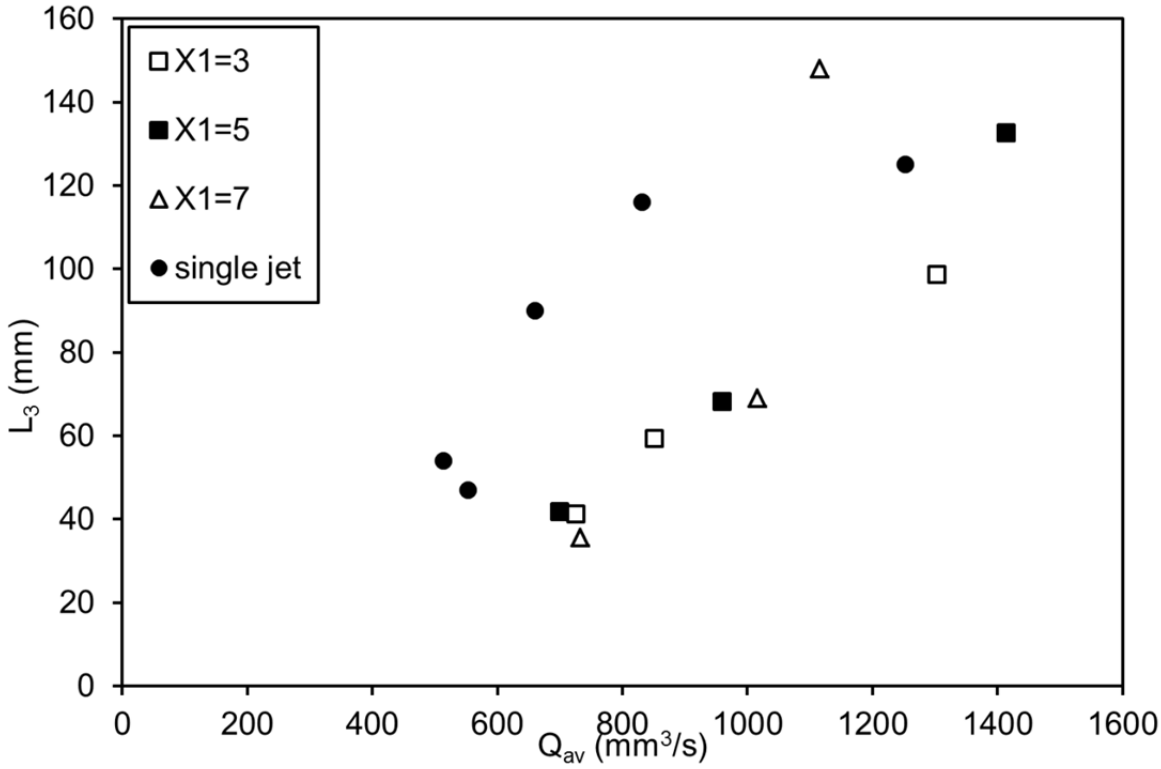

Figure 5-4: Jet breakup length versus jet flow rate and spacing.

5.1.3 Influence of jet breakup length and spacing on droplet diameter

In Figure 5-1(*b*) and Figure 5-5; it was indicated that both the breakup length and resultant droplet diameter varied as a function of both flow rate Q_{av} and nozzle separation distance X_1. In Figure 5-5, droplet diameter has been plotted as a function of the jet breakup length. It can be seen that, for the range of experimental conditions examined at least, d_d exhibited a linear relationship with L_3 that was independent of the nozzle separation distance. Moreover, the measurements were consistent with the theoretical droplet size of Teng, Kinoshita et al. (1995) at zero jet breakup length. For single jet analysis, linear relationship is observed for lower jet breakup length (lower flow rates). However, non-linearity observed at higher breakup length (higher flow rates).

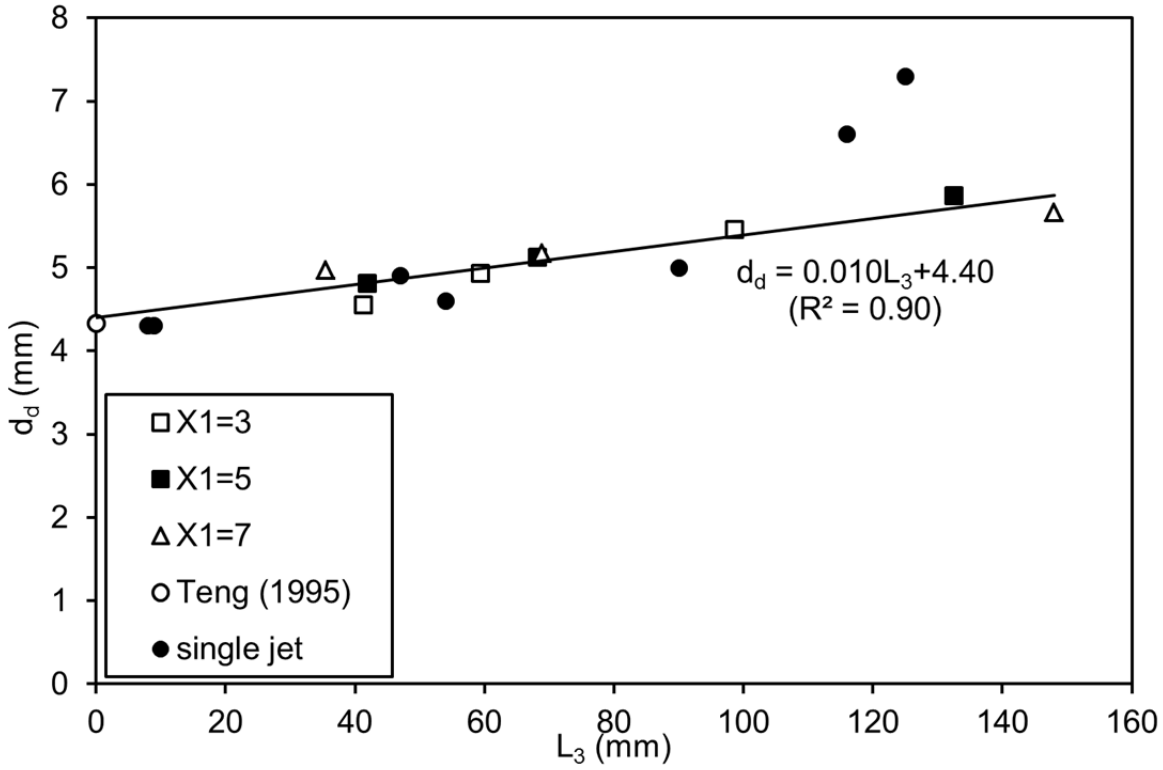

Figure 5-5: Droplet diameter versus jet breakup length and spacing.

5.1.4 Multiple jet interactions

Experiments on double jet system were carried out for understanding of jet-jet interaction in terms of in and out-of-phase breakup phenomena and its implications on jet breakup and subsequently droplet formation process. This can be explained with axial and radial component of velocity and critical distance between two jets. As discussed by Knops, Slot et al. (2001) that the observed that neighbouring threads may break up in-phase or out-of-phase. They employed principle of minimal dissipation of energy to approach the problem and found that the dissipation term due to the interaction of the thread depends on the relative distance $\hat{b} = b/a$ between the threads. Gunawan, Molenaar et al. (2002) agreed with the outcome of Knops, Slot et al. (2001) however, they seem to disagree with the principle of dissipation of energy and the value of critical distance between two jets.

Axial and radial component of the velocity for two adjacent jets is vitally important for in phase and out-of-phase deformation. Moreover, critical distance between two

jets is equally important. Experimentally, two jets were immersed into continuous phase and the distances between two jets were varied from 3 mm to 7 mm. As shown in Figure 5-6 in phase deformation was observed for 3 mm distance between two jets. However, this deformation transformed into out-of-phase near jet breakup point and droplets formed were at out-of-phase. However, out of phase deformation was observed for 5 mm and 7 mm distance between two jets (Figure 5-7, Figure 5-8) and Figure 5-9 explained radial and axial velocity component in the out-of-phase deformation.

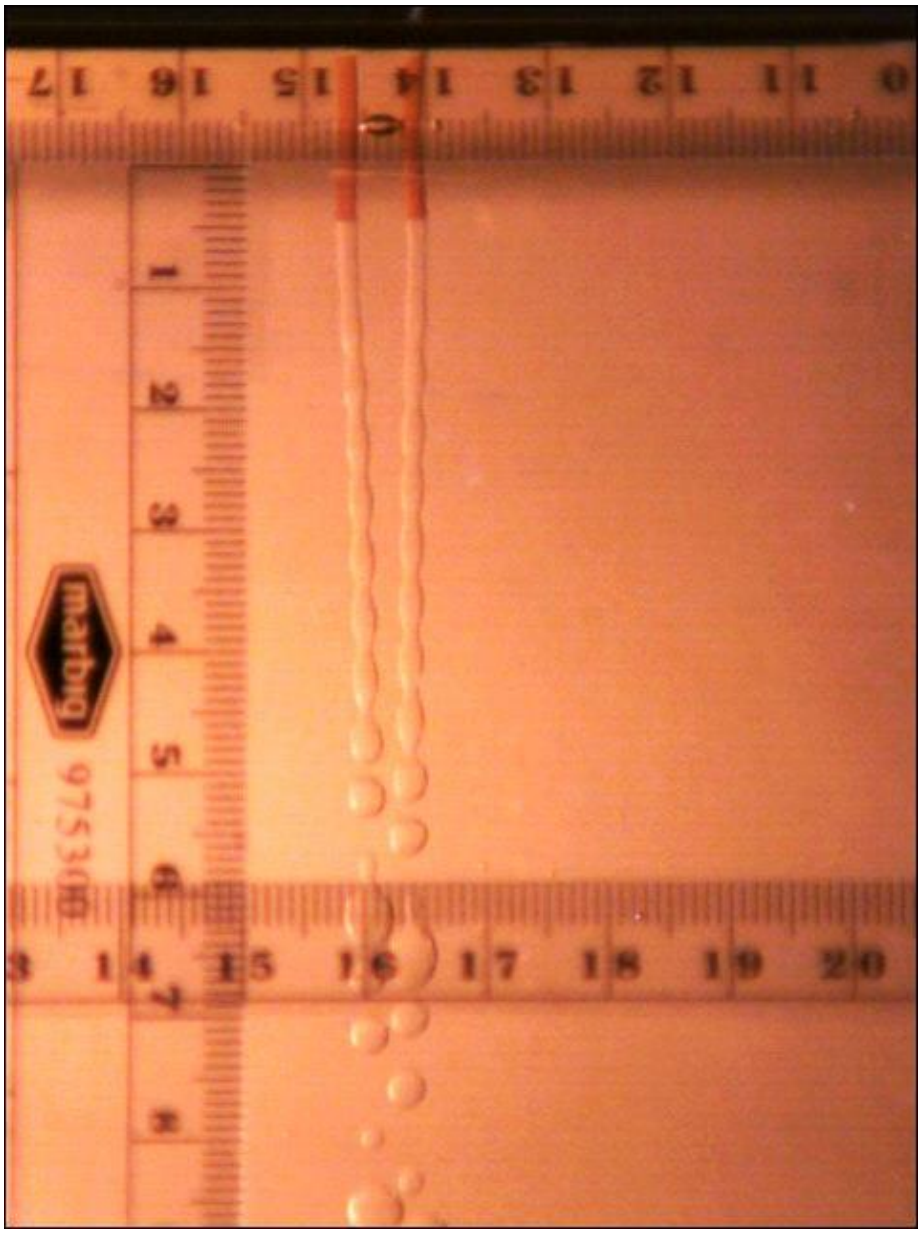

Figure 5-6: In- phase deformation between two adjacent jets (distance between two jets was 3 mm).

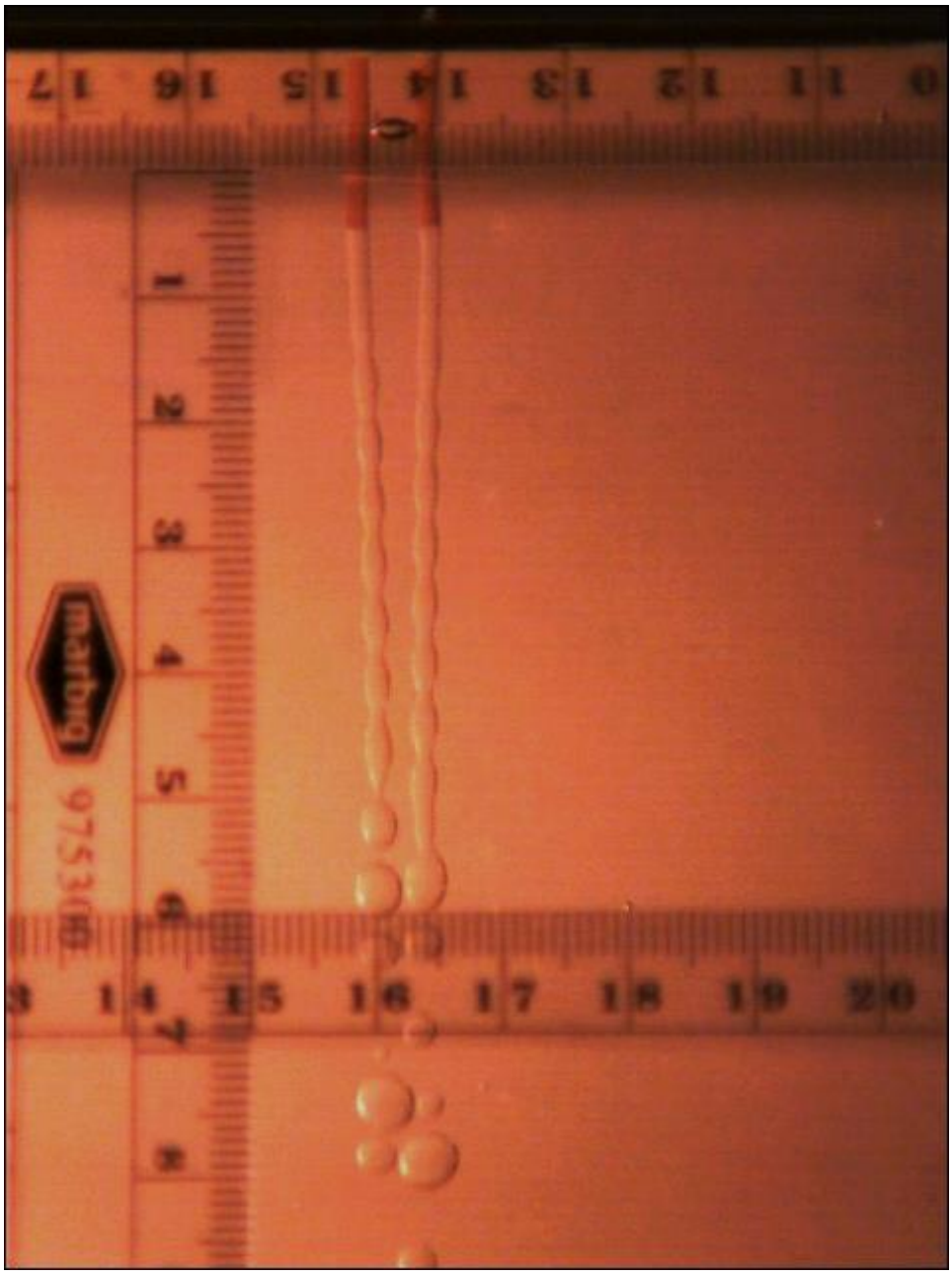

Figure 5-7: Out-of- phase deformation between two adjacent jets (distance between two jets was 5 mm).

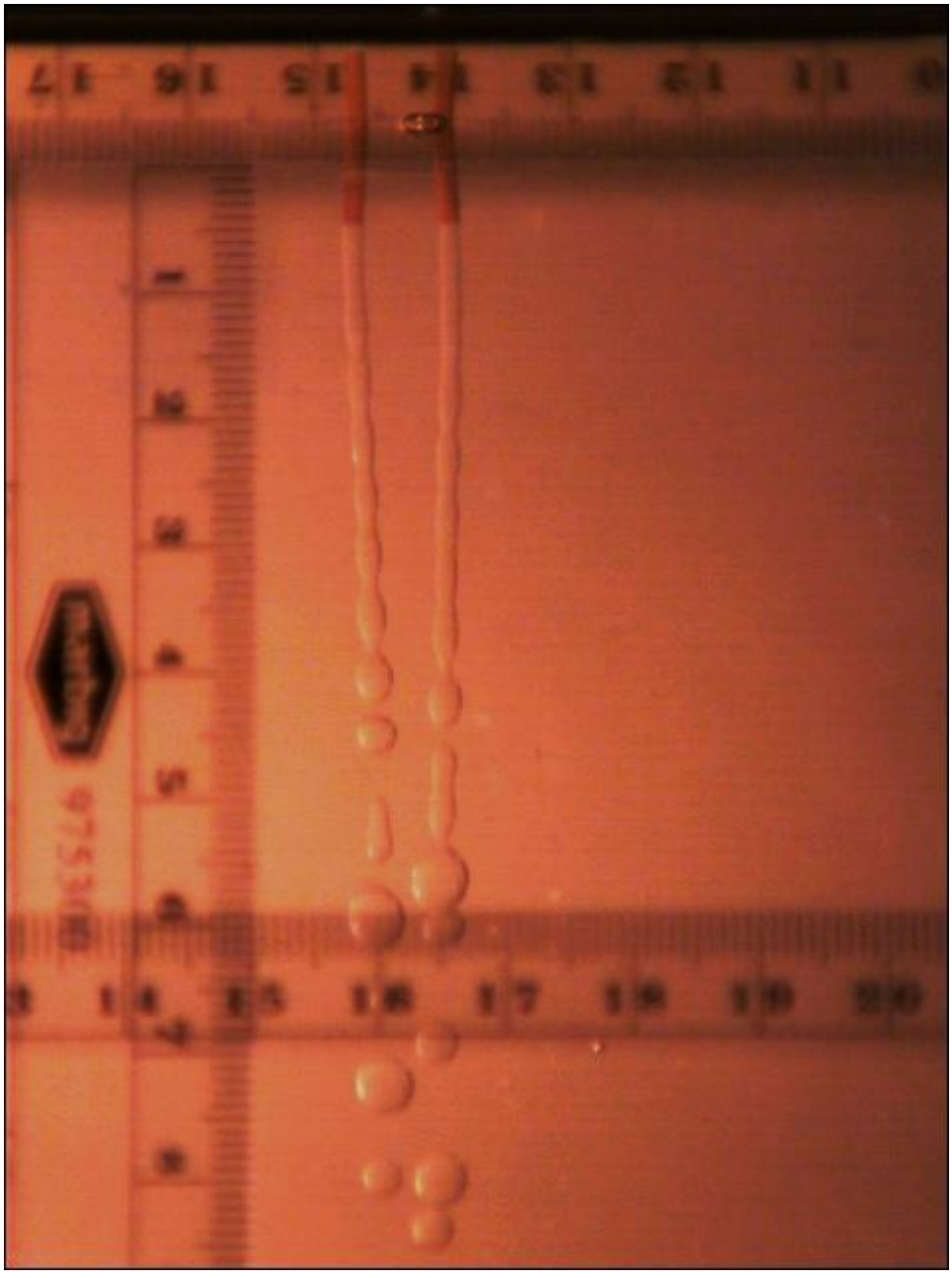

Figure 5-8: Out-of- phase deformation between two adjacent jets (distance between two jets was 7 mm).

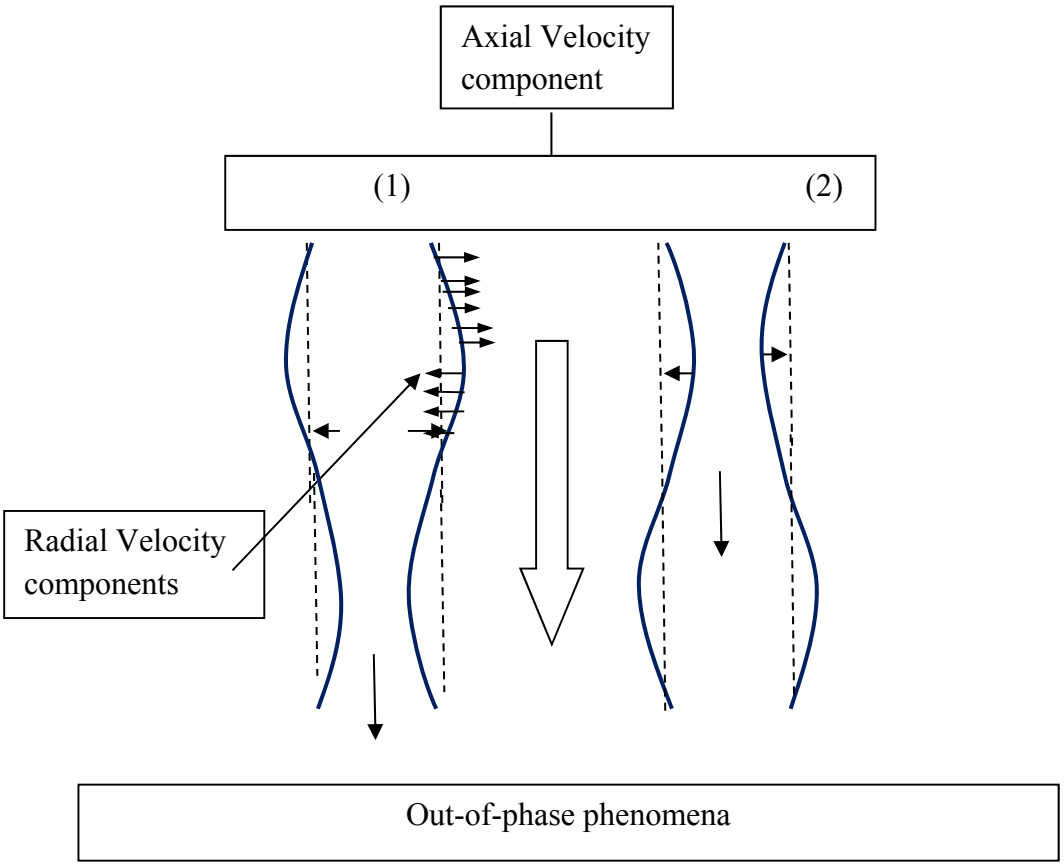

Figure 5-9: Interaction between two jets on the basis of velocity field, showing off-phase relationship.

Figure 5-10 shows comparison of resultant droplet diameter from experiments and simulation as a function of volumetric flow rate. For the double jet, the experimental and CFD observations are in good agreement for all three regimes.

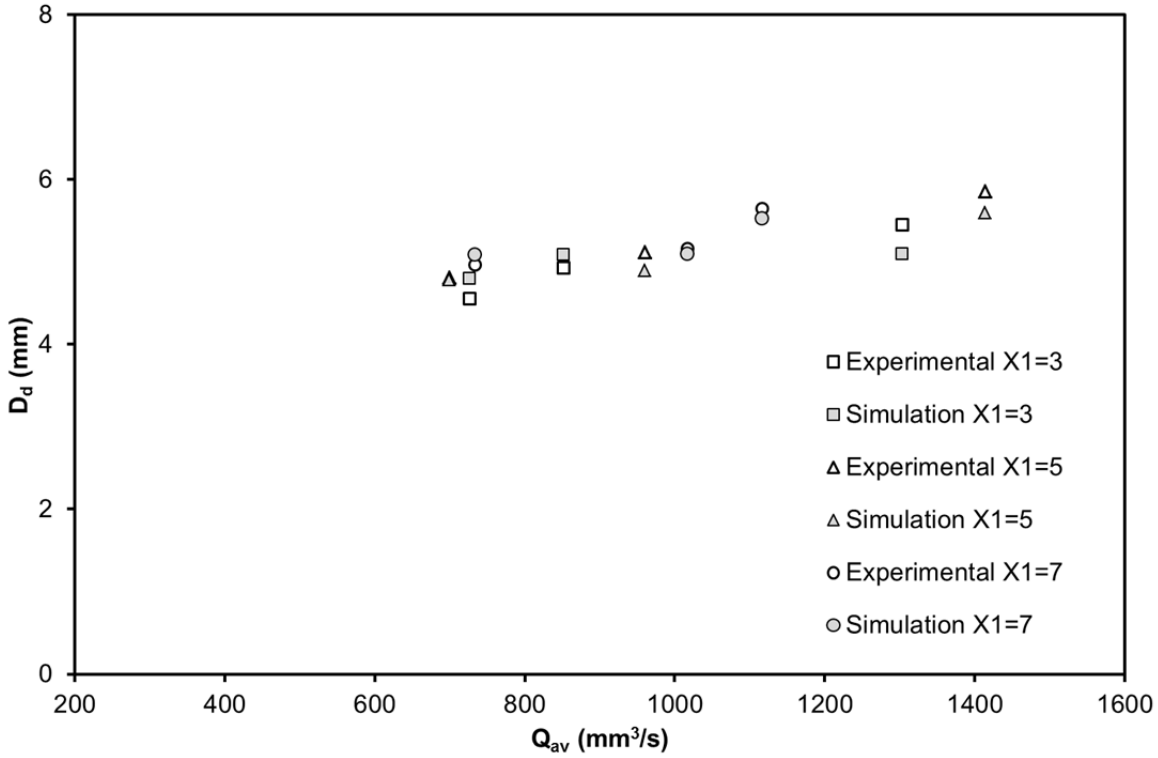

Figure 5-10: Comparison of droplet diameter obtained from experiments and CFD versus Qav for multiple jets with three different spacing between two jets.

5.2 Simulation results and discussions

5.2.1 Multiple jet interactions

Computational fluid dynamics simulations were employed to validate instability phenomena for multiple jets systems. As shown in Figure 5-11 (*a*), no instability was observed for double jet system when *X* and *Y* slices were taken at *t*=4.9 seconds and flow rate was 1252 ± 50 mm^3/s. Pressure contour extracted (Figure 5-11 (*b*)) from simulations to show the effect of pressure gradient between two jets. The induced pressure gradient between two jets was in balance and therefore resulted in more regular breakup, smaller droplet diameter and shorter breakup length.

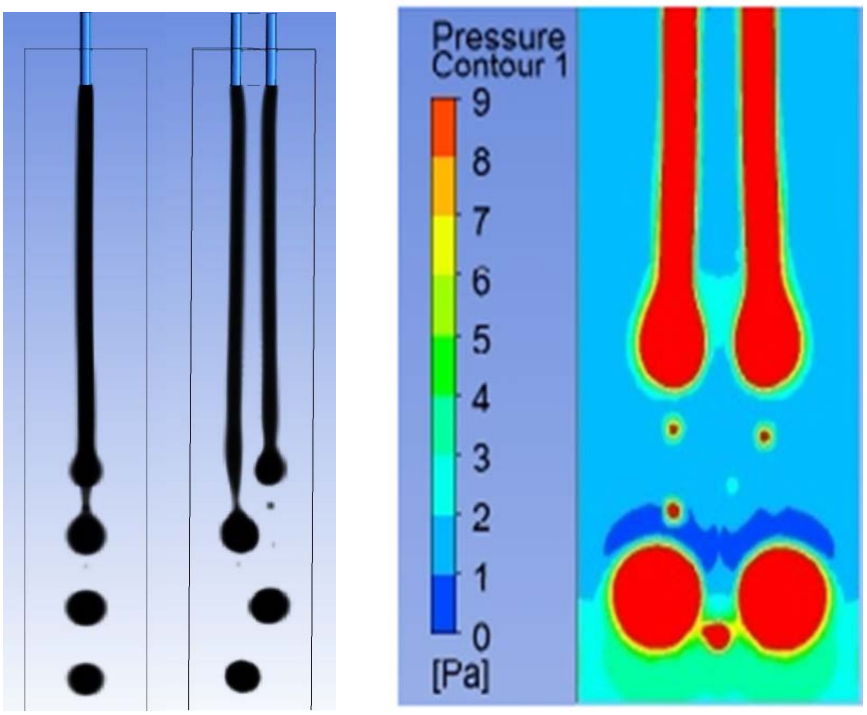

(a) X and Y slice t= 4.9 s *(b)* Pressure contour

Figure 5-11: *(a)* double jet system (x and y plane respectively) *(b)* Pressure contours between two jets and outside region.

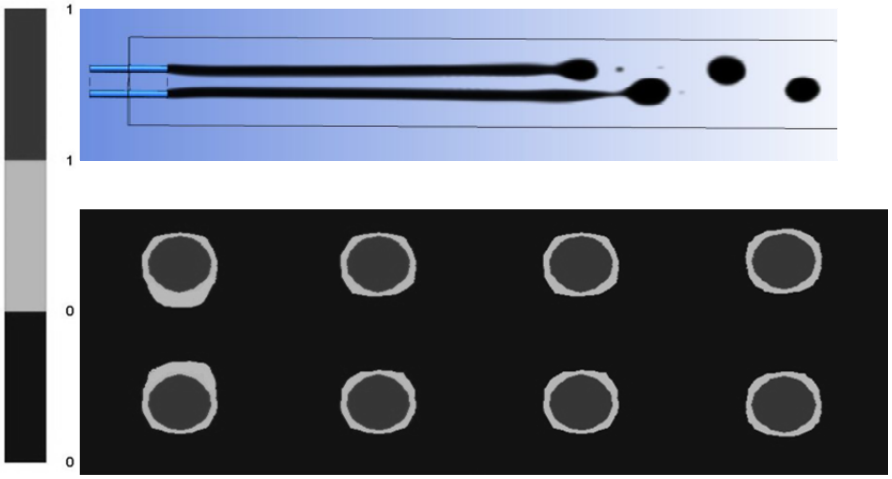

(a) *(b)* *(c)* *(d)*

Figure 5-12: Double jet mean volume fraction on a *XZ* plane at *(a)* z = 45 mm *(b)* z = 60 mm *(c)* z = 75 mm *(d)* z = 90 mm.

Double jet system simulation was analysed to find mean volume fraction contours, as shown in Figure 5-12. At the beginning, jet swing towards each other due to jet-jet interaction. Afterwards, the two jets swing very little (as evidenced by the thin green area).

5.2.2 Jet interaction at nozzle opening

For the two channels simulation, the simultaneous jets are moving slightly closer and remain on the same axis throughout the path of the jet. The distance between jets before breakup was observed at 1.8 mm. "In-phase" mode observed initially but "out-of-phase" was observed after steady state (Figure 5-13(*a*)) was reached. In case of three channels, the simultaneous velocity field in the cross section of the nozzle exit (inset) and volume fraction of dispersed and continuous phase and velocity pattern nozzle exit is shown in Figure 5-13(*b*). Strong interactions between outer and middle jets cause outer jets to bend inward initially and then three jets remain parallel until breakup. The distance between these parallel jets is approximately 1.6 mm, i.e. ~ *D*.

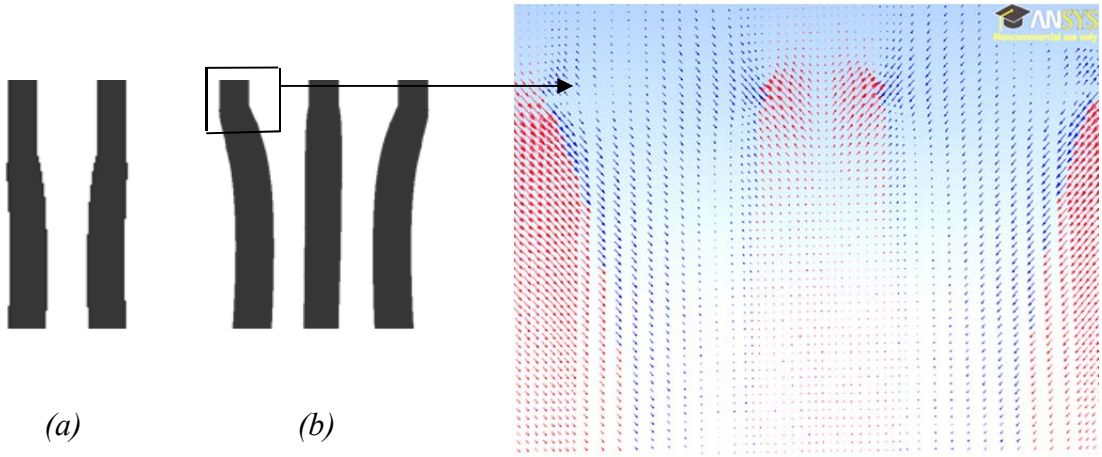

Figure 5-13: Velocity pattern of continuous and dispersed phase at nozzle exit (*a*) two jets (*b*) three jets.

5.2.3 Jet breakup process

Breakup processes of two and three simultaneous jets were studied using 3 dimensional VOF simulations and shown in Figure 5-14. An “in-phase”

phenomenon was observed between two outer jets as they are breaking in symmetric pattern. Time of breakage and droplet size was identical for both jets. However, In case of three simultaneous jets, "out-of-phase "mode observed between middle and outer jets. Adjacent jets observed radial component dominance and hence jet breakup experienced out-of-phase mode. Out-of-phase breakup is more influenced by radial velocity by component than axial component of velocity, which can be seen in Figure 5-15.

Figure 5-14: Instantaneous volume fraction of dispersed phase (Water) in continuous phase (Canola oil) after: 3 s, 4.1 s and 5.6 s respectively. (All three images were taken as 25 mm below the nozzle exit).

As shown in Figure 5-15, velocity pattern at the time of droplet breakup suggest the radial component and axial component effect. Initially, axial velocity component is much higher than radial component due to moving jet velocity. However, near the breakup region (approximately 25 mm below nozzle exit); the radial component gets stronger and dominates jet breakup process. Such a high value of radial velocity demonstrated the linear instability analysis (Knops, Slot et al. 2001), which was based on small velocities, is not appropriate for this system. Radial component affected both side of the jet and hence these two sides can breakup as "in-phase".

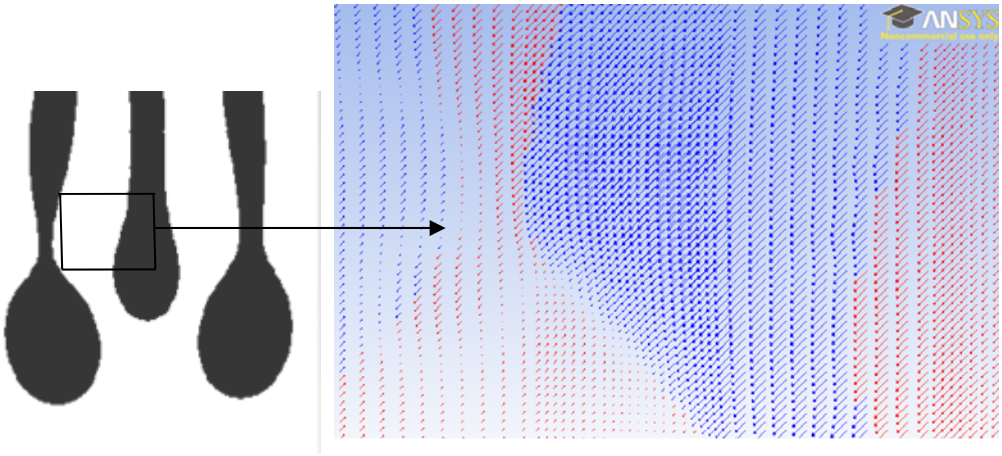

Figure 5-15: Velocity pattern of continuous and dispersed phase at drop formation process.

5.3 Summary

Multiple jet emulsifications are vitally important for the industry where high production rate of emulsions are essential. Interfacial interaction of multiple jet and its subsequent effects on jet breakup length and resultant droplet diameter were quantified in this chapter. Droplet diameters were found to decrease with jet-jet interaction. This is a key advantage of multiple jet system over single jet. Moreover, asymmetric instability was not observed in the multiple jet system. Experimental observation and computational fluid dynamics simulations are in a good agreement.

In and out-of-phase phenomena was observed in multiple jet system. Critical distance between two jets is a deciding factor for these phenomena. Furthermore, droplet breakup process was visualised in the multiple jet system. Jet-jet interaction, in and out-of-phase phenomena were also observed in three jet system. It can be concluded that the radial component of velocity dominated out-of-phase breakup and axial component of velocity dominated in-phase breakup. Jets interaction and breaking-up can be explained by considering the pressure distribution along the jet, which is obtainable from the simulation. Summarily, the droplet size can be optimized by manipulating jet-jet distance and flow-rate. Moreover, a successful optimization requires a complimentary combination of experimental and simulation analysis.

Chapter 6. Conclusions and Recommendations

Experimental and simulation studies were performed in the course of this thesis for emulsification process and resultant droplet size in the multiple jet system, which is essential for higher production rate. Single jet system was employed initially in order to visualise and study droplet formation process at lower flow rates. Furthermore, computational fluid dynamics and volume of fluid method was employed for the droplet breakup process and instability phenomena at higher flow rates. Both rectangular and circular nozzles were taken into consideration for the droplet size in the emulsification process. Multiple jet system was further experimented in order to visualise interfacial jet-jet interaction phenomena. Smaller droplet size were obtained and validated computationally for multiple jet system. The following conclusions were drawn based on the study.

6.1 Single jet

The results from single jet are:

1. Regular jet breakup was observed at flow rate below 831 $\pm$ 50 mm^3/s. Single jet system observed two types of instability (axis symmetric and asymmetric) above these flow rate ranges.
2. Higher droplet sizes were observed during single jet breakup when instability is evident. Instability phenomena were observed as flow of the fluid from neck to swell region due to induced pressure gradient.
3. Continuous phase interfacial properties and higher volumetric flow rate cause amplification in both the instabilities and resulted in jet *swing*.
4. Computational fluid dynamic study of rectangular nozzle was in good agreement with the experimental observations and showed that for given nozzle dimensions the equilibrium jet diameter increased with increasing volumetric flow rate.
5. It was also found that for a given liquid flow rate the equilibrium jet diameter was a function of aspect ratio. There appears to be an optimum aspect ratio of

between 5 and 7 for generating minimum sized droplets that are approximately 30% less than for a circular nozzle with the same cross-sectional area.

6. Existence of instability phenomena within the single jet system were quantified computationally and this information will be important for the modelling of single jet instability.

6.2 Multiple jets

The results from multiple jets are:

1. Droplet diameters were found to decrease with jet-jet interfacial interaction. Moreover, instability was not observed in the multiple jet system in which a jet-jet interfacial interaction is played a major role.
2. Experimental observation and computational fluid dynamics simulations are in a good agreement for multiple jet system and no instability was found due to balanced induced pressure gradient between two jets.
3. Induced pressure gradient between two jets resulted in more regular breakup, smaller droplet diameter and shorter breakup length.
4. Critical distance between two jets is an important factor for producing smaller emulsion droplets. Critical distance between two jets leads to in and out-of-phase phenomena in multiple jet system.
5. Summarily, multiple jets are easier to control and more advantaged over single jet for emulsion production.

6.3 Recommendations and future work

Primary goal of this study is to quantify the hydrodynamic behaviour of single and multiple jets in immiscible liquid-liquid system and its effect on jet breakup length and droplet size. This study allows us to identify the future work in order to fill more gaps in the area of study. These recommendations are mentioned below:

1. Array of nozzle would be employed for further experiments on the effect of jet-jet interaction on jet breakup length and droplet size. Circular and/or

rectangular shape of nozzles can be arrayed in different configurations and size for the further development and optimisation of micro reactor for the production of water in oil and oil in water emulsions.

2. Computational fluid dynamics would be then used to validate experimental observation and further modelling of emulsification process. Emulsification process will only happens in narrow conditions. Hence, the modelling will be critical for the successful process.
3. Various surfactants i.e. water soluble and oil soluble; can be consumed for the stability of produced emulsion droplets. Modelling would be necessary to predict time in which all emulsion droplets are covered with surfactant and attain steady state.
4. Micro jetting system would be developed and strategies for the modelling from lab scale to industrial scale can be applied for successful implementation.
5. As the next generation of micro-devices are routinely produced with precise size-control and arrangements, the study can applied to the new system. For the practical application, the distribution should be optimized in 2-D formation. However, this expect the results from this study, especially jet-jet interaction remains valid.
6. Three dimensional arrangements can also be optimised for jet-jet interaction computationally and experimentally.

Appendices

List of appendices

1. Single jet data

FR1								Average values			
Droplet	**t**	**Δt**	**L_3**	**D_j**	**d_d**	**V_d**	**$\sum V_d$**	**L_3**	**Q_{av}**	**n_d**	**$(d_d)_{av}$**
	(s)	**(s)**	**(mm)**	**(mm)**	**(mm)**	**(mm^3)**	**(mm^3)**	**(mm)**	**(mm^3/s)**	**(1/s)**	**(mm)**
1	0.128	0	5	2.2	3.25	18	18	**5**	**124**	**6.9**	**3.3**
2	0.272	0.144	5	2.2	3.25	18	36				
3	0.424	0.296	5	2.2	3.25	18	54				
4	0.576	0.448	5	2.2	3.25	18	72				
5	0.728	0.6	5	2.2	3.25	18	90				
6	0.888	0.76	5	2.2	3.25	18	108				
7	1.04	0.912	5	2.2	3.25	18	126				
8	1.192	1.064	5	2.2	3.25	18	144				
9	1.336	1.208	5	2.2	3.25	18	162				
10	1.488	1.36	5	2.2	3.25	18	180				
11	1.648	1.52	5	2.2	3.25	18	198				
12	1.8	1.672	5	2.2	3.25	18	216				
13	1.952	1.824	5	2.2	3.25	18	234				
14	2.096	1.968	5	2.2	3.25	18	252				
15	2.24	2.112	5	2.2	3.25	18	270				
16	2.392	2.264	5	2.2	3.25	18	288				
17	2.552	2.424	5	2.2	3.25	18	306				
18	2.696	2.568	5	2.2	3.25	18	324				
19	2.856	2.728	5	2.2	3.25	18	342				
20	3.016	2.888	5	2.2	3.25	18	359				

FR2								Average values			
Droplet	**t**	**Δt**	**L_3**	**D_j**	**d_d**	**V_d**	**$\sum V_d$**	**L_3**	**Q_{av}**	**n_d**	**$(d_d)_{av}$**
	(s)	**(s)**	**(mm)**	**(mm)**	**(mm)**	**(mm^3)**	**(mm^3)**	**(mm)**	**(mm^3/s)**	**(1/s)**	**(mm)**
1	0.04	0	10	2.2	5.5	87	87	**8**	**270**	**6.7**	**4.3**
2	0.096	0.056	6	2.2	3	14	101				
3	0.344	0.304	10	2.2	4	34	135				
4	0.416	0.376	8	2.2	4	34	168				
5	0.592	0.552	9	2.2	3.5	22	191				
6	0.824	0.784	7	2.2	5.5	87	278				
7	1.016	0.976	9	2.2	4	34	311				
8	1.136	1.096	9	2.2	3.25	18	329				
9	1.376	1.336	10	2.2	5.25	76	405				
10	1.432	1.392	6	2.2	2.75	11	416				
11	1.664	1.624	10	2.2	4.75	56	472				
12	1.752	1.712	8	2.2	3.25	18	490				
13	1.92	1.88	9	2.2	3.5	22	513				
14	2.16	2.12	9	2.2	5.5	87	600				
15	2.208	2.168	5	2.2	3	14	614				
16	2.456	2.416	10	2.2	4	34	647				
17	2.536	2.496	8	2.2	3.5	22	670				
18	2.72	2.68	8	2.2	4	34	703				
19	2.968	2.928	9	2.2	5.5	87	790				
20	3.024	2.984	7	2.2	3	14	804				

FR3								Average values			
Droplet	**t**	**Δt**	**L_3**	**D_j**	**d_d**	**V_d**	**$\sum V_d$**	**L_3**	**Q_{av}**	**n_d**	**$(d_d)_{av}$**
	(s)	**(s)**	**(mm)**	**(mm)**	**(mm)**	**(mm^3)**	**(mm^3)**	**(mm)**	**(mm^3/s)**	**(1/s)**	**(mm)**
1	0.04	0	13	2.2	3	14	14	**9**	**272**	**6.7**	**4.3**
2	0.256	0.216	12	2.2	6	113	127				
3	0.296	0.256	10	2.2	3	14	141				
4	0.416	0.376	8	2.2	4	34	175				
5	0.592	0.552	9	2.2	3.5	22	197				
6	0.824	0.784	7	2.2	5.5	87	284				
7	1.016	0.976	9	2.2	4	34	318				
8	1.136	1.096	9	2.2	3.25	18	336				
9	1.376	1.336	10	2.2	5.25	76	412				
10	1.432	1.392	6	2.2	2.75	11	423				
11	1.664	1.624	10	2.2	4.75	56	479				
12	1.752	1.712	8	2.2	3.25	18	497				
13	1.92	1.88	9	2.2	3.5	22	519				
14	2.16	2.12	9	2.2	5.5	87	606				
15	2.208	2.168	5	2.2	3	14	620				
16	2.456	2.416	10	2.2	4	34	654				
17	2.536	2.496	8	2.2	3.5	22	676				
18	2.72	2.68	8	2.2	4	34	710				
19	2.968	2.928	9	2.2	5.5	87	797				
20	3.024	2.984	7	2.2	3	14	811				

FR4								Average values			
Droplet	**t**	**Δt**	**L_3**	**D_j**	**d_d**	**V_d**	**$\sum V_d$**	**L_3**	**Q_{av}**	**n_d**	**$(d_d)_{av}$**
	(s)	**(s)**	**(mm)**	**(mm)**	**(mm)**	**(mm^3)**	**(mm^3)**	**(mm)**	**(mm^3/s)**	**(1/s)**	**(mm)**
1	0.072	0	53	2.2	5	65	65	**54**	**514**	**10.4**	**4.6**
2	0.272	0.2	53	2.2	7.5	221	286				
3	0.52	0.448	54	2.2	7.5	221	507				
4	0.696	0.624	56	2.2	5.5	87	594				
5	0.712	0.64	52	2.2	3	14	608				
6	0.712	0.64	46	2.2	3.5	22	631				
7	0.76	0.688	44	2.2	3.5	22	653				
8	0.792	0.72	41	2.2	3.25	18	671				
9	1	0.928	53	2.2	3.5	22	694				
10	1.064	0.992	47	2.2	3.5	22	716				
11	1.248	1.176	48	2.2	4.5	48	764				
12	1.296	1.224	47	2.2	3.5	22	786				
13	1.52	1.448	56	2.2	3.5	22	809				
14	1.608	1.536	61	2.2	4	34	842				
15	1.68	1.608	60	2.2	4	34	876				
16	1.704	1.632	56	2.2	4	34	909				
17	1.952	1.88	71	2.2	3.5	22	932				
18	1.952	1.88	59	2.2	3.5	22	954				
19	1.968	1.896	61	2.2	3.5	22	977				
20	2	1.928	57	2.2	3	14	991				

FR5								Average values			
Droplet	**t**	**Δt**	**L_3**	**D_j**	**d_d**	**V_d**	**$\sum V_d$**	**L_3**	**Q_{av}**	**n_d**	**$(d_d)_{av}$**
	(s)	**(s)**	**(mm)**	**(mm)**	**(mm)**	**(mm^3)**	**(mm^3)**	**(mm)**	**(mm^3/s)**	**(1/s)**	**(mm)**
1	0.016	0	45	2.2	3	14	14	**47**	**553**	**8.9**	**4.9**
2	0.344	0.328	55	2.2	6.25	128	142				
3	0.416	0.4	54	2.2	3.25	18	160				
4	0.624	0.608	55	2.2	6	113	273				
5	0.672	0.656	53	2.2	3	14	287				
6	0.824	0.808	45	2.2	9	382	669				
7	0.848	0.832	40	2.2	3	14	683				
8	1.112	1.096	50	2.2	4	34	717				
9	1.168	1.152	49	2.2	3.5	22	739				
10	1.352	1.336	57	2.2	4	34	772				
11	1.36	1.344	48	2.2	3.25	18	790				
12	1.392	1.376	45	2.2	3	14	805				
13	1.56	1.544	42	2.2	5	65	870				
14	1.584	1.568	39	2.2	3	14	884				
15	1.64	1.624	38	2.2	3	14	898				
16	1.96	1.944	56	2.2	7	180	1078				
17	2	1.984	43	2.2	3	14	1092				
18	2.224	2.208	46	2.2	6.25	128	1220				
19	2.248	2.232	44	2.2	3	14	1234				
20	2.272	2.256	38	2.2	3	14	1248				

FR6								Average values			
Droplet	**t**	**Δt**	**L_3**	**D_j**	**d_d**	**V_d**	**$\sum V_d$**	**L_3**	**Q_{av}**	**n_d**	**$(d_d)_{av}$**
	(s)	**(s)**	**(mm)**	**(mm)**	**(mm)**	**(mm^3)**	**(mm^3)**	**(mm)**	**(mm^3/s)**	**(1/s)**	**(mm)**
1	0.08	0	88	2.2	6	113	113	**90**	**660**	**10.1**	**5.0**
2	0.112	0.032	83	2.2	2.5	8	121				
3	0.464	0.384	101	2.2	6.5	144	265				
4	0.696	0.616	103	2.2	6.5	144	409				
5	0.528	0.448	102	2.2	3	14	423				
6	0.568	0.488	100	2.2	3	14	437				
7	0.624	0.544	98	2.2	3	14	451				
8	0.8	0.72	105	2.2	4.25	40	491				
9	0.808	0.728	89	2.2	6	113	605				
10	0.84	0.76	88	2.2	3.25	18	623				
11	0.888	0.808	84	2.2	3.5	22	645				
12	1.112	1.032	99	2.2	6.5	144	789				
13	1.152	1.072	88	2.2	3.5	22	811				
14	1.36	1.28	93	2.2	5	65	877				
15	1.392	1.312	90	2.2	3	14	891				
16	1.544	1.464	82	2.2	7	180	1070				
17	1.608	1.528	78	2.2	3.25	18	1088				
18	1.968	1.888	89	2.2	7	180	1268				
19	2.008	1.928	61	2.2	3.25	18	1286				
20	2.056	1.976	83	2.2	3.25	18	1304				

FR7								Average values			
Droplet	**t**	**Δt**	**L_3**	**D_j**	**d_d**	**V_d**	**$\sum V_d$**	**L_3**	**Q_{av}**	**n_d**	**$(d_d)_{av}$**
	(s)	**(s)**	**(mm)**	**(mm)**	**(mm)**	**(mm^3)**	**(mm^3)**	**(mm)**	**(mm^3/s)**	**(1/s)**	**(mm)**
1	0.168	0	113	2.2	8.5	322	322	**116**	**831**	**5.5**	**6.6**
2	0.224	0.056	111	2.2	3.5	22	344				
3	0.632	0.464	118	2.2	7.5	221	565				
4	0.712	0.544	117	2.2	3.5	22	587				
5	0.944	0.776	111	2.2	9	382	969				
6	0.968	0.8	95	2.2	3.5	22	991				
7	1.568	1.4	133	2.2	8	268	1260				
8	1.624	1.456	128	2.2	3.75	28	1287				
9	1.816	1.648	129	2.2	7	180	1467				
10	1.872	1.704	127	2.2	3.5	22	1489				
11	2.168	2	129	2.2	8	268	1757				
12	2.168	2	110	2.2	6.5	144	1901				
13	2.168	2	100	2.2	3.5	22	1924				
14	2.576	2.408	109	2.2	8	268	2192				
15	2.896	2.728	114	2.2	7.5	221	2413				
16	3.136	2.968	118	2.2	7	180	2592				
17	3.36	3.192	120	2.2	7	180	2772				
18	3.392	3.224	118	2.2	3.5	22	2794				
19	3.456	3.288	104	2.2	3.5	22	2817				
20	3.824	3.656	113	2.2	7.5	221	3038				

FR8								Average values			
Droplet	**t**	**Δt**	**L_3**	**D_j**	**d_d**	**V_d**	**$\sum V_d$**	**L_3**	**Q_{av}**	**n_d**	**$(d_d)_{av}$**
	(s)	**(s)**	**(mm)**	**(mm)**	**(mm)**	**(mm^3)**	**(mm^3)**	**(mm)**	**(mm^3/s)**	**(1/s)**	**(mm)**
1	0.04	0	139	2.2	3.5	22	22	**125**	**1252**	**6.2**	**7.3**
2	0.224	0.184	113	2.2	15	1767	1790				
3	0.28	0.24	110	2.2	7.5	221	2010				
4	0.744	0.704	133	2.2	7.5	221	2231				
5	0.768	0.728	129	2.2	3.5	22	2254				
6	1.008	0.968	139	2.2	5.5	87	2341				
7	1.024	0.984	129	2.2	3.5	22	2363				
8	1.24	1.2	131	2.2	6	113	2476				
9	1.256	1.216	129	2.2	3	14	2491				
10	1.44	1.4	120	2.2	8	268	2759				
11	1.48	1.44	116	2.2	3.5	22	2781				
12	1.896	1.856	124	2.2	9	382	3163				
13	2.168	2.128	133	2.2	6.5	144	3307				
14	2.184	2.144	128	2.2	3.5	22	3329				
15	2.224	2.184	109	2.2	7.5	221	3550				
16	2.24	2.2	105	2.2	3.5	22	3572				
17	2.704	2.664	130	2.2	6.5	144	3716				
18	2.76	2.72	125	2.2	5	65	3782				
19	3.024	2.984	128	2.2	5	65	3847				
20	3.256	3.216	132	2.2	7	180	4027				

Double jet data

X_1=3mm

X_1=3 mm									Average values			
Jet	**Droplet**	**t (s)**	**Δt (s)**	**L_3 (mm)**	**D_j (mm)**	**d_d (mm)**	**V_d (mm^3)**	**$\sum V_d$ (mm^3)**	**L_3 (mm)**	**Q_{av} (mm^3/s)**	**n_d (1/s)**	**$(d_d)_{av}$ (mm)**
LHS	1	49.784	0	97	2.2	4.5	48	48	**100**	**1330**	**14.6**	**5.6**
	2	49.832	0.048	98	2.2	4.5	48	95				
	3	50	0.216	112	2.2	6.5	144	239				
	4	50.024	0.24	99	2.2	4.5	48	287				
	5	50.144	0.36	93	2.2	8.5	322	608				
	6	50.168	0.384	91	2.2	4.5	48	656				
	7	50.216	0.432	92	2.2	4.5	48	704				
	8	50.264	0.48	92	2.2	4.5	48	752				
	9	50.296	0.512	91	2.2	4.5	48	799				
	10	50.464	0.68	97	2.2	6.5	144	943				
	11	50.496	0.712	94	2.2	6.5	144	1087				
	12	50.544	0.76	95	2.2	4.5	48	1135				
	13	50.696	0.912	105	2.2	5.5	87	1222				
	14	50.728	0.944	99	2.2	4.5	48	1269				
	15	50.76	0.976	96	2.2	4.5	48	1317				
	16	50.984	1.2	110	2.2	7.5	221	1538				
	17	51	1.216	105	2.2	4.5	48	1586				
	18	51.024	1.24	103	2.2	4.5	48	1633				
	19	51.108	1.324	111	2.2	6.5	144	1777				
	20	51.156	1.372	112	2.2	4.5	48	1825				

X_1=3 mm									Average values			
Jet	**Droplet**	**t**	**Δt**	**L_3**	**D_j**	**d_d**	**V_d**	**$\sum V_d$**	**L_3**	**Q_{av}**	**n_d**	**$(d_d)_{av}$**
		(s)	**(s)**	**(mm)**	**(mm)**	**(mm)**	**(mm^3)**	**(mm^3)**	**(mm)**	**(mm^3/s)**	**(1/s)**	**(mm)**
	1	49.784	0	91	2.2	4.5	48	48	**98**	**1260**	**15.9**	**5.3**
	2	49.824	0.04	92	2.2	4.5	48	95				
	3	49.992	0.208	98	2.2	6.5	144	239				
	4	50.016	0.232	94	2.2	4.5	48	287				
	5	50.048	0.264	93	2.2	4.5	48	335				
	6	50.104	0.32	94	2.2	4.5	48	382				
	7	50.136	0.352	94	2.2	4.5	48	430				
	8	50.192	0.408	93	2.2	4.75	56	486				
	9	50.232	0.448	93	2.2	4.5	48	534	**L_3**	**Q_{av}**	**n_d**	**$(d_d)_{av}$**
RHS	10	50.272	0.488	93	2.2	4.5	48	582	**(mm)**	**(mm^3/s)**	**(1/s)**	**(mm)**
	11	50.312	0.528	93	2.2	4.5	48	629	**99**	**1295**	**15.3**	**5.5**
	12	50.464	0.68	103	2.2	6.5	144	773				
	13	50.48	0.696	99	2.2	4.5	48	821				
	14	50.536	0.752	100	2.2	4.75	56	877				
	15	50.568	0.784	99	2.2	4.5	48	925				
	16	50.616	0.832	99	2.2	4.5	48	972				
	17	50.752	0.968	104	2.2	7.5	221	1193				
	18	50.8	1.016	102	2.2	4.5	48	1241				
	19	50.992	1.208	111	2.2	8.25	294	1535				
	20	51.04	1.256	110	2.2	4.5	48	1583				

X_1=3 mm									Average values			
Jet	**Droplet**	**t**	**Δt**	**L_3**	**D_j**	**d_d**	**V_d**	**$\sum V_d$**	**L_3**	**Q_{av}**	**n_d**	**$(d_d)_{av}$**
		(s)	**(s)**	**(mm)**	**(mm)**	**(mm)**	**(mm^3)**	**(mm^3)**	**(mm)**	**(mm^3/s)**	**(1/s)**	**(mm)**
LHS	1	37.272	0	56	2.2	6.5	144	144	**59**	**862**	**13.3**	**5.0**
	2	37.304	0.032	54	2.2	4.5	48	192				
	3	37.344	0.072	53	2.2	4.5	48	239				
	4	37.504	0.232	55	2.2	5.5	87	326				
	5	37.536	0.264	54	2.2	4	34	360				
	6	37.688	0.416	56	2.2	5.5	87	447				
	7	37.737	0.465	54	2.2	4.5	48	495				
	8	37.88	0.608	60	2.2	6	113	608				
	9	37.912	0.64	57	2.2	4	34	641				
	10	38.072	0.8	63	2.2	5.5	87	728				
	11	38.104	0.832	60	2.2	3.5	22	751				
	12	38.224	0.952	63	2.2	5.75	100	850				
	13	38.264	0.992	62	2.2	4	34	884				
	14	38.44	1.168	67	2.2	5.5	87	971				
	15	38.48	1.208	63	2.2	3.75	28	999				
	16	38.552	1.28	60	2.2	6	113	1112				
	17	38.576	1.304	60	2.2	4	34	1145				
	18	38.688	1.416	63	2.2	5.25	76	1221				
	19	38.728	1.456	60	2.2	4.5	48	1269				
	20	38.776	1.504	60	2.2	3.75	28	1296				

X_1=3 mm									Average values			
Jet	**Droplet**	**t**	**Δt**	**L_3**	**D_j**	**d_d**	**V_d**	**$\sum V_d$**	**L_3**	**Q_{av}**	**n_d**	**$(d_d)_{av}$**
		(s)	**(s)**	**(mm)**	**(mm)**	**(mm)**	**(mm^3)**	**(mm^3)**	**(mm)**	**(mm^3/s)**	**(1/s)**	**(mm)**
RHS	1	37.256	0	57	2.2	4.5	48	48	**60**	**834**	**13.7**	**4.9**
	2	37.416	0.16	61	2.2	6.5	144	192				
	3	37.464	0.208	64	2.2	4.25	40	232				
	4	37.504	0.248	61	2.2	5.25	76	307				
	5	37.64	0.384	65	2.2	4.25	40	348				
	6	37.704	0.448	55	2.2	4.25	40	388				
	7	37.864	0.608	60	2.2	5.5	87	475				
	8	37.904	0.648	59	2.2	4.25	40	515				
	9	38.064	0.808	63	2.2	5.5	87	602				
	10	38.088	0.832	60	2.2	4.25	40	642	**L_3**	**Q_{av}**	**n_d**	**$(d_d)_{av}$**
	11	38.256	1	65	2.2	7.25	200	842	**(mm)**	**(mm^3/s)**	**(1/s)**	**(mm)**
	12	38.296	1.04	62	2.2	4.25	40	882	**59**	**848**	**13.5**	**4.9**
	13	38.344	1.088	60	2.2	3.5	22	905				
	14	38.456	1.2	65	2.2	4.5	48	952				
	15	38.464	1.208	58	2.2	3.75	28	980				
	16	38.488	1.232	58	2.2	4.25	40	1020				
	17	38.6	1.344	60	2.2	5	65	1086				
	18	38.632	1.376	55	2.2	4.5	48	1133				
	19	38.672	1.416	54	2.2	4.25	40	1174				
	20	38.712	1.456	53	2.2	4.25	40	1214				

X_1=3 mm									Average values			
Jet	**Droplet**	**t**	**Δt**	**L_3**	**D_j**	**d_d**	**V_d**	**$\sum V_d$**	**L_3**	**Q_{av}**	**n_d**	**$(d_d)_{av}$**
		(s)	**(s)**	**(mm)**	**(mm)**	**(mm)**	**(mm^3)**	**(mm^3)**	**(mm)**	**(mm^3/s)**	**(1/s)**	**(mm)**
LHS	1	22.88	0	43	2.2	3.5	22	22	**40**	**673**	**14.1**	**4.5**
	2	22.912	0.032	41	2.2	3.5	22	45				
	3	23.016	0.136	43	2.2	5.25	76	121				
	4	23.064	0.184	42	2.2	3.5	22	143				
	5	23.104	0.224	41	2.2	3.5	22	166				
	6	23.24	0.36	42	2.2	5.5	87	253				
	7	23.288	0.408	41	2.2	3.5	22	275				
	8	23.328	0.448	40	2.2	3.5	22	298				
	9	23.352	0.472	38	2.2	3.5	22	320				
	10	23.464	0.584	41	2.2	5.25	76	396				
	11	23.488	0.608	38	2.2	3.5	22	418				
	12	23.664	0.784	42	2.2	6.5	144	562				
	13	23.696	0.816	41	2.2	3.5	22	584				
	14	23.752	0.872	37	2.2	3.5	22	607				
	15	23.792	0.912	36	2.2	3.5	22	629				
	16	23.952	1.072	39	2.2	5.5	87	716				
	17	23.984	1.104	37	2.2	3.5	22	739				
	18	24.088	1.208	40	2.2	4.5	48	787				
	19	24.128	1.248	38	2.2	3.5	22	809				
	20	24.296	1.416	41	2.2	6.5	144	953				

X_1=3 mm									Average values			
Jet	**Droplet**	**t**	**Δt**	**L_3**	**D_j**	**d_d**	**V_d**	**$\sum V_d$**	**L_3**	**Q_{av}**	**n_d**	**$(d_d)_{av}$**
		(s)	**(s)**	**(mm)**	**(mm)**	**(mm)**	**(mm^3)**	**(mm^3)**	**(mm)**	**(mm^3/s)**	**(1/s)**	**(mm)**
	1	22.912	0	46	2.2	3.5	22	22	**43**	**704**	**13.7**	**4.6**
	2	22.992	0.08	41	2.2	5.5	87	110				
	3	23.128	0.216	42	2.2	5.5	87	197				
	4	23.248	0.336	46	2.2	5.5	87	284				
	5	23.28	0.368	43	2.2	3.5	22	306				
	6	23.304	0.392	40	2.2	3.5	22	329				
	7	23.512	0.6	44	2.2	7.5	221	550				
	8	23.528	0.616	41	2.2	3.25	18	568				
	9	23.544	0.632	38	2.2	3.5	22	590				
RHS	10	23.672	0.76	42	2.2	4.5	48	638				
	11	23.696	0.784	39	2.2	3.5	22	660	**L_3**	**Q_{av}**	**n_d**	**$(d_d)_{av}$**
	12	23.84	0.928	46	2.2	5.5	87	747	**(mm)**	**(mm^3/s)**	**(1/s)**	**(mm)**
	13	23.856	0.944	41	2.2	3.25	18	765	**41**	**688**	**13.9**	**4.6**
	14	23.896	0.984	40	2.2	3.5	22	788				
	15	24.008	1.096	43	2.2	5	65	853				
	16	24.04	1.128	41	2.2	3.5	22	876				
	17	24.184	1.272	48	2.2	3.5	22	898				
	18	24.24	1.328	42	2.2	3.5	22	921				
	19	24.336	1.424	44	2.2	5.5	87	1008				
	20	24.376	1.464	43	2.2	3.5	22	1030				

X_1=5mm

X_1=5 mm									Average values			
Jet	**Droplet**	**t**	**Δt**	**L_3**	**D_j**	**d_d**	**V_d**	**$\sum V_d$**	**L_3**	**Q_{av}**	**n_d**	**$(d_d)_{av}$**
		(s)	**(s)**	**(mm)**	**(mm)**	**(mm)**	**(mm^3)**	**(mm^3)**	**(mm)**	**(mm^3/s)**	**(1/s)**	**(mm)**
LHS	1	60.024	0	140	2.2	4	34	34	**131**	**1415**	**14.5**	**5.7**
	2	60.224	0.2	152	2.2	8	268	302				
	3	60.24	0.216	140	2.2	3.5	22	324				
	4	60.296	0.272	137	2.2	3.5	22	346				
	5	60.408	0.384	129	2.2	8.75	351	697				
	6	60.472	0.448	131	2.2	4.5	48	745				
	7	60.512	0.488	128	2.2	4.5	48	793				
	8	60.736	0.712	144	2.2	5.25	76	868				
	9	60.744	0.72	136	2.2	7.75	244	1112				
	10	60.752	0.728	130	2.2	4	34	1146				
	11	60.84	0.816	125	2.2	4.5	48	1193				
	12	60.872	0.848	125	2.2	3.75	28	1221				
	13	61.008	0.984	128	2.2	5.75	100	1321				
	14	61.04	1.016	125	2.2	4	34	1354				
	15	61.176	1.152	132	2.2	4.25	40	1394				
	16	61.216	1.192	130	2.2	5.25	76	1470				
	17	61.272	1.248	131	2.2	5	65	1535				
	18	61.312	1.288	120	2.2	7.75	244	1779				
	19	61.368	1.344	121	2.2	6	113	1892				
	20	61.408	1.384	118	2.2	5	65	1958				

X_1=5 mm									Average values			
Jet	**Droplet**	**t**	**Δt**	**L_3**	**D_j**	**d_d**	**V_d**	**$\sum V_d$**	**L_3**	**Q_{av}**	**n_d**	**$(d_d)_{av}$**
		(s)	**(s)**	**(mm)**	**(mm)**	**(mm)**	**(mm^3)**	**(mm^3)**	**(mm)**	**(mm^3/s)**	**(1/s)**	**(mm)**
RHS	1	59.968	0	127	2.2	5	65	65	**134**	**1414**	**12.5**	**6.0**
	2	60.192	0.224	136	2.2	9	382	447				
	3	60.224	0.256	132	2.2	4.5	48	495				
	4	60.232	0.264	128	2.2	4	34	528				
	5	60.448	0.48	134	2.2	8.5	322	850				
	6	60.48	0.512	133	2.2	4	34	883				
	7	60.592	0.624	138	2.2	5.25	76	959				
	8	60.648	0.68	137	2.2	4.25	40	999	**L_3**	**Q_{av}**	**n_d**	**$(d_d)_{av}$**
	9	60.792	0.824	138	2.2	7.5	221	1220	**(mm)**	**(mm^3/s)**	**(1/s)**	**(mm)**
	10	60.824	0.856	137	2.2	3.75	28	1248	**133**	**1414**	**13.5**	**5.9**
	11	60.904	0.936	132	2.2	7.25	200	1447				
	12	61.104	1.136	141	2.2	7.5	221	1668				
	13	61.12	1.152	139	2.2	2.5	8	1677				
	14	61.12	1.152	132	2.2	3.75	28	1704				
	15	61.232	1.264	138	2.2	4.25	40	1744				
	16	61.272	1.304	136	2.2	3.75	28	1772				
	17	61.392	1.424	129	2.2	8.5	322	2093				
	18	61.472	1.504	133	2.2	4.5	48	2141				
	19	61.496	1.528	126	2.2	4.25	40	2181				
	20	61.572	1.604	134	2.2	5.5	87	2269				

X_1=5 mm									Average values			
Jet	**Droplet**	**t**	**Δt**	**L_3**	**D_j**	**d_d**	**V_d**	**$\sum V_d$**	**L_3**	**Q_{av}**	**n_d**	**$(d_d)_{av}$**
		(s)	**(s)**	**(mm)**	**(mm)**	**(mm)**	**(mm^3)**	**(mm^3)**	**(mm)**	**(mm^3/s)**	**(1/s)**	**(mm)**
LHS	1	38.048	0	71	2.2	4	34	34	**64**	**922**	**11.7**	**5.3**
	2	38.072	0.024	63	2.2	8	268	302				
	3	38.288	0.24	64	2.2	3	14	316				
	4	38.304	0.256	73	2.2	4	34	349				
	5	38.448	0.4	69	2.2	5.25	76	425				
	6	38.472	0.424	69	2.2	4.5	48	473				
	7	38.504	0.456	63	2.2	4.25	40	513				
	8	38.544	0.496	61	2.2	3.25	18	531				
	9	38.584	0.536	58	2.2	3.5	22	553				
	10	38.616	0.568	57	2.2	3.5	22	576				
	11	38.792	0.744	60	2.2	6.5	144	720				
	12	38.824	0.776	58	2.2	3.5	22	742				
	13	39	0.952	63	2.2	5.25	76	818				
	14	39.032	0.984	60	2.2	3.5	22	840				
	15	39.208	1.16	66	2.2	6.5	144	984				
	16	39.36	1.312	68	2.2	6.5	144	1128				
	17	39.344	1.296	60	2.2	3	14	1142				
	18	39.56	1.512	65	2.2	8	268	1410				
	19	39.6	1.552	65	2.2	3.25	18	1428				
	20	39.752	1.704	65	2.2	6.5	144	1572				

X_1=5 mm									Average values			
Jet	**Droplet**	**t**	**Δt**	**L_3**	**D_j**	**d_d**	**V_d**	**$\sum V_d$**	**L_3**	**Q_{av}**	**n_d**	**$(d_d)_{av}$**
		(s)	**(s)**	**(mm)**	**(mm)**	**(mm)**	**(mm^3)**	**(mm^3)**	**(mm)**	**(mm^3/s)**	**(1/s)**	**(mm)**
RHS	1	38.176	0	77	2.2	7	180	180	**73**	**938**	**15.0**	**4.9**
	2	38.328	0.152	82	2.2	6	113	293				
	3	38.367	0.191	79	2.2	4.5	48	340				
	4	38.4	0.224	76	2.2	3.25	18	358				
	5	38.448	0.272	76	2.2	3.25	18	376				
	6	38.552	0.376	78	2.2	5	65	442				
	7	38.584	0.408	75	2.2	4.5	48	490				
	8	38.624	0.448	75	2.2	4.5	48	537	**L_3**	**Q_{av}**	**n_d**	**$(d_d)_{av}$**
	9	38.672	0.496	74	2.2	4.5	48	585	**(mm)**	**(mm^3/s)**	**(1/s)**	**(mm)**
	10	38.712	0.536	70	2.2	4.5	48	633	**68**	**930**	**13.4**	**5.1**
	11	38.896	0.72	76	2.2	6.5	144	776				
	12	38.92	0.744	73	2.2	3.5	22	799				
	13	38.92	0.744	70	2.2	3.5	22	821				
	14	38.952	0.776	68	2.2	3.75	28	849				
	15	39.024	0.848	63	2.2	3.75	28	877				
	16	39.216	1.04	67	2.2	6.5	144	1020				
	17	39.24	1.064	65	2.2	3.75	28	1048				
	18	39.408	1.232	70	2.2	6.5	144	1192				
	19	39.448	1.272	68	2.2	3.75	28	1219				
	20	39.512	1.336	68	2.2	4	34	1253				

X_1=5 mm									Average values			
Jet	**Droplet**	**t**	**Δt**	**L_3**	**D_j**	**d_d**	**V_d**	**$\sum V_d$**	**L_3**	**Q_{av}**	**n_d**	**$(d_d)_{av}$**
		(s)	**(s)**	**(mm)**	**(mm)**	**(mm)**	**(mm^3)**	**(mm^3)**	**(mm)**	**(mm^3/s)**	**(1/s)**	**(mm)**
LHS	1	33.056	0	42	2.2	5.5	87	87	**40**	**652**	**11.5**	**4.8**
	2	33.096	0.04	41	2.2	3.25	18	105				
	3	33.24	0.184	42	2.2	5.5	87	192				
	4	33.28	0.224	40	2.2	3.25	18	210				
	5	33.424	0.368	46	2.2	4.25	40	250				
	6	33.448	0.392	40	2.2	3.75	28	278				
	7	33.472	0.416	36	2.2	3.25	18	296				
	8	33.68	0.624	38	2.2	6.5	144	440				
	9	33.856	0.8	41	2.2	5.5	87	527				
	10	33.896	0.84	40	2.2	3.25	18	545				
	11	34.032	0.976	40	2.2	5.5	87	632				
	12	34.064	1.008	39	2.2	3	14	646				
	13	34.224	1.168	40	2.2	6.5	144	790				
	14	34.264	1.208	39	2.2	3.25	18	808				
	15	34.416	1.36	40	2.2	6.5	144	952				
	16	34.448	1.392	39	2.2	3.25	18	970				
	17	34.496	1.44	37	2.2	3.25	18	988				
	18	34.536	1.48	36	2.2	3.25	18	1006				
	19	34.568	1.512	32	2.2	3.25	18	1024				
	20	34.8	1.744	44	2.2	6	113	1137				

X_1=5 mm									Average values			
Jet	**Droplet**	**t**	**Δt**	**L_3**	**D_j**	**d_d**	**V_d**	**$\sum V_d$**	**L_3**	**Q_{av}**	**n_d**	**$(d_d)_{av}$**
		(s)	**(s)**	**(mm)**	**(mm)**	**(mm)**	**(mm^3)**	**(mm^3)**	**(mm)**	**(mm^3/s)**	**(1/s)**	**(mm)**
RHS	1	33.048	0	42	2.2	6	113	113	**44**	**678**	**11.4**	**4.8**
	2	33.192	0.144	42	2.2	5.5	87	200				
	3	33.232	0.184	42	2.2	3	14	214				
	4	33.392	0.344	44	2.2	6	113	327				
	5	33.432	0.384	44	2.2	3	14	342				
	6	33.592	0.544	46	2.2	6	113	455				
	7	33.776	0.728	51	2.2	6	113	568				
	8	33.792	0.744	47	2.2	3	14	582	**L_3**	**Q_{av}**	**n_d**	**$(d_d)_{av}$**
	9	33.816	0.768	44	2.2	3	14	596	**(mm)**	**(mm^3/s)**	**(1/s)**	**(mm)**
	10	33.968	0.92	46	2.2	6	113	709	**42**	**665**	**11.4**	**4.8**
	11	34	0.952	44	2.2	3.25	18	727				
	12	34.048	1	44	2.2	3.5	22	750				
	13	34.2	1.152	46	2.2	6	113	863				
	14	34.344	1.296	51	2.2	5	65	928				
	15	34.344	1.296	41	2.2	3.5	22	951				
	16	34.368	1.32	39	2.2	3	14	965				
	17	34.6	1.552	44	2.2	6	113	1078				
	18	34.616	1.568	41	2.2	3	14	1092				
	19	34.784	1.736	44	2.2	5.5	87	1179				
	20	34.808	1.76	41	2.2	3	14	1193				

X_1=7mm

X_1=7 mm									Average values			
Jet	**Droplet**	**t**	**Δt**	**L_3**	**D_j**	**d_d**	**V_d**	**$\sum V_d$**	**L_3**	**Q_{av}**	**n_d**	**$(d_d)_{av}$**
		(s)	**(s)**	**(mm)**	**(mm)**	**(mm)**	**(mm^3)**	**(mm^3)**	**(mm)**	**(mm^3/s)**	**(1/s)**	**(mm)**
LHS	1	62.44	0	121	2.2	4.75	56	56	**174**	**1234**	**12.0**	**5.8**
	2	62.464	0.024	1178	2.2	4.25	40	96				
	3	62.648	0.208	123	2.2	6.25	128	224				
	4	62.696	0.256	123	2.2	4.25	40	264				
	5	62.744	0.304	119	2.2	4.25	40	305				
	6	62.76	0.32	114	2.2	5.25	76	380				
	7	62.808	0.368	113	2.2	4.25	40	420				
	8	62.864	0.424	112	2.2	4.25	40	461				
	9	63.096	0.656	118	2.2	8.5	322	782				
	10	63.128	0.688	117	2.2	4.25	40	822				
	11	63.32	0.88	124	2.2	5.5	87	910				
	12	63.376	0.936	120	2.2	4.75	56	966				
	13	63.56	1.12	126	2.2	6.5	144	1109				
	14	63.6	1.16	125	2.2	4.25	40	1150				
	15	63.7	1.26	131	2.2	6.5	144	1293				
	16	63.808	1.368	128	2.2	4.25	40	1334				
	17	63.968	1.528	120	2.2	9.5	449	1783				
	18	64.008	1.568	119	2.2	4.25	40	1823				
	19	64.064	1.624	118	2.2	4.25	40	1863				
	20	64.112	1.672	124	2.2	7.25	200	2062				

X_1=7 mm									Average values			
Jet	**Droplet**	**t**	**Δt**	**L_3**	**D_j**	**d_d**	**V_d**	**$\sum V_d$**	**L_3**	**Q_{av}**	**n_d**	**$(d_d)_{av}$**
		(s)	**(s)**	**(mm)**	**(mm)**	**(mm)**	**(mm^3)**	**(mm^3)**	**(mm)**	**(mm^3/s)**	**(1/s)**	**(mm)**
RHS	1	62.344	0	125	2.2	4.25	40	40	**122**	**1228**	**14.1**	**5.5**
	2	62.528	0.184	131	2.2	7	180	220				
	3	62.56	0.216	129	2.2	4.5	48	268				
	4	62.608	0.264	129	2.2	4.25	40	308				
	5	62.608	0.264	119	2.2	4.5	48	355				
	6	62.664	0.32	118	2.2	5	65	421				
	7	62.704	0.36	114	2.2	4.75	56	477				
	8	62.904	0.56	124	2.2	6.5	144	621	**L_3**	**Q_{av}**	**n_d**	**$(d_d)_{av}$**
	9	62.936	0.592	123	2.2	4.5	48	668	**(mm)**	**(mm^3/s)**	**(1/s)**	**(mm)**
	10	62.992	0.648	124	2.2	4.25	40	709	**148**	**1231**	**13.0**	**5.7**
	11	63.12	0.776	130	2.2	5.5	87	796				
	12	63.12	0.776	118	2.2	4.5	48	844				
	13	63.176	0.832	118	2.2	4.75	56	900				
	14	63.232	0.888	119	2.2	4.5	48	947				
	15	63.288	0.944	118	2.2	5	65	1013				
	16	63.48	1.136	125	2.2	7.5	221	1234				
	17	63.512	1.168	123	2.2	3.75	28	1261				
	18	63.56	1.216	118	2.2	4.5	48	1309				
	19	63.736	1.392	122	2.2	9	382	1691				
	20	63.76	1.416	120	2.2	4.5	48	1738				

X_1=7 mm									Average values			
Jet	**Droplet**	**t**	**Δt**	**L_3**	**D_j**	**d_d**	**V_d**	**$\sum V_d$**	**L_3**	**Q_{av}**	**n_d**	**$(d_d)_{av}$**
		(s)	**(s)**	**(mm)**	**(mm)**	**(mm)**	**(mm^3)**	**(mm^3)**	**(mm)**	**(mm^3/s)**	**(1/s)**	**(mm)**
LHS	1	29.488	0	66	2.2	6.5	144	144	**64**	**954**	**12.9**	**5.2**
	2	29.632	0.144	67	2.2	6.5	144	288				
	3	29.648	0.16	63	2.2	4.5	48	335				
	4	29.72	0.232	64	2.2	4.5	48	383				
	5	29.808	0.32	62	2.2	5.5	87	470				
	6	29.84	0.352	60	2.2	4.25	40	510				
	7	30.024	0.536	64	2.2	6.5	144	654				
	8	30.072	0.584	64	2.2	4.25	40	694				
	9	30.232	0.744	69	2.2	6.5	144	838				
	10	30.248	0.76	63	2.2	4.25	40	878				
	11	30.296	0.808	62	2.2	4.5	48	926				
	12	30.36	0.872	63	2.2	4.5	48	974				
	13	30.384	0.896	60	2.2	4.25	40	1014				
	14	30.416	0.928	60	2.2	4.25	40	1054				
	15	30.632	1.144	62	2.2	4.5	48	1102				
	16	30.808	1.32	69	2.2	6.5	144	1246				
	17	30.848	1.36	64	2.2	4.5	48	1293				
	18	30.88	1.392	62	2.2	4.25	40	1334				
	19	31.016	1.528	68	2.2	5.75	100	1433				
	20	31.04	1.552	65	2.2	4.5	48	1481				

X_1=7 mm									Average values			
Jet	**Droplet**	**t**	**Δt**	**L_3**	**D_j**	**d_d**	**V_d**	**$\sum V_d$**	**L_3**	**Q_{av}**	**n_d**	**$(d_d)_{av}$**
		(s)	**(s)**	**(mm)**	**(mm)**	**(mm)**	**(mm^3)**	**(mm^3)**	**(mm)**	**(mm^3/s)**	**(1/s)**	**(mm)**
RHS	1	29.48	0	74	2.2	4.5	48	48	**74**	**978**	**13.8**	**5.1**
	2	29.648	0.168	77	2.2	6.6	151	198				
	3	29.696	0.216	77	2.2	4.5	48	246				
	4	29.848	0.368	78	2.2	6.5	144	390				
	5	29.856	0.376	79	2.2	4.5	48	437				
	6	29.872	0.392	76	2.2	4	34	471				
	7	29.896	0.416	72	2.2	4.5	48	519				
	8	29.952	0.472	72	2.2	4.5	48	566	**L_3**	**Q_{av}**	**n_d**	**$(d_d)_{av}$**
	9	29.992	0.512	71	2.2	4.25	40	607	**(mm)**	**(mm^3/s)**	**(1/s)**	**(mm)**
	10	30.024	0.544	68	2.2	4.5	48	654	**69**	**966**	**13.3**	**5.2**
	11	30.232	0.752	76	2.2	6	113	767				
	12	30.24	0.76	72	2.2	4.25	40	808				
	13	30.28	0.8	72	2.2	4.5	48	855				
	14	30.448	0.968	75	2.2	6.5	144	999				
	15	30.608	1.128	82	2.2	5.5	87	1086				
	16	30.608	1.128	71	2.2	5	65	1152				
	17	30.816	1.336	75	2.2	6.5	144	1295				
	18	30.84	1.36	71	2.2	4.25	40	1336				
	19	30.88	1.4	71	2.2	4.25	40	1376				
	20	30.928	1.448	71	2.2	4.25	40	1416				

X_1=7 mm									Average values			
Jet	**Droplet**	**t**	**Δt**	**L_3**	**D_j**	**d_d**	**V_d**	**$\sum V_d$**	**L_3**	**Q_{av}**	**n_d**	**$(d_d)_{av}$**
		(s)	**(s)**	**(mm)**	**(mm)**	**(mm)**	**(mm^3)**	**(mm^3)**	**(mm)**	**(mm^3/s)**	**(1/s)**	**(mm)**
LHS	1	16.208	0	29	2.2	4.5	48	48	**34**	**712**	**12.1**	**4.8**
	2	16.48	0.272	39	2.2	6.5	144	192				
	3	16.52	0.312	36	2.2	4.5	48	239				
	4	16.56	0.352	35	2.2	4.25	40	279				
	5	16.728	0.52	37	2.2	5.5	87	367				
	6	16.768	0.56	35	2.2	4.75	56	423				
	7	16.816	0.608	34	2.2	4.25	40	463				
	8	16.856	0.648	33	2.2	4.25	40	503				
	9	16.888	0.68	30	2.2	4	34	537				
	10	16.928	0.72	28	2.2	4	34	570				
	11	17.184	0.976	36	2.2	6	113	683				
	12	17.224	1.016	35	2.2	4	34	717				
	13	17.224	1.016	35	2.2	4.25	40	757				
	14	17.256	1.048	32	2.2	4.25	40	797				
	15	17.56	1.352	38	2.2	4.5	48	845				
	16	17.712	1.504	38	2.2	7	180	1024				
	17	17.736	1.528	35	2.2	4.25	40	1065				
	18	17.784	1.576	35	2.2	4	34	1098				
	19	17.84	1.632	34	2.2	4.25	40	1138				
	20	17.864	1.656	31	2.2	4.25	40	1178				

X_1=7 mm									Average values			
Jet	**Droplet**	**t**	**Δt**	**L_3**	**D_j**	**d_d**	**V_d**	**$\sum V_d$**	**L_3**	**Q_{av}**	**n_d**	**$(d_d)_{av}$**
		(s)	**(s)**	**(mm)**	**(mm)**	**(mm)**	**(mm^3)**	**(mm^3)**	**(mm)**	**(mm^3/s)**	**(1/s)**	**(mm)**
RHS	1	16.456	0	36	2.2	4.25	40	40	**37**	**752**	**10.8**	**5.1**
	2	16.624	0.168	39	2.2	6.5	144	184				
	3	16.648	0.192	35	2.2	3.5	22	206				
	4	16.696	0.24	34	2.2	3.75	28	234				
	5	16.744	0.288	33	2.2	4.25	40	274				
	6	16.768	0.312	29	2.2	3.5	22	297				
	7	17.04	0.584	40	2.2	6.5	144	440				
	8	17.08	0.624	37	2.2	3.5	22	463	**L_3**	**Q_{av}**	**n_d**	**$(d_d)_{av}$**
	9	17.12	0.664	36	2.2	4.25	40	503	**(mm)**	**(mm^3/s)**	**(1/s)**	**(mm)**
	10	17.296	0.84	40	2.2	6.5	144	647	**35**	**732**	**11.4**	**5.0**
	11	17.328	0.872	37	2.2	4.5	48	695				
	12	17.448	0.992	41	2.2	5.5	87	782				
	13	17.448	0.992	32	2.2	4.25	40	822				
	14	17.536	1.08	30	2.2	4.25	40	862				
	15	17.8	1.344	40	2.2	6.5	144	1006				
	16	17.816	1.36	33	2.2	3.75	28	1034				
	17	17.864	1.408	34	2.2	3.75	28	1061				
	18	18.136	1.68	45	2.2	6.5	144	1205				
	19	18.152	1.696	40	2.2	4.5	48	1253				
	20	18.312	1.856	41	2.2	6.5	144	1396				

References

Anna, S., N. Bontoux and H. Stone (2003). "Formation of dispersions using “flow focusing” in microchannels." Applied Physics Letters **82**: 364.

Baird, M. H. I. and J. F. Davidson (1962). "Annular jets-I: Fluid dynamics." Chemical Engineering Science **17**(6): 467-472.

Bashforth, F. and J. C. Adams (1883). An attempt to test the theories of capillary action: by comparing the theoretical and measured forms of drops of fluid. With an explanation of the method of integration employed in constucting the tables which give the theoretical forms of such drops, University Press.

Becher, P. (1965). Emulsions: theory and practice, Reinhold Pub. Corp.

Bogy, D. (1979). "Drop formation in a circular liquid jet." Annual Review of Fluid Mechanics **11**(1): 207-228.

Brackbill, J. U., D. B. Kothe and C. Zemach (1992). "A continuum method for modeling surface tension." Journal of Computational Physics **100**(2): 335-354.

Brenner, M. P., J. Eggers, K. Joseph, S. R. Nagel and X. D. Shi (1997). "Breakdown of scaling in droplet fission at high Reynolds number." Physics of Fluids **9**(6): 1573-1590.

Bright, A. (1985). "Minimum drop volume in liquid jet breakup." Chemical Engineering Research and Design **63**(a): 59-66.

Buszello, K. and B. Muller (2000). "Emulsions as drug delivery systems." Pharmaceutical emulsions and suspensions: 191-228.

Chandrasekhar, S. (1961). Hydrodynamic and hydromagnetic stability, Courier Dover Publications.

Chandrasekhar, S. (1961). "Hydrodynamic and hydromagnetic stability." International Series of Monographs on Physics, Oxford: Clarendon, 1961 **1**.

Chaudhary, K. and T. Maxworthy (1980a). "The nonlinear capillary instability of a liquid jet. Part 2. Experiments on jet behaviour before droplet formation." J. Fluid Mech **96**(5): 275-286.

Chaudhary, K. and T. Maxworthy (1980b). "The nonlinear capillary instability of a liquid jet. Part 3. Experiments on satellite drop formation and control." J. Fluid Mech **96**(5): 287-297.

Chazal, L. E. M. d. and J. T. Ryan (1971). "Formation of organic drops in water." AIChE Journal **17**(5): 1226-1229.

Chen, Y., L. Wu and C. Zhang (2013). "Emulsion droplet formation in coflowing liquid streams." Physical Review E **87**(1): 013002.

Clanet, C. and J. C. Lasheras (1999). "Transition from dripping to jetting." Journal of Fluid Mechanics **383**(1): 307-326.

Cohen, I., M. P. Brenner, J. Eggers and S. R. Nagel (1999). "Two fluid drop snap-off problem: Experiments and theory." Physical Review Letters **83**(6): 1147-1150.

Cramer, C., B. Berüter, P. Fischer and E. J. Windhab (2002). "Liquid Jet Stability in a Laminar Flow Field." Chemical Engineering & Technology **25**(5): 499-506.

Cramer, C., P. Fischer and E. J. Windhab (2004). "Drop formation in a co-flowing ambient fluid." Chemical Engineering Science **59**(15): 3045-3058.

Das, T. (1997). "Prediction of jet breakup length in liquid-liquid systems using the Rayleigh-Tomotika analysis." Atomization and Sprays **7**(5): 549.

Debye, P. and J. Daen (1959). "Stability Considerations on Nonviscous Jets Exhibiting Surface or Body Tension." Physics of Fluids **2**(4): 416-421.

Degim, T. and N. Çelebi (2007). "Controlled delivery of peptides and proteins." Current pharmaceutical design **13**(1): 99-117.

Delteil, J., S. Vincent, A. Erriguible and P. Subra-Paternault (2011). "Numerical investigations in Rayleigh breakup of round liquid jets with VOF methods." Computers & Fluids **50**(1): 10-23.

Donnelly, R. J. and W. Glaberson (1966). "Experiments on the Capillary Instability of a Liquid Jet." Proceedings of the Royal Society of London. Series A. Mathematical and Physical Sciences **290**(1423): 547-556.

Edgerton, H. E., E. A. Hauser and W. B. Tucker (1937). "Studies in Drop Formation as Revealed by the High-speed Motion Camera." The Journal of Physical Chemistry **41**(7): 1017-1028.

Eggers, J. (2006). A Brief History of Drop Formation. Nonsmooth Mechanics and Analysis. P. Alart, O. Maisonneuve and R. T. Rockafellar, Springer US. **12:** 163-172.

Eggers, J. and E. Villermaux (2008). "Physics of liquid jets." Reports on progress in physics **71**(3): 036601.

Ehrfeld, W., V. Hessel and V. Haverkamp (2000). Microreactors, Wiley Online Library.

Elemans, P., J. Van Wunnik and R. Van Dam (1997). "Development of morphology in blends of immiscible polymers." AIChE Journal **43**(6): 1649-1651.

Fletcher, P. D. I., S. J. Haswell, E. Pombo-Villar, B. H. Warrington, P. Watts, S. Y. F. Wong and X. Zhang (2002). "Micro reactors: principles and applications in organic synthesis." Tetrahedron **58**(24): 4735-4757.

Gañán-Calvo, A. M. and J. M. Gordillo (2001). "Perfectly Monodisperse Microbubbling by Capillary Flow Focusing." Physical Review Letters **87**(27): 274501.

Garcia, F. J. and H. Gonzalez (2008). "Normal-mode linear analysis and initial conditions of capillary jets." Journal of Fluid Mechanics **602**: 81-117.

Garstecki, P., M. J. Fuerstman, H. A. Stone and G. M. Whitesides (2006). "Formation of droplets and bubbles in a microfluidic T-junction-scaling and mechanism of break-up." Lab on a Chip **6**(3): 437-446.

Geer, J. F. and J. C. Strikwerda (1983). "Vertical slender jets with surface tension." Journal of Fluid Mechanics **135**: 155-169.

Goedde, E. and M. C. Yuen (1970). "Experiments on liquid jet instability." J. Fluid Mech **40**(3): 495-511.

Gopala, V. R. and B. G. M. van Wachem (2008). "Volume of fluid methods for immiscible-fluid and free-surface flows." Chemical Engineering Journal **141**(1-3): 204-221.

Gun, T. and S. Martin (2007). CFD modelling of drop formation in a liquid-liquid system, 6th International Conference on Multiphase Flow.

Gunawan, A. Y., J. Molenaar and A. A. F. van de Ven (2002). "In-phase and out-of-phase break-up of two immersed liquid threads under influence of surface tension." European Journal of Mechanics - B/Fluids **21**(4): 399-412.

Gunawan, A. Y., J. Molenaar and A. A. F. van de Ven (2004). "Break-up of a set of liquid threads under influence of surface tension." Journal of Engineering Mathematics **50**(1): 25-49.

Haenlein, A. (1931). "Über den Zerfall eines Flüssigkeitsstrahles." Forschung auf dem Gebiet des Ingenieurwesens A **2**(4): 139-149.

Harkins, W. D. and F. Brown (1919). "The determination of surface tension (free surface energy), and the weight of falling drops: The surface tension of water and benzene by the capillary height method." Journal of the American Chemical Society **41**(4): 499-524.

Harris, C. K., D. Roekaerts, F. J. J. Rosendal, F. G. J. Buitendijk, P. Daskopoulos, A. J. N. Vreenegoor and H. Wang (1996). "Computational fluid dynamics for chemical reactor engineering." Chemical Engineering Science **51**(10): 1569-1594.

Hartland, S. and R. W. Hartley (1976). Axisymmetric fluid-liquid interfaces: tables giving the shape of sessile and pendant drops and external menisci, with examples of their use, Elsevier Scientific Publishing Company.

Harvie, D. J. E. and D. F. Fletcher (2000). "A New Volume of Fluid Advection Algorithm: The Stream Scheme." Journal of Computational Physics **162**(1): 1-32.

Haverkamp, V., W. Ehrfeld, K. Gebauer, V. Hessel, H. Löwe, T. Richter and C. Wille (1999). "The potential of micromixers for contacting of disperse liquid phases." Fresenius' Journal of Analytical Chemistry **364**(7): 617-624.

Hayworth, C. B. and R. E. Treybal (1950). "Drop Formation in Two-Liquid-Phase Systems." Industrial & Engineering Chemistry **42**(6): 1174-1181.

Helmholtz, H. (1869). "The mechanism of the ossicles of the ear and membrana tympani." Pflugers Arch Physiologie **1**.

Hessel, V., H. Löwe and F. Schönfeld (2005). "Micromixers—a review on passive and active mixing principles." Chemical Engineering Science **60**(8–9): 2479-2501.

Hessel, V., H. Löwe and F. Schönfeld (2005). "Micromixers - a review on passive and active mixing principles." Chemical Engineering Science **60**(8-9): 2479-2501.

Hirt, C. W. and B. D. Nichols (1981). "Volume of fluid (VOF) method for the dynamics of free boundaries." Journal of Computational Physics **39**(1): 201-225.

Homma, S., J. Koga, S. Matsumoto, M. Song and G. Tryggvason (2006). "Breakup mode of an axisymmetric liquid jet injected into another immiscible liquid." Chemical Engineering Science **61**(12): 3986-3996.

Homma, S., M. Yokotsuka and J. Koga (2010). "Numerical Simulation of the Formation of a Jet and Droplets from a Capillary in a Co-Flowing Ambient Fluid." Journal of Chemical Engineering of japan **43**(1): 7-12.

Hong, Y. and F. Wang (2007). "Flow rate effect on droplet control in a co-flowing microfluidic device." Microfluidics and Nanofluidics **3**(3): 341-346.

Hoorfar, M., M. A. Kurz and A. W. Neumann (2005). "Evaluation of the surface tension measurement of axisymmetric drop shape analysis (ADSA) using a shape parameter." Colloids and Surfaces A: Physicochemical and Engineering Aspects **260**(1–3): 277-285.

Hoorfar, M. and A. W. Neumann (2004). "Axisymmetric Drop Shape Analysis (ADSA) for the determination of sutface tension and contact angle." The Journal of Adhesion **80**(8): 727-743.

Hoorfar, M. and A. W. Neumann (2006). "Recent progress in Axisymmetric Drop Shape Analysis (ADSA)." Advances in Colloid and Interface Science **121**(1-3): 25-49.

Hua, J., B. Zhang and J. Lou (2007). "Numerical simulation of microdroplet formation in coflowing immiscible liquids." AIChE Journal **53**(10): 2534-2548.

Huang, J. S. and R. Varadaraj (1996). "Colloid and interface science in the oil industry." Current Opinion in Colloid & Interface Science **1**(4): 535-539.

Keller, J. B. (1983). "Capillary waves on a vertical jet." Journal of Fluid Mechanics **135**: 171-173.

Kitamura, Y., H. Mishima and T. Takahashi (1982). "Stability of jets in liquid-liquid systems." The Canadian Journal of Chemical Engineering **60**(6): 723-731.

Knops, Y. M. M., J. J. M. Slot, P. H. M. Elemans and M. J. H. Bulters (2001). "Simultaneous breakup of multiple viscous threads surrounded by viscous liquid." AIChE Journal **47**(8): 1740-1745.

Kobayashi, I., S. Hirose, T. Katoh, Y. Zhang, K. Uemura and M. Nakajima (2008). "High-aspect-ratio through-hole array microfabricated in a PMMA plate for monodisperse emulsion production." Microsystem Technologies **14**(9-11): 1349-1357.

Kobayashi, I., S. Mukataka and M. Nakajima (2004). "CFD Simulation and Analysis of Emulsion Droplet Formation from Straight-Through Microchannels." Langmuir **20**(22): 9868-9877.

Kobayashi, I., S. Mukataka and M. Nakajima (2005). "Effects of Type and Physical Properties of Oil Phase on Oil-in-Water Emulsion Droplet Formation in Straight-Through Microchannel Emulsification, Experimental and CFD Studies." Langmuir **21**(13): 5722-5730.

Kobayashi, I., S. Mukataka and M. Nakajima (2005). "Novel Asymmetric Through-Hole Array Microfabricated on a Silicon Plate for Formulating Monodisperse Emulsions." Langmuir **21**(17): 7629-7632.

Kobayashi, I., S. Mukataka and M. Nakajima (2005). "Production of Monodisperse Oil-in-Water Emulsions Using a Large Silicon Straight-Through Microchannel Plate." Industrial & Engineering Chemistry Research **44**(15): 5852-5856.

Kobayashi, I. and M. Nakajima (2006). "Generation and multiphase flow of emulsions in microchannels."

Kobayashi, I., T. Takano, R. Maeda, Y. Wada, K. Uemura and M. Nakajima (2008). "Straight-through microchannel devices for generating monodisperse emulsion droplets several microns in size." Microfluidics and Nanofluidics **4**(3): 167-177.

Kobayashi, I., K. Uemura and M. Nakajima (2007). "CFD Analysis of Generation of Soybean Oil-in-Water Emulsion Droplets Using Rectangular Straight-Through Microchannels." Food Science and Technology Research **13**(3): 187-192.

Kobayashi, I., G. T. Vladisavljević, K. Uemura and M. Nakajima (2011). "CFD analysis of microchannel emulsification: Droplet generation process and size effect of asymmetric straight flow-through microchannels." Chemical Engineering Science **66**(22): 5556-5565.

Kowalewski, T. A. (1996). "On the separation of droplets from a liquid jet." Fluid Dynamics Research **17**(3): 121-145.

Lafrance, P. (1975). "Nonlinear breakup of a laminar liquid jet." Physics of Fluids **18**(4): 428-432.

Laplace, P. S. (1805). Traité de mécanique céleste/par PS Laplace...; tome premier [-quatrieme], de l'Imprimerie de Crapelet.

Leal-Calderon, F., V. Schmitt and J. Bibette (2007). Emulsion science: basic principles, Springer Verlag.

Lenard, P. (1887). "Ueber die Schwingungen fallender Tropfen." Annalen der Physik **266**(2): 209-243.

Lister, J. R. and H. A. Stone (1998). "Capillary breakup of a viscous thread surrounded by another viscous fluid." Physics of Fluids **10**(11): 2758-2764.

Longmire, E. K., T. L. Norman and D. L. Gefroh (2001). "Dynamics of pinch-off in liquid/liquid jets with surface tension." International Journal of Multiphase Flow **27**(10): 1735-1752.

Martín-Banderas, L., M. Flores-Mosquera, P. Riesco-Chueca, A. Rodríguez-Gil, Á. Cebolla, S. Chávez and A. M. Gañán-Calvo (2005). "Flow Focusing: A Versatile Technology to Produce Size-Controlled and Specific-Morphology Microparticles." Small **1**(7): 688-692.

Mason, T. G. and J. Bibette (1997). "Shear Rupturing of Droplets in Complex Fluids." Langmuir **13**(17): 4600-4613.

Maze, C. and G. Burnet (1969). "A non-linear regression method for calculating surface tension and contact angle from the shape of a sessile drop." Surface Science **13**(2): 451-470.

Maze, C. and G. Burnet (1971). "Estimation of non-equilibrium surface tension." Surface Science **27**(3): 411-418.

Meister, B. and G. Scheele (1967). "Generalized solution of the Tomotika stability analysis for a cylindrical jet." AIChE Journal **13**(4): 682-688.

Meister, B. and G. Scheele (1969a). "Drop formation from cylindrical jets in immiscible liquid systems." AIChE Journal **15**(5): 700-706.

Meister, B. J. and G. F. Scheele (1969b). "Prediction of jet length in immiscible liquid systems." AIChE Journal **15**(5): 689-699.

Milosevic, I. N. and E. K. Longmire (2002). "Pinch-off modes and satellite formation in liquid/liquid jet systems." International Journal of Multiphase Flow **28**(11): 1853-1869.

Muschiolik, G. (2007). "Multiple emulsions for food use." Current Opinion in Colloid & Interface Science **12**(4-5): 213-220.

Nie, Z., M. Seo, S. Xu, P. Lewis, M. Mok, E. Kumacheva, G. Whitesides, P. Garstecki and H. Stone (2008). "Emulsification in a microfluidic flow-focusing device: effect of the viscosities of the liquids." Microfluidics and Nanofluidics **5**(5): 585-594.

Nigel, P. W. and F. T. Joe (1998). Fundamental Concepts and Approaches. Handbook of Grid Generation, CRC Press.

Nisisako, T. (2008). "Microstructured Devices for Preparing Controlled Multiple Emulsions." Chemical Engineering & Technology **31**(8): 1091-1098.

Nisisako, T., T. Torii and T. Higuchi (2002). "Droplet formation in a microchannel network." Lab on a Chip **2**(1): 24-26.

Null, H. R. and H. F. Johnson (1958). "Drop formation in liquid-liquid systems from single nozzles." AIChE Journal **4**(3): 273-281.

Okochi, H. and M. Nakano (2000). "Preparation and evaluation of w/o/w type emulsions containing vancomycin." Advanced drug delivery reviews **45**(1): 5-26.

Ouyang, Y., R. Mansell and R. Rhue (1995). "Emulsion-mediated transport of nonaqueous-phase liquid in porous media: a review." Critical reviews in environmental science and technology **25**(3): 269-290.

Oxley, J. C. (1998). "The chemistry of explosives." Explosive Effects Appl: 137–172.

Pennemann, H., S. Hardt, V. Hessel, P. Loeb and F. Weise (2005). "Micromixer based liquid/liquid dispersion." Chemical Engineering & Technology **28**(4): 501-508.

Peregrine, D., G. Shoker and A. Symon (1990). "The bifurcation of liquid bridges." Journal of Fluid Mechanics **212**: 25-39.

Perrut, M. and R. Loutaty (1972). "Drop size in a liquid--liquid dispersion: Formation in jet Break-up." The Chemical Engineering Journal **3**: 286-293.

Phan, C. and G. Evans (2008). "Influence of Jet Velocity on Jet Breakup in Immiscible Liquid-Liquid Systems." Chemeca 2008: Towards a Sustainable Australasia: 1087.

Pimbley, W. T. and H. C. Lee (1977). "Satellite Droplet Formation in a Liquid Jet." IBM Journal of Research and Development **21**(1): 21-30.

Plateau, J. (1843). "Mémoire sur les phénomènes que présente une masse liquide et soustraite à l'action de la pesanteur." Nouveaux mémoires de l'Académie Royale des Sciences et Belles-Lettres de Bruxelles **16**: 1.

Plateau, J. (1849). Recherches expérimentales et théoriques sur les figures d'équilibre d'une masse liquide sans pesanteur, sn.

Plateau, J. (1873). "Experimental and theoretical statics of liquids subject to molecular forces only." Gauthier-Villars, Paris.

Ranz, W. and W. Dreier Jr (1964). "Initial instability of a viscous fluid interface." Industrial & Engineering Chemistry Fundamentals **3**(1): 53-60.

Rayleigh, L. (1878). "On the instability of jets." Proceedings of the London Mathematical Society **1**(1): 4.

Rayleigh, L. (1891). "Some applications of photography." Nature **44**(1133): 249-254.

Richards, J., A. Beris and A. Lenhoff (1995). "Drop formation in liquid-liquid systems before and after jetting." Physics of Fluids **7**(11): 2617-2630.

Rowlinson, J. S. (2002). Cohesion: a scientific history of intermolecular forces, Cambridge University Press.

Savart, F. (1833). "Mémoire sur la constitution des veines liquides lancées par des orifices circulaires en mince paroi." Ann. Chim. Phys **53**(337): 1833.

Scheele, G. F. and B. J. Meister (1968a). "Drop formation at low velocities in liquid-liquid systems: Part I. Prediction of drop volume." AIChE Journal **14**(1): 9-15.

Scheele, G. F. and B. J. Meister (1968b). "Drop formation at low velocities in liquid-liquid systems: Part II. Prediction of jetting velocity." AIChE Journal **14**(1): 15-19.

Schramm, L. L. (2005). Emulsions, foams, and suspensions: fundamentals and applications, Vch Verlagsgesellschaft Mbh.

Shi, X., M. P. Brenner and S. R. Nagel (1994). "A cascade of structure in a drop falling from a faucet." science-Newyork then Washington: 219-219.

Soleymani, A., A. Laari and I. Turunen (2008). "Simulation of drop formation in a single hole in solvent extraction using the volume-of-fluid method." Chemical Engineering Research and Design **86**(7A): 731-738.

Sugiura, S., M. Nakajima and M. Seki (2002). "Effect of Channel Structure on Microchannel Emulsification." Langmuir **18**(15): 5708-5712.

Taylor, G. (1934). "The formation of emulsions in definable fields of flow." Proceedings of the Royal Society of London. Series A **146**(858): 501.

Taylor, K. C. and B. F. Hawkins (1992). "Emulsions in enhanced oil recovery." Emulsions: Fundamentals and Applications in the Petroleum Industry, Schramm, LL (Ed.), American Chemical Society, Washington, DC: 263-294.

Teng, H., C. M. Kinoshita and S. M. Masutani (1995). "Prediction of droplet size from the breakup of cylindrical liquid jets." International Journal of Multiphase Flow **21**(1): 129-136.

Thomas, S. (2008). "Récupération assistée du pétrole : panorama." Oil & Gas Science and Technology - Rev. IFP **63**(1): 9-19.

Thorsen, T., R. W. Roberts, F. H. Arnold and S. R. Quake (2001). "Dynamic Pattern Formation in a Vesicle-Generating Microfluidic Device." Physical Review Letters **86**(18): 4163-4166.

Timgren, A., G. Trägårdh and C. Trägårdh (2009). "Effects of cross-flow velocity, capillary pressure and oil viscosity on oil-in-water drop formation from a capillary." Chemical Engineering Science **64**(6): 1111-1118.

Timgren, A., G. Trägårdh and C. Trägårdh (2010). "A model for drop size prediction during cross-flow emulsification." Chemical Engineering Research and Design **88**(2): 229-238.

Tomotika, S. (1935). "On the instability of a cylindrical thread of a viscous liquid surrounded by another viscous fluid." Proceedings of the Royal Society of London. Series A, Mathematical and Physical Sciences **150**(870): 322-337.

Tomotika, S. (1936). "Breaking up of a Drop of Viscous Liquid Immersed in Another Viscous Fluid Which is Extending at a Uniform Rate." Proceedings of the Royal Society of London. Series A, Mathematical and Physical Sciences **153**(879): 302-318.

Tyler, E. (1933). "Instability of liquid jets." Phil. Mag **16**(7): 505-518.

Vasiljevic, D., J. Parojcic, M. Primorac and G. Vuleta (2006). "An investigation into the characteristics and drug release properties of multiple W/O/W emulsion systems containing low concentration of lipophilic polymeric emulsifier." International journal of pharmaceutics **309**(1-2): 171-177.

Vassallo, P. and N. Ashgriz (1991). "Satellite Formation and Merging in Liquid Jet Breakup." Proceedings of the Royal Society of London. Series A: Mathematical and Physical Sciences **433**(1888): 269-286.

Versteeg, H. K. (1995). An introduction to computational fluid dynamics the finite volume method, 2/E, Pearson Education India.

Walters, T. and E. Marschall (1988). "Drop formation in liquid-liquid systems." Experiments in Fluids **7**(3): 210-213.

Wang, W., K. H. Ngan, J. Gong and P. Angeli (2009). "Observations on single drop formation from a capillary tube at low flow rates." Colloids and Surfaces A: Physicochemical and Engineering Aspects **334**(1-3): 197-202.

Weber, C. (1931). "Disintegration of liquid jets." Zeitschrift für Angewandte Mathematik und Mechanik **11**(2): 136-159.

Webster, D. and E. Longmire (2001). "Jet pinch-off and drop formation in immiscible liquid–liquid systems." Experiments in Fluids **30**(1): 47-56.

Xu, Q., M. Hashimoto, T. T. Dang, T. Hoare, D. S. Kohane, G. M. Whitesides, R. Langer and D. G. Anderson (2009). "Preparation of Monodisperse Biodegradable Polymer

Microparticles Using a Microfluidic Flow-Focusing Device for Controlled Drug Delivery." Small **5**(13): 1575-1581.

Yahaya Khan, M., Z. A. Abdul Karim, F. Y. Hagos, A. R. A. Aziz and I. M. Tan (2014). "Current Trends in Water-in-Diesel Emulsion as a Fuel." The Scientific World Journal **2014**: 15.

Young, T. (1804). "The Bakerian lecture: Experiments and calculations relative to physical optics." Philosophical transactions of the Royal Society of London **94**: 1-16.

Zhang, D. F. and H. A. Stone (1997). "Drop formation in viscous flows at a vertical capillary tube." Physics of Fluids (1994-present) **9**(8): 2234-2242.

Zhang, W. W. and J. R. Lister (1999). "Similarity solutions for capillary pinch-off in fluids of differing viscosity." Physical Review Letters **83**(6): 1151-1154.

Zhang, X. (1999a). "Dynamics of Growth and Breakup of Viscous Pendant Drops into Air." Journal of Colloid and Interface Science **212**(1): 107-122.

Zhang, X. (1999b). "Dynamics of drop formation in viscous flows." Chemical Engineering Science **54**(12): 1759-1774.

Zhang, X. and O. A. Basaran (1995). "An experimental study of dynamics of drop formation." Physics of Fluids (1994-present) **7**(6): 1184-1203.

Zhang, X. and O. A. Basaran (1995). "An experimental study of dynamics of drop formation." Physics of Fluids **7**(6): 1184-1203.

Zuo, Y. Y., M. Ding, A. Bateni, M. Hoorfar and A. W. Neumann (2004). "Improvement of interfacial tension measurement using a captive bubble in conjunction with axisymmetric drop shape analysis (ADSA)." Colloids and Surfaces A: Physicochemical and Engineering Aspects **250**(1–3): 233-246.

Every reasonable effort has been made to acknowledge the owners of copyright material. I would be pleased to hear from any copyright owner who has been omitted or incorrectly acknowledged.